Mémoire

Auteur : Piette, Aurélien
Promoteur(s) : 8568; Jehin, Emmanuel
Faculté : Faculté des Sciences
Diplôme : Master en sciences spatiales, à finalité spécialisée
Année académique : 2020-2021
URI/URL : http://hdl.handle.net/2268.2/12754

University of Liège

A Thesis Submitted in Partial Fulfilment of the
Requirements for the Degree of Master in Space Science

Effects of the meteorite and comet impacts on the degassing of volatile contained in martian heterogeneous regolith

Supervisors :
DEHANT Véronique
JEHIN Emmanuël
Readers :
BONFOND Bertrand
JAVAUX Emmanuelle
KARATEKIN Ozgur

Candidate :
PIETTE Aurélien

2^{nd} master in space sciences and astrophysics
Academic year 2020-2021

Abstract

The goal of this master's thesis iw to better understand Mars and its complex processes and more specifcally to understand if the heterogeneity of the martian regolith may impact the degassing of volatile due to small impactors.

To do so the increase of temperature as a result of impact energy is theoretically and numerically investigated. A modelisation of the increase of impact-induced temperature is proposed with an analytcial method : the Murnaghan equation of state.

Then a comparison with a hydrocode (numerical method) is considered. To study the environmental effect, the evolution of the temperature following an impact for a martian year is calculated using the Crank-Nicholson method.

The effect of the heterogeneity of the martuian subsurface is then studied with the use of different plausible scenarii of different locations of interest on Mars. Finally, the results for each scenarii are compared with the depth of the ice table or the clathrate stability zone to assess its destabilization and thus degassing of methane.

Acknowledgements

First of all, I would like to thank Véronique Dehant for her enthusiasm and for proposing me interesting thesis subjects to address. I also want to warmly thank Elodie Gloesener, Ozgur Karatekin, Orkun Temel and Cem Berk Senel for their needed help, advices and their time spent to help me throughout this work.

About the end of my master, I want to sincerely thank several teachers, especially Michaël De Becker, Denis Grodent, Emmanuel Jehin and Christian Barbier for their contagious passion that has fueled my interest and curiosity for space scienes.

In the end , I would like to thank Lina and my family for their support during this year, for their curiosity and interest about my studies. It helped me a lot to stay motivated.

Contents

List of Figures

List of Tables

1 Introduction

Since several years, Mars is a source of questions and of interest. Answering those questions is the key to understand Mars, the planet formation, the solar system and finally to learn more about our own planet, Earth.

After the first detection of methane, astrobiological questions about life on Mars and the origin of methane became recurrent. The quest for potential life beyond Earth found a new track. However with the non-detection of methane [Korablev et al., 2019] and the intermittence of detection [Webster et al., 2015], it became clear that Mars has still a lot of mysteries and that there are a lot of processes that need to be undertsood. Methane clathrates, cavities trapping methane in the subsurface, may be a potential answer to solve the methane mystery [Gloesener et al., 2018, Chastain and Chevrier, 2007].

However remote-sensing and in situ obervations help to get a better grasp of understanding to the reddish planet. New missions like ExoMars 2022, will continue to improve the knowledge gathered about Mars and its history. Hystory which can be revealed through the study of impacts on Mars. Due to the very thin atmosphere on Mars (600 Pa at the surface), erosion processes on Mars are scarce and it allows to keep the remnant of past ages on Mars.

From the impacts, the timeline of Mars was separated in epochs and from them the major geological processes that affect the mineralogy of Mars, from a global coverage of basaltic crust to the presence of several minerals on specific regions. The evolution of the martian mineralogy leads to a heterogeneity of the regolith's composition [Ehlmann and Edwards, 2014]. This heterogeneity could lead to different behavior or the subsurface when being hit by impactors. After which it may lead or not to the destabilization of methane clathrates. The effect of small impactors on the destabilization of clathrates was already investigated [Joiret, 2020].

This work will focus on the effect of the meteorite and comet impacts on heterogeneous regolith. A subsurface structure was developped for different locations of interest based on available observations. Then an analytical model (Murnaghan equation of state) was used to simulate the effect of small impactors (lower than 2m in diameter) and its evolution over one martian years. The increase of temperature following an impact was compared to the iSALE-2D shock physics hydrocode.

2 Methane observation on Mars

With the detection [Mumma et al., 2009] and non-detection [Korablev et al., 2019] of methane in the atmopshere of Mars, a need for an understanding came about the probable sources and sinks of the the methane.

Since 2003, instruments on board of martian orbiters and Earth-based instruments have been measuring methane in the atmosphere of Mars up to tens of parts per billion by volume (ppbv) [Mumma et al., 2009].

Recently, the Curiosity rover has detected methane with background levels of 0.41 ± 0.16 ppbv and episodic releases of 7 ppbv [Webster et al., 2015]. Curiosity measurements also led to a hypothesis to explain the background level of methane. Indeed it seems this level is seasonal [Webster et al., 2015]. Lately, no methane was detected from the ExoMars Trace Gas Orbiter (TGO) even though one of the main purpose of the TGO is to search trace levels of methane. Moreover the TGO has a lower upper limit (about 0.05 ppbv) than the previous detection of methane in the atmosphere [Korablev et al., 2019, Webster et al., 2021].

As it is a question of sinks and sources, at the moment only two sinks are accepted. The first one is the photolysis by the Lyman α line. This photochemical destruction of methane happens above ≈ 80 km altitude. The second sink happens below ≈ 80 km altitude and is due to the oxidation of methane by OH or O(1D) [Haberle et al., 2017].

The lifetime of a chemical species is limited by its sink and for the methane in the atmosphere of Mars the lifetime is about 300 terrestrial years [Lefèvre and Forget, 2009]. If chemical species have a lifetime longer than its mixing in the atmosphere, it could lead to a homogenisation of the concentration of the chemical species. For the methane the vertical mixing time is about 10 days and the horizontal mixing time is about half a year [Temel et al., 2019]. However observations from in situ and remote sensing instruments are showing susbtantial change in the mixing ratio of the atmospheric methane.

Those observations indicate a shorter lifetime for the methane, about 200 days, and thus implying localized sources and faster sinks, all leading to shorter time scales. The big discrepancy in the lifetime of methane leaded to a debate over the validity of the methane observations. However unvalid observations seem unlikely based on the fact that ground-based obsersations [Mumma et al., 2009] so as Curiosity measurements [Webster et al., 2013] did not detect any trace of methane.

To explain the presence of intermittent methane peaks and the non-detection of the Trace gas Orbiter a new and faster sink of methane is needed. Several sinks are suggested :

- heterogeneous chemistry
- triboelectricity [1]

[1] Triboelectricity refers to the electrification of different objects or materials occurred due to the collision resulting in

- physical and chemical sequestration in the regolith

At the moment the new and swift sink mechanism has still not been found.

As the variation of a chemical species, here methane, comes from the balance between its sinks and sources, the question of the origin of the methane is investigated. From the proposition of a biological origin to a geological origin or even an exogenous generation mechanism it was decided that the second proposition will be the focus for this work. Indeed based on [Chastain and Chevrier, 2007], this master's thesis will follow the hypothesis that the methane detected on Mars could come from clathrate hydrates as a sink mechanism but the origin of the methane will not be discussed.

Those subsurface reservoirs have the capacity to store methane formed in the past or more recently. As a matter of fact, the annual dissociation of 2×10^3 m^3 of clathrates hydrates, which can trap large amount of gas[2], would lead to a background value of 10 ppb in the martian atmosphere [Gloesener et al., 2021].

3 Clathrate

3.1 Molecular structure

Clathrates or clathrate hydrates are an organized structure of cages formed by a three dimensional assembly of hydrogen-bonded water molecules. These crystalline compounds form cavities (or cages) that can trap a large variety of guest molecules [Chatti et al., 2005].

By means of weak Van der Waals forces the water cage have the capacity to interact with their entrapped gas molecule to lower the free energy hence becoming more stable [Buffett, 2000].

Clathrates can be found under five different type of molecular structure. The different cages and their configuration are shown in 3.1. To refer to the different types a specific nomenclature is used : s^f. Where s is the side of each face and f is the number of faces per cage.

the phenomenal flow of electrons from one material to other balancing the potential difference.

[2] $1m^3$ of clathrates hydrates can store more than $160m^3$

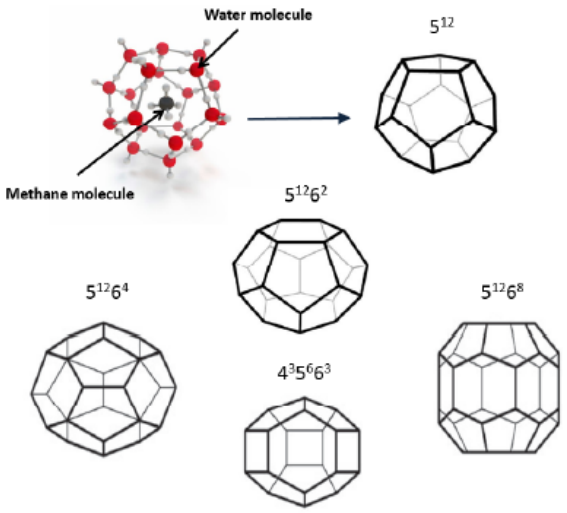

Figure 3.1: The 5 structures of cavity in clathrate hydrates. Top left (credits: Mikkel Juul Jensen) the 5^{12} cage with the methane and water molecules in detail. For the other schema, the line intersections represent the positions of oxygen atoms.

- The first type is the pentagonal dodecahedron (5^{12} , with 12 pentagonal faces) which is prevalent to all clathrate hydrate structures. It contains 20 water molecules.
- The second type is the tetrakaidecahedron ($5^{12}6^2$ with 14 faces composed by 2 facing hexagons and 12 connecting pentagons). This type contains 24 water molecules.
- The third type is the hexakaidecahedron ($5^{12}6^4$, with 16 faces consisting of 4 hexagons ringed completely by pentagonal faces). It is the most spherical cage and it contains 28 water molecules.
- The next type is the dodecahedron ($4^35^66^3$, with 12 faces where two groups of three pentagons face each other and are separated by a band that alternates squares and hexagons). It contains 20 water molecules.
- The last type is the isocahedron ($5^{12}6^8$, with 20 faces where 2 facing hexagons ringed by pentagons and separated by a central band composed of 6 hexagons). It is the most oblate cage and it contains 36 water molecules.

From these 5 different types, three distinct structures have been deduced from x-ray diffraction studies. These structures are composed by an arrangement of cavities where the cage type (detailed above) and the number of cavities are specific to a given structure.

Three structures are the most commonly found in nature. These structures are the cubic structure and the hexagonal structures. The cubic structures correspond to structure I (sI) and structure II and the hexagonal one corresponds to structure H. Their properties can be seen in Table 3.1.

In resume

From the 3 three structures discussed it is possible to resume their parameters. Those parameters are listed in Table 3.1.

Table 3.1: Synthesis of the three clathrate hydrate structures with their parameters [Sloan and Koh, 2007] .

	sI		sII		sH		
Cavity type	Small	Large	Small	Large	Small	Medium	Large
Description	5^{12}	$5^{12}6^2$	5^{12}	$5^{12}6^4$	5^{12}	$4^35^66^3$	$5^{12}6^8$
Number of cages per unit cell	2	6	16	8	3	2	1
Average cavity radius[a] (Å)	3.95	4.33	3.91	4.73	3.94	4.04	5.79
Coordination number[b]	20	24	20	28	20	20	36
H_2O molecules per unit cell	46		136		34		

[a] The cavity radius will change with temperature, pressure and guest composition.
[b] The number of water molecules per cavity.

Commonly there is a guest molecule in each cage. This presence of guest molecule helps to prevent the collapse of the clathrate by the repulsive interactions between the guest molecule and the cage or between the guest molecule and another guest molecule trapped in the neighboring cages. This is why clathrate need a minimal occupancy level to be stable [Sloan and Koh, 2007].

3.2 Properties of clathrate

The properties of clathrate depends strongly on the guest molecule. To be able to be trapped, the guest molecule must have a specific chemical nature, a specific shape and size :

1. The guest molecule can not carry a strong hydrogen-bonding group or several moderately strong hydrogen-bonding groups [Jeffrey, 1984].

2. The guest molecule has to fit in the cavity in order to maximize the van derWaals interactions between the water molecules and the guest molecule. Thus its shape and size have to be adequate for the cavity.
   On one hand if less than 0.76 for the guest/cavity size ratio, the guest is too small. It can enter the cavity but the van der Waals interactions are weak and contribute less to the stability of the cage.
   On the the other hand, if the ratio is bigger than 1, then the guest molecule is too big for the cage and it cannot enter without distorting the cage [Sloan and Koh, 2007].

In conclusion, a guest species will occupy the type of cage which fits the best with its size and thus it leads to the crystallization of a specific type of structure. Figure 3.2 shows the best fit of cavities for each cavities for simple clathrates. .

From the three predominant structure found in nature (sI,sII and sH), the cubic one (sI and sII) are the common one.
During the crystallization, the structure is mainly determined by the size of the guest molecule (sI clathrate for e-methane and carbon dioxide and sII for nitrogen and argon). Moreover the three-dimensional structure from sI, sII or sH determines some properties of the clathrate as the equilibrium temperature and the pressure of the different clathrate phases [Sloan and Koh, 2007].

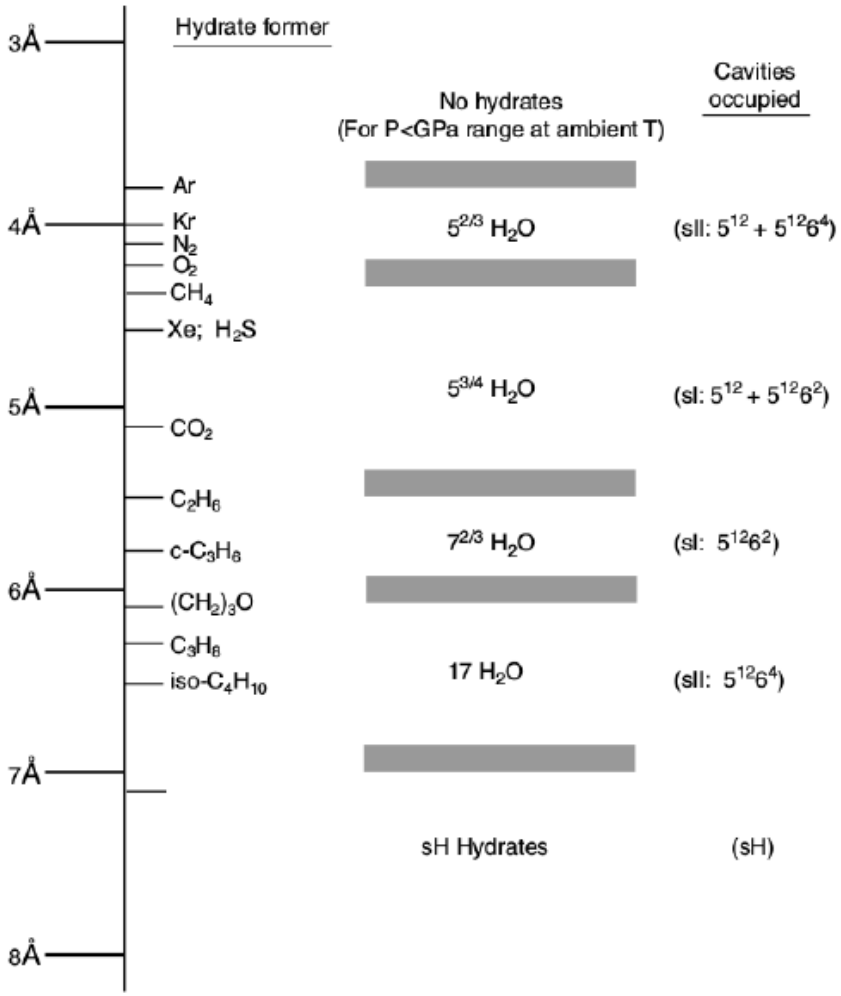

Figure 3.2: Comparison between the size of guest molecules and the cavities they occupy in simple clathrates [Sloan and Koh, 2007]. The corresponding hydration numbers are listed in the central column.

Due to the formation of the cavities by molecule of water it is possible to approximate clathrate hydrates properties with the properties of Ice Ih. Indeed a typical clathrate structure is made of $\leq 85\%$ water and even if the water molecules form a cavity, the system of hydrogen-bonded H2O connection can be assimilated with the one of water ice. Indeed the bond lengths and the O-H bond angles in clathrate are approximately the same as the one in water ice Ih [Sloan and Koh, 2007].

Nonetheless the properties of the cavity (such as mechanical strength, thermal conductivity and density) is still dependent of the presence of guest molecules as the guest molecule impacts the molecular interaction. The variation in thermo-physical properties are shown in Table 3.2.

3.3 Stability of clathrate hydrates

As explained before, the common clathrate structure is composed of at least 85% water and thus some of the clathrate physical properties are analogous to the physical properties of water ice Ih. Still there are some difference due to the presence of gas molecule trapped in the cavities of the clathrate hydrate. And those difference can lead to affect greatly geological processes of planetary environments

Table 3.2: Thermo-physical properties of water ice and of methane clathrate [Sloan and Koh, 2007] .

Property	Water ice Ih	CH_4 clathrate
Density (kg m^{-3})	916[a]	912[a]
H_2O diffusion jump time (μs)	2.7	> 200
Dielectric constant at 273 K	94[a]	~58[a]
Young's modulus at 268 K (GPa)	9.5	~8.4
Poisson's ratio	0.3301	0.3140
Thermal conductivity at 263 K (W m^{-1} K^{-1})	2.18	0.51
Heat capacity within 250 - 270 K (J kg^{-1} K^{-1})	1900 (250 K)- 2100 (270 K)	2080
Linear thermal expansion at 200 K (10^{-6} K^{-1})	56	77
Heat of dissociation (kJ mol^{-1})	6	18.01 ($\rightarrow$ ice + gas)[b] 53.5 ($\rightarrow$ liquid water + gas)[b]

[a] Max (2003)
[b] Anderson (2004)

[Komatsu et al., 2011].

The guest molecule and more precisely, its nature and its partial pressure, plays an important role in the stability of clathrates hydrates. But the stability of the clathrates hydrates is also affected by the presence of inhibitors such as ammonia, salts and alcohols [Sloan and Koh, 2007].

More specifically to the case of Mars, the dissociation curves of the different clathrates considered on Mars are represented in Figure 3.3 together with the phase diagram of H_2O.

.

To link the clathrate with the detection of methane the first step is to evaluate the clathrate stability zone (CSZ), or in other words, where the clathrates are lasting. The thickness of the CSZ is determined by the local geothermal gradient. But it is a complex determination as it depends in practice on many factors like the salinity and nature of dissolved solids in the groundwater, the pressure, the average surface temperature, the recent thermal history of the crust and the subsurface heterogeneity [Gloesener et al., 2018, Mousis et al., 2013].

In Figure 3.4 a case of CSZ for methane clathrate in permafrost is shown where the pressure was converted to depth assuming hydrostatic conditions.

.

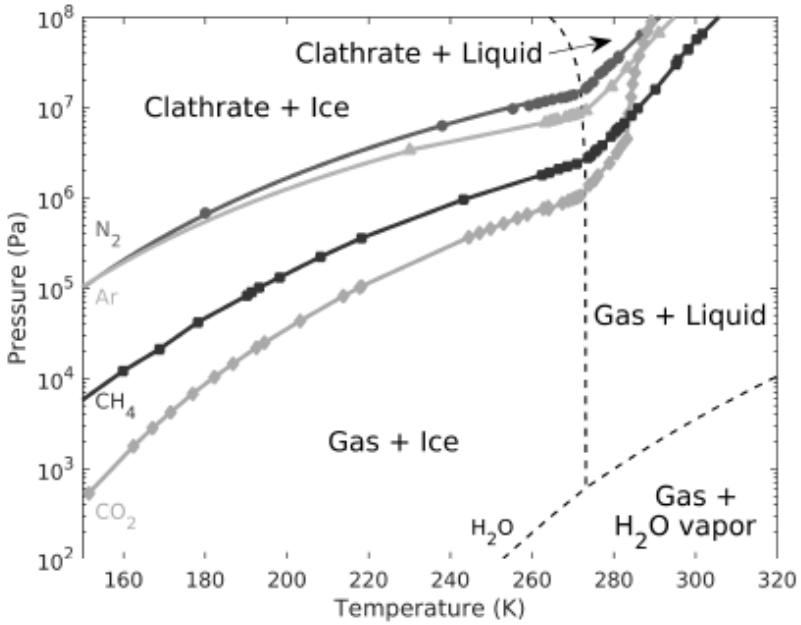

Figure 3.3: Dissociation curves of the different clathrate types considered on Mars together with the phase diagram of H2O (black dotted line) [Gloesener et al., 2021].

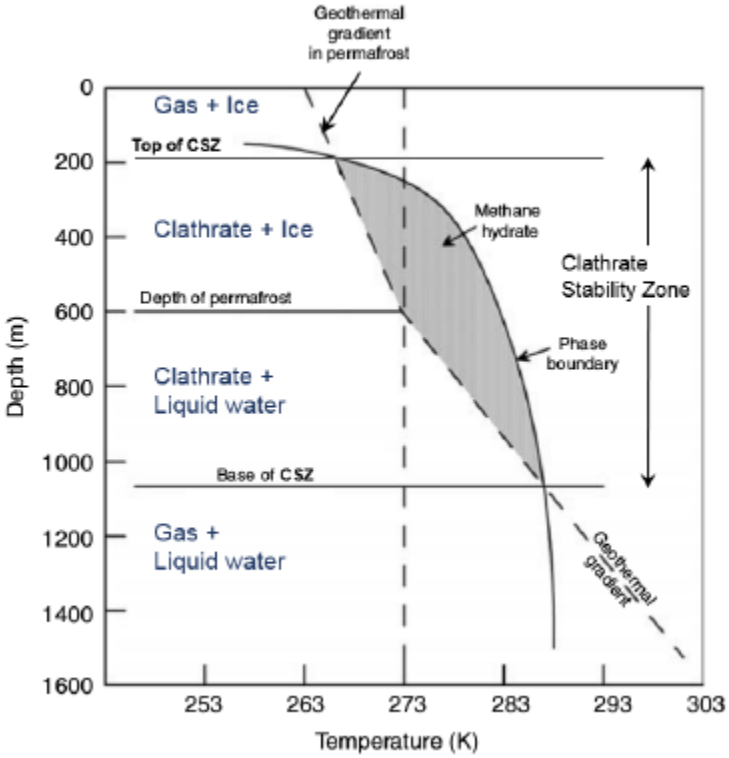

Figure 3.4: Methane clathrate stability zone in permafrost [Gloesener, 2019].

From Figure 3.4 it is possible to see that the clathrate stability zone can correspond to large subsurface areas. However a stability zone does not mean a zone where the clathrate are actually present.

As a matter of fact the most critical factor ruling the existence of clathrate is the methane availability.

To conclude, the clathrate stability zone based only on temperature-pressure conditions gives thus an upper bound to possible clathrate occurrences [Gloesener, 2019, Gloesener et al., 2019].

3.4 Clathrate formation

To understand the availibity of methane, it is needed to first understand the formation of clathrate. Even though the availibity of methane is not linked with the formation of clathrates, the second one is needed in order to have the possibiliy to trap methane. This formation has some similarities with crystallization. Indeed it can be separated in 2 successive steps:

1. A nucleation phase
2. A growth phase

The first phase (the nucleation phase) is unpredictable as it is stochastic, it usually begins when a a metastable supercooled and supersaturated fluid is either at the water-gas interface or on solid substrates (the nucleation is then called heterogeneous nucleation). It consists of the assemblage of water and gas until those assemblage are big enough to launch the next phase: the growth phase.

The next phase consists of the spontaneously growth of the small assemblage. Nonetheless a supersaturated fluid is not always a guarantee for the initiaiton of the nucleation phase and thus for clathrate formation. In fact there are several levels of supersaturation and it is unlikely for spontaneous crystallization to occur below a certain level of supersaturation even though if the temperarture and pressure are favorable. Finally all along the spontaneously growth of the small assemblage, two processes become crucial [Sloan and Koh, 2007]:

1. Mass transfer during which components are adsorbed on the growing.
2. Crystal surface and heat transfer related to the exothermic nature of clathrate formation.

4 Clathrate hydrate on Mars

Assuming a serpentinization process followed by Fischer-Tropsch reactions [3] it is possible to consider the formation of methane in the crust. But even with those assumptions, there are still barriers to cross in order to get the methane from the crust to the atmosphere.

First, methane either in the form of gas bubbles or in the form of a methane-saturated fluids, will have to rise through regolith layers thanks to faults and fractures till it reach the Clathrate Stability Zone (CSZ). There, the nucleation phase of clathrate hydrates can begin at the gas-water interface.

The first formed clathrates hydrate are under the form of a thin film along the surface of the gas bubble . The gas bubble will continue to rise until it interacts with the pre-existing permafrost layer and then it will freeze at the transition between liquid water and water ice. In the end the water ice matrix will

[3] A collection of chemical reactions that converts a mixture of carbon monoxide and hydrogen or water gas into liquid hydrocarbons

contain methane clathrate as small inclusions [Chassefière and Leblanc, 2011].

However given the very low abundance of methane on Mars, methane rich clathrate hydrates cannot be formed from the current planet's atmosphere [Thomas et al., 2009]. That means that if methane rich clathrates are present on Mars it should have been former with a subsurface source or an early martian atmosphere, richer in methane. Moreover it is known that the presence of methan rich clathrates on Mars also depends on different factors as :

- The obliquity variations
- The thermal history
- The composition of the crust
- The dissociation rate of clathrates
- The amount of methane available either in the subsurface or in the early Mars atmosphere

It is still possible that these methane reservoirs have remained trapped at depth until now. And that at this moment the current stability zone of methane rich clathrate hydrates is close to the surface leading to the release of methane from these reservoirs. This release could explain transient CH4 plumes that have been observed on the surface during the past years. To confirm this hypothesis, it is hoped that The ExoMars Trace Gas Orbiter will provide valuable measurements to understand the volatile reservoirs on Mars and particularly the sources and the sinks of methane [Gloesener et al., 2018].

4.1 Dissociation of the clathrate

To release the methane trapped in the cavities, it is needed to dissociate (or destabilize) the clathrate. This dissociation is an endothermic process and occurs when the hydrogen bonds as well as the van der Waals interaction forces between the guest molecule and host cage break. This destabilization can be triggerred by :

- heating
- depressurization
- thermodynamic inhibitor injection

Small and disseminated clathrate reservoirs are easily decomposed, while massive deposits undergo a much slower dissociation. There are tw o reasons for that. The first one is becasue of the low surface to volume ratio [Sloan and Koh, 2007].

The second one is beacuse of the "self-preservation" effect where a protective ice layer forms from dissociated clathrates and prevents the rest from further dissociation [Yakushev and Istomin, 1992].

To be noted, the dissociation of methane clathrate in ice and gas requires less heat than its decomposition in water and gas [Gloesener, 2019].

4.2 Clathrate on present-day Mars

On present-day Mars, the stability conditions of CH_4-rich clathrates are met in the shallow subsurface. A representation of the Clathrate Stability Zone in present-day martian subsurface is shown in Figure 4.1.

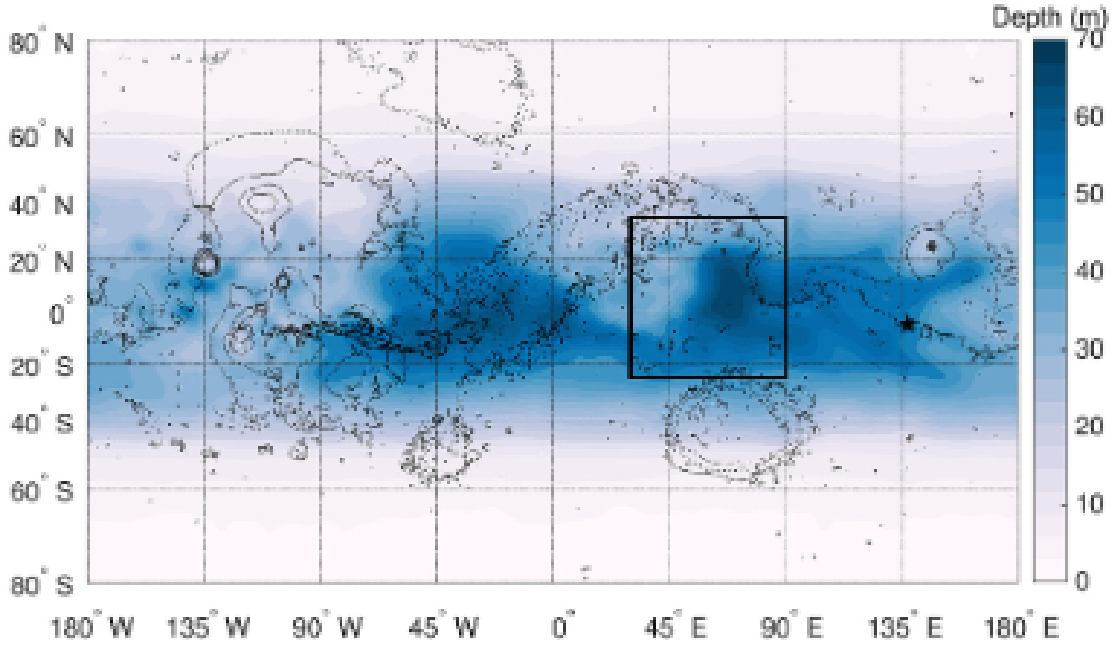

Figure 4.1: Depth (m) of the beginning of hydrate stability zone in present-day martian subsurface for CH4-rich clathrates formed from a gas phase with 90% of methane[Gloesener et al., 2021].

On present-day Mars clathrate hydrate can be stable very near the surface at high latitudes, and can be as close as 20 m to the surface in the tropics. Nevertheless, the top of their stability zone is the deepest (-68 m) in regions where methane has been locally reported, notably in the area observed by [Mumma et al., 2009].

At -68m of depth the clathrate are too deep to be affected by seasonal changes in temperature [Ishimaru et al., 2010]. However the stability field can be shifted upwards with tilted surfaces oriented towards the pole as these slopes experience colder surface temperature. The shallowest stability zone at -4.6 °N and 30°N has been found to occur with a slope angle of 70°and 60 °respectively [Gloesener, 2019].

Furthemore some equator-facing slopes can also bring the clathrate stability zone closer to the surface if these slopes are located at very low latitude. For concrete example, in the equatorial regions, the destabilization of methane clathrates by surface processes could thus be easier on crater walls, especially as sloped surfaces are more likely to landslides [Gloesener, 2019].

Another factor is the presence of eutectic Mg(ClO4)2 brine, whenever brine is present the methane clathrate will form at shallower depth, more precisely the base of the stability zone is shifted upwards [Gloesener et al., 2021].

Another possibility may come from the base of the clathrate stability zone, where it can be closer to the surface on the condition that eutectic NaCl, $CaCl_2$ and $Mg(ClO4)_2$ brines are present [Gloesener et al., 2021]. The base of the clathrate zone could also be decomposed by being in contact with high salinity fluid-sleading to the release of volatile [Madden et al., 2007].

Despite the non-detection of the Trace Gas Orbiter, it does not prevent potential future observations, especially if the methane is outgassed only episodically. Moreover with the launch of ExoMars2022 and with the landing of the new Mars Rover Perseverance it could bring a a series of geochemical analyses including measurements of CH4 (below the ground if possible). The new data will hopefully lead to a new step to solve the methane mystery.

5 Impacts on Mars

5.1 Impacts rate

From 2005 to 2015, almost 500 new dated impact sites have been identified on Mars based on imaging a location before and after impacts [Daubar et al., 2015]. Impacts are common on Mars and the impact rate is estimated to be $1.8 \times 10^{-6} km^{-2} yr^{-1}$ for a diameter larger than 3.9m [Daubar et al., 2015]. Another way to reprensent what falls on Mars is from the InSight data [Banerdt et al., 2020, Daubar et al., 2020] where it was measured that 1kg falls every $1.47 * 10^{-4} km^{-2} yr^{-1}$ and an impactor of 1kg on Mars roughly leads to a crater between 1.2 and 2.8m of diameter.

It is known that small impacts are much more abundant [Hartmann, 2005] but it is harder to estimate the rate for small impactor (impactors with a diameter lower than $2m$) because there is a bias on the data from Insigt for the small impactors. Indeed, small impacts provide a much weaker seismic source and thus are only detectable regionally and that requires the seismometer to be near the impact site. That is why InSight has not detected any small impacts [Daubar et al., 2015]. For now on, the only way to detect small impacts is with the image camera from orbiters. A recent impact can be seen in Figure

Figure 5.1: Before and after image of a small impacts near InSight. Impact coordinates : 4.66°N,226.01°W. Credits : Ingrid Daubar

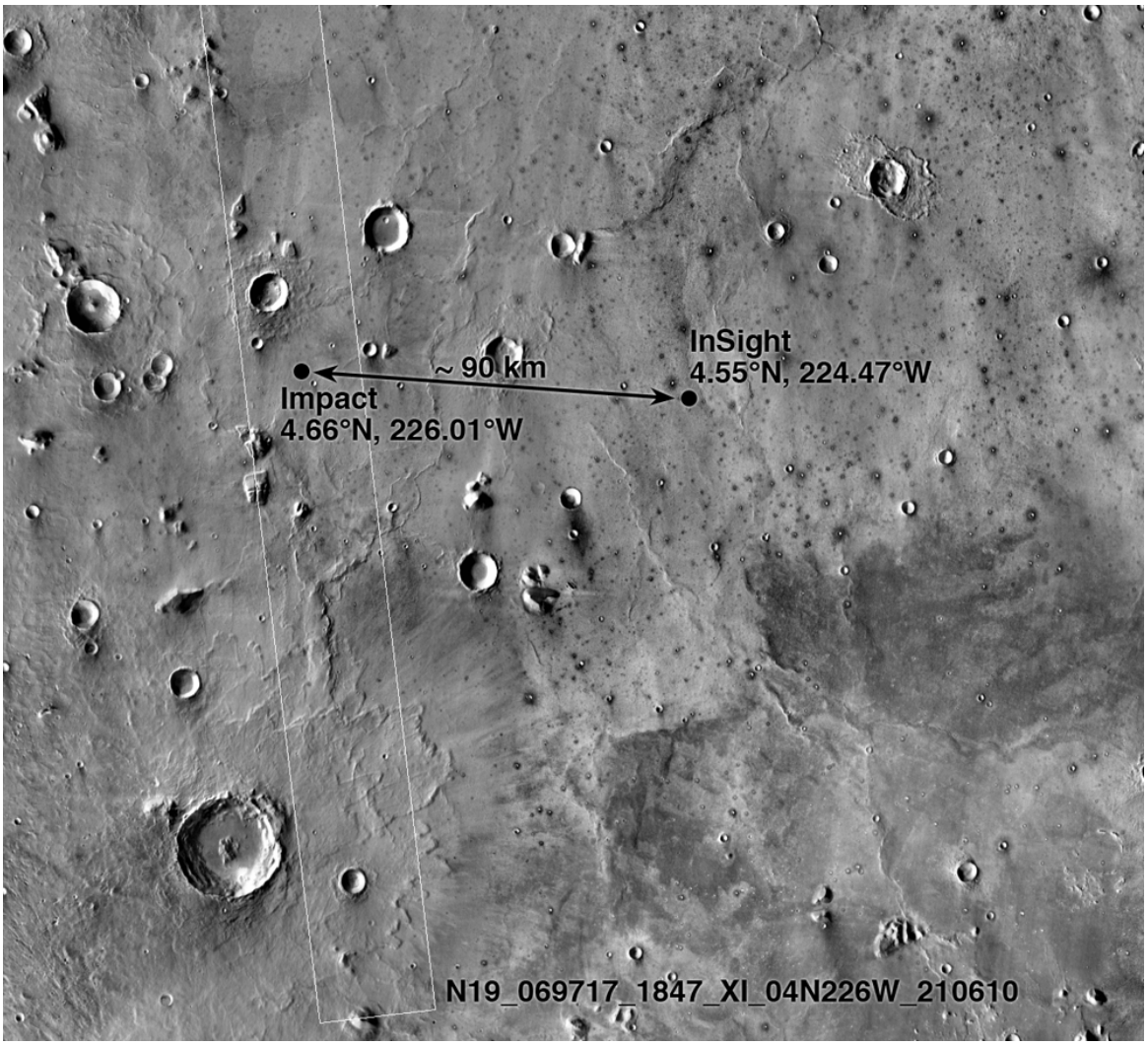

Figure 5.2: Recent impacts on the surface of Mars.Credits : Ingrid Daubar

Small impactor with high velocities can lead to the increase of temperature in the subsurface on Mars as the Martian atmosphere is much thinner than Earth's. In comparison the atmospheric pressure on Mars is 600 Pa compared to the 101325 Pa of the Earth's atmosphere. Figure 5.3 shows the recent impacts on the surface of Mars.

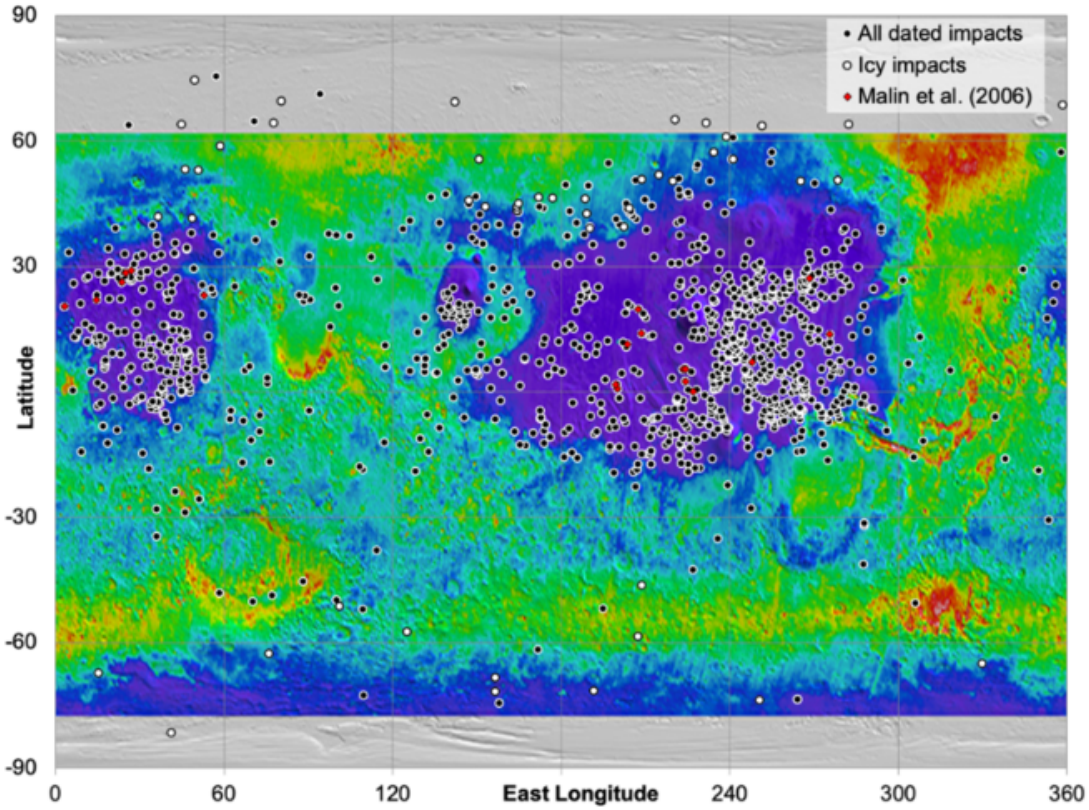

Figure 5.3: Recent impacts on the surface of Mars [Munje et al., 2020].

To be noted, when entering the atmosphere of Mars, impactors may break up. This fragmentation of the impactor in Mars's atmosphere often leads to clusters of impact craters. As a result, most small craters on Mars could be secondaries [Munje et al., 2020].

5.2 Crater ejecta morphology

Fresh craters on the Moon or on Mercury display radial patterns but on Mars, it is different. As shown by Viking and Mars Global Surveyor (MGS) imagery, fresh impact craters on Mars are generally encircled by a layered or lobate ejecta morphology. To explain the difference in morphology, two hypotheses were proposed [Barlow and Perez, 2003] :

- Impact into and vaporization of subsurface volatiles
- Ejecta entrainment into the thin Martian atmosphere.

From the fresh Martian impact craters three dominant fluidized (or layered from the preferred nomenclature) ejecta morphologies are displayed :

- Single layer ejecta (SLE)
- Double layer ejecta (DLE)
- Multiple layer ejecta (MLE)

It is commonly thought that the heating and vaporization of subsurface volatiles during crater forma-

tion leads to those fluidized appearances [Barlow and Perez, 2003]. The three dominant layered ejecta morphologies are shown on figure 5.4 and 5.5.

The most common ejecta morphology, the SLE, is constituting more than 70% of all ejecta morphologies studied within the $\pm 60°$ latitude zone on Mars. The two other morphologies (DLE and MLE) are much less common, but these morphologies often found in localized regions of Mars. Those three ejecta morphologies are often found in lower latitudes [Barlow and Perez, 2003]. The correlation between the ejecta morphology with their frequency and their latitute would be explained by subsurface volatiles which act a crucial role for the formation of the different morphologies [Barlow and Perez, 2003].

There are two types of double layer ejecta (DLE) crater exist on Mars. The first one, Type 1 DLE crater, is characterized by two complete ejecta layers where the inner layer is less extensive, more circular in planform, has a broader distal rampart, and is thicker than the outer layer. The Type 2 DLE craters are morphologically transitional between SLE and MLE [Boyce et al., 2016].

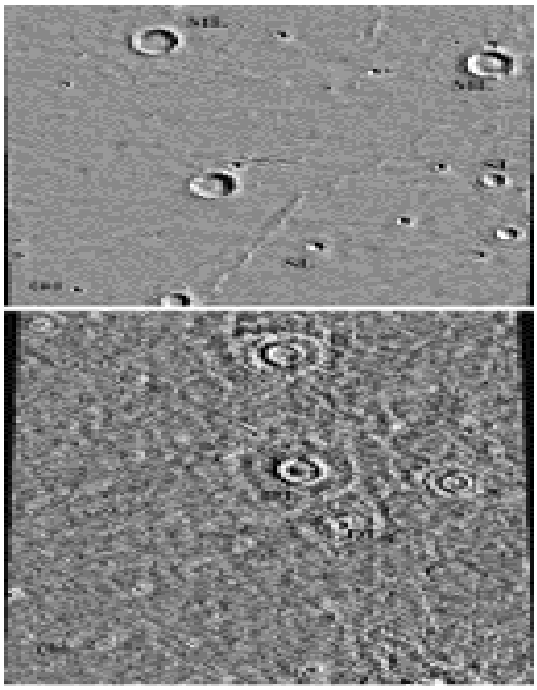

Figure 5.4: Examples of ejecta morphologies. (a) Examples of the SLE and MLE ejecta morphologies. MLE crater at upper right is located at $16.0°S 275.4°E$ and is 18.8 km in diameter. SLE crater is located at $18.7°S 276.6°E$ and is 7.4 km in diameter. (b) Example of the DLE morphology. Central DLE crater is 13.8 km in diameter and is located at $41.3°N 98.3°E$ [Barlow and Perez, 2003].

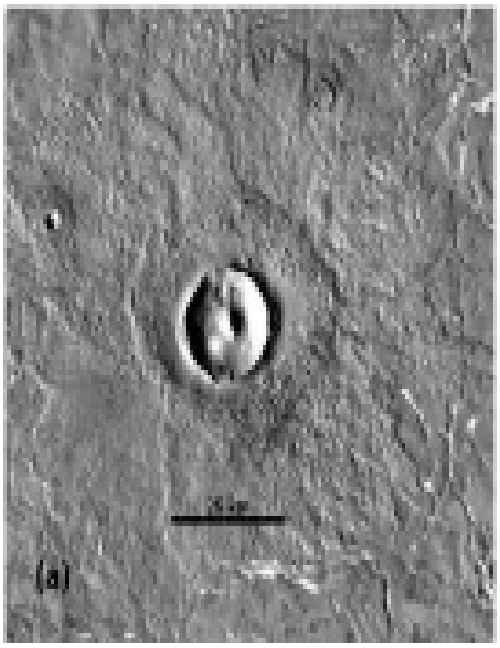

Figure 5.5: Double Layer ejecta[Barlow and Boyce, 2016].

In higher latitudes, other ejecta morphologies can be found [Barlow and Boyce, 2016] :

- Low-aspect Ratio layered ejecta (LARLE)
- Pedestal crater (Pd)
- Pancake crater (Pn)

Low-aspect Ratio layered ejecta are ejecta deposit morphology displaying an extensive, thin ($< 10m$) and sinuous outer deposit beyond the normal layered ejecta blanket [Barlow and Boyce, 2016]. A LARLE can be seen in figure 5.6.

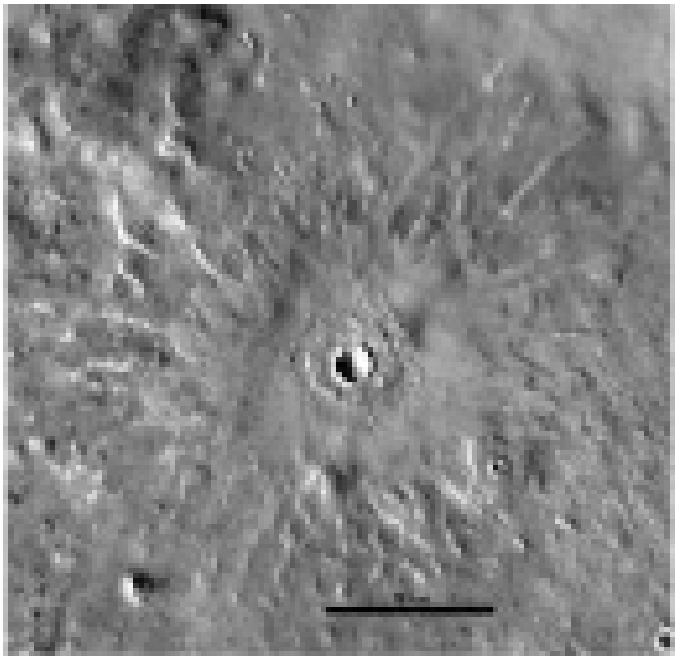

Figure 5.6: 5.5 km of diameter LARLE crater centered at $68.27°N$ $266.36°E$ [Barlow and Boyce, 2016].

Pancake crater are characterized by a single thick ejecta deposit. At first, Pn crater were thought to be the inner ejecta layer of DLE craters where the outer layer was not detectable. But morphometric measurements linked with higher resolution image led to confirm that Pn craters are eroded versions of Type 1 DLE craters where only the inner ejecta layer is resolved or present [Barlow and Boyce, 2016]. A Pancake crater can be seen in Figure 5.7.

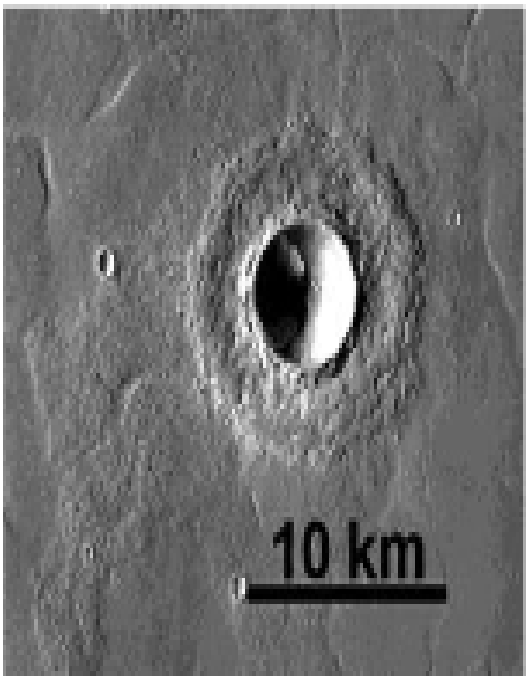

Figure 5.7: 5.0 km of diameter Pancake crater at $32.19°N103.86°E$ [Barlow and Boyce, 2016].

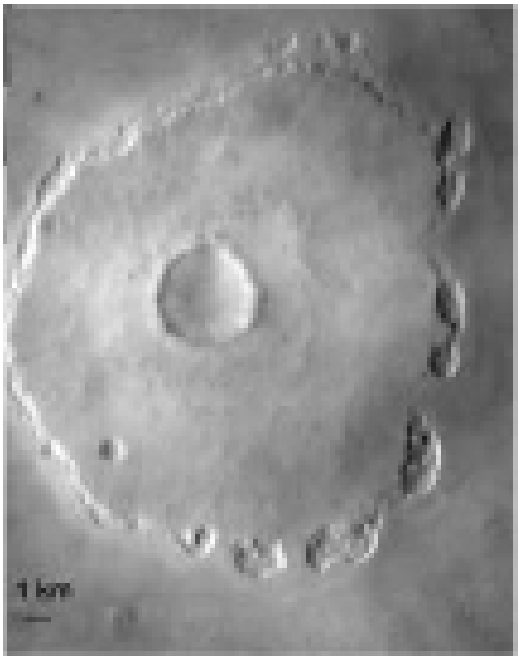

Figure 5.8: 3.4 km of diameter Pd crater with marginal sublimation pits, centered at $62.4°N 99.4°E$ [Barlow and Boyce, 2016].

Pedestal (Pd) craters are characterized by a crater and its layered ejecta blanket onto an roughly circular elevated plateau. based on their properties (distribution, diameter range, and morphology), it is advanced that Pedestal (Pd) craters are eroded LARLE craters. It is supported by the fact that Pd craters are found in the same locations and diameter ranges as LARLE craters [Barlow and Boyce, 2016, Kadish et al., 2008]. A pedestal crater can be seen in Figure 5.8.

From the morphologies of Martian impacts and based on models for the distribution of subsurface volatiles [Clifford, 1993] it was suggested that the SLE morphology came from impact into subsurface ice [Barlow and Perez, 2003].

Moreover, still based on theoretical distribution of subsurface volatiles [Clifford, 1993], on the depth analysis and in comparison with the Mars Odyssey Gamma Ray Spectrometer (GRS) data (showed in Figure 5.9) it is probable that Martian impact craters displaying any of the three layered ejecta morphologies can provide information about the distribution of subsurface H2O and perhaps its physical state.

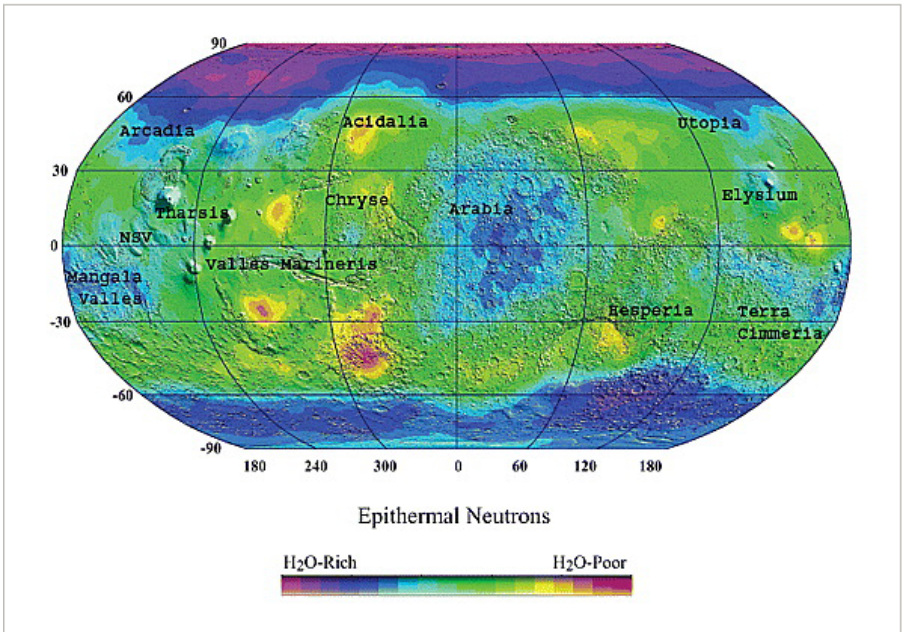

Figure 5.9: GRS epithermal neutron map. This map shows the distribution of the epithermal neutron flux as measured by the Neutron Spectrometer (part of the GRS instrument package) during northern hemisphere summer. Regions with low epithermal neutron flux are interpreted as high water concentration and are with the highest concentrations of DLE and MLE craters. (Map courtesy of William Boynton and the GRS Science Team) [Boynton et al., 2002].

6 Martian mineralogy

From the beginning of 2000, orbital infrared spectroscopy and in situ exploration from landers or in situ data from Mössbauer spectroscopy [4] of Fe-bearing minerals and X-ray diffraction (XRD) have helped a lot to understand and reveal the composition and history of Mars. It is a key point to understand Mars as the martian rocks and sediments contain the record of the evolution of the Red Planet. Indeed, minerals keep track of geological processes that happened on Mars [Ehlmann and Edwards, 2014].

First of all, the red planet is called like that due to the presence of a reddish, fine-grained ($< 5\mu m$) dust. This reddish dust is present everywhere on the surface of Mars and it covers and obscures large portions of the planet. However, dust cover is incomplete, and beneath the dust of Mars lie bedrock and sediments of distinctive composition.

Then, Mars has basaltic upper crust with some regionally variation of the quantity of pyroxene, olivine and silicate. Each regional variation is associated with different terrains. It indicates changes in magma composition and generation over time and space [Ehlmann and Edwards, 2014].

6.1 Martian time periods

As the history of Mars reveals that it was possible to discriminate the Martian time periods in several epochs. The Noachian epoch ($> 3.7Ga$), The Hesperian epoch (3.7 - 3.1 Ga), and the Amazonian epochs ($< 3.1Ga$). Each epoch with specific major processes affects the mineralogy. Those processes are resumed in Figure 6.1.

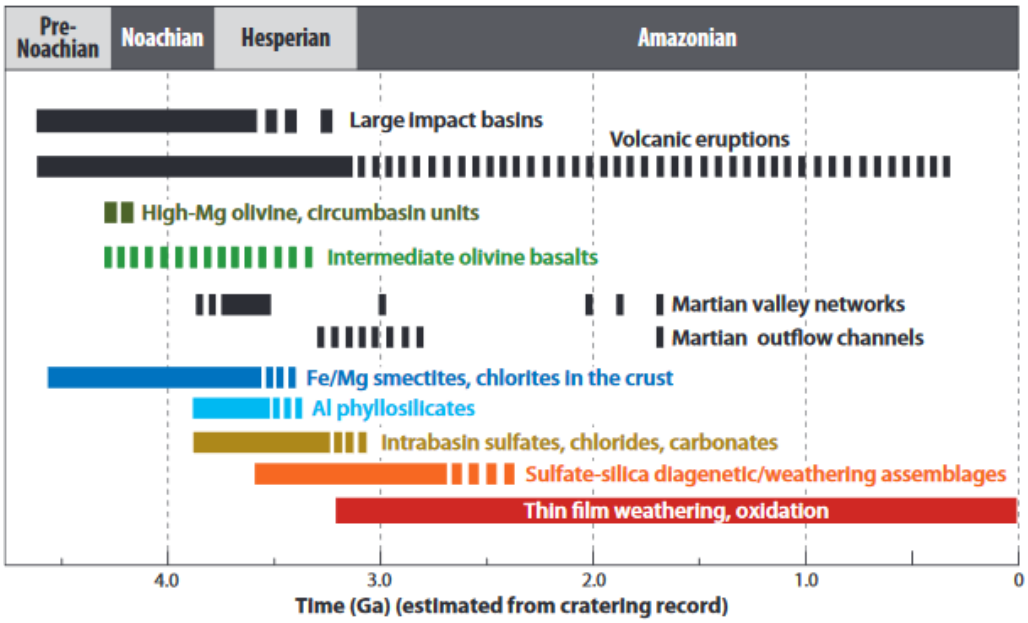

Figure 6.1: Timeline of the major processes affecting the mineralogic composition of Mars and the ages of large-scale units [Ehlmann and Edwards, 2014].

Linked with the facts that many Noachian and Hesperian lavas on Mars are enriched ($> 20\%$) in

[4] It consists of the nearly recoil-free emission and absorption of nuclear gamma rays in solids.

intermediate-Mg-number olivine it indicates the excavation of the upper mantle or localized high-temperature lavas induced by an impact[Ehlmann and Edwards, 2014].

Evolved rocks are rare on Mars but are found locally. It indicates a local-scale igneous fractional crystallization of magmas with different composition, or other different processes.

It is well known that water was present on early Mars, and that water affected the mineralogy of Mars. Indeed, it is possible to find clay minerals where the Noachian crust is exposed. And the presence of clay minerals imply aqueous alteration early in Mars past history. Some portion of this alteration was hydrothermal and some was near-surface weathering. Noachian and Hesperian sediments are composed of clays, carbonates, sulfates, and chlorides [Ehlmann and Edwards, 2014].

About the late Hesperian to Amazonian mineralogic record of water, it is sparser. However sulfates and silica are found in some locations indicating local availability of ground and surface waters even in the most recent geologic epoch. Nevertheless Amazonian units do not generally have crystalline alteration minerals, suggesting that less water was present late in Mars history and thus less aqueous alteration occured in late Mars history [Ehlmann and Edwards, 2014].

6.2 Minerals on Mars

As water ran on early Mars, its properties, like salinity and pH but also the relative importance of detrital and precipitated sediments, changed regionally. It leads to variations in the mineral assemblage of the altered rocks. In addition to that, groundwater was also a major factor during the formation and the diagenesis of clay minerals. Actually, when groundwater rose to the surface, it produced large deposits of sulfates, hematite, and chlorides. From the hydrated mineral assemblages of the Hesperian it was deduced that there were more acidic conditions later in Mars history in some locations leading to the formation of iron and aluminum sulfates [Ehlmann and Edwards, 2014].

Finally, carbonate-bearing rocks associated with olivine have been detected, and carbonate is present in small quantities in dust and soil even though its present-day distribution is not fully understood [Ehlmann and Edwards, 2014].

The minerals detected on Mars can be seen in Table 6.1 and the distribution of major classes of aqueous minerals is shown in Figure 6.2.

Table 6.1: Minerals detected on Mars from landed and orbital data sets [Ehlmann and Edwards, 2014].

	Class	Group/mineral/phase	Formula
Primary	Framework silicates	Olivines	$(Mg, Fe)_2SiO_4$
		Orthopyroxenes	$(Mg, Fe, Ca)Si_2O_6$
		Clinopyroxenes	$(Ca, Mg, Fe)Si_2O_6$
		Plagioclase feldspars	$(Ca, Na)(Al, Si)_4O_8$
		Alkali feldspars	$(K, Na)(Al, Si)_4O_8$
	Sulfides	Pyrrhotite[b]	$Fe_{1-x}S$
		Pyrite/marcasite[c]	FeS_2
	Oxides	Magnetite[d]	$Fe_{3-x}Ti_xO_4$
		Ilmenite[d]	$FeTiO_3$
Secondary	Oxides	Hematite	Fe_2O_3
		Goethite[d]	$FeO(OH)$
		Akaganeite[b]	$Fe(O, OH, Cl)$
	Phyllosilicates (clay minerals)	Fe/Mg smectites (e.g., nontronite, saponite)	$(Ca, Na)_{0.3-0.5}(Fe, Mg, Al)_{2-3}(Al, Si)_4O_{10}(OH)_2 \cdot nH_2O$
		Al smectite (e.g., montmorillonite, beidellite)	$(Na, Ca)_{0.3-0.5}(Al, Mg)_2(Al, Si)_4O_{10}(OH)_2 \cdot nH_2O$
		Kaolin group minerals (e.g., kaolinite, halloysite)	$Al_2Si_2O_5(OH)_4$
		Chlorite	$(Mg, Fe^{2+})_5Al(Si_3Al)O_{10}(OH)_8$
		Serpentine[e]	$(Mg, Fe)_3Si_2O_5(OH)_4$
		High-charge Al/K phyllosilicate (e.g., muscovite, illite)	$(K, H_3O)(Al, Mg, Fe)_2Al_xSi_{4-x}O_{10}(OH)_2$
	Other hydrated silicates	Prehnite	$Ca_2Al(AlSi_3O_{10})(OH)_2$
		Analcime	$NaAlSi_2O_6 \cdot H_2O$
		Opaline silica ($n > 0$), quartz ($n = 0$)	$SiO_2 \cdot nH_2O$
	Carbonates	Mg/Ca/Fe carbonates	$(Mg, Fe, Ca)CO_3$
	Sulfates	Kieserite ($MgSO_4 \cdot H_2O$); szomolnokite ($FeSO_4 \cdot H_2O$); Fe(II)-, Fe(III)-, and Mg-polyhydrated sulfates	$(Fe, Mg)SO_4 \cdot nH_2O$
		Gypsum ($n = 2$), bassanite ($n = 0.5$), anhydrite ($n = 0$)	$CaSO_4 \cdot nH_2O$
		Alunite	$KAl_3(SO_4)_2(OH)_6$
		Jarosite	$KFe_3(OH)_6(SO_4)_2$
		Not a named mineral	$Fe^{3+}SO_4(OH)$
	Chlorides	Chlorides	e.g., $NaCl$, $MgCl_2$
	Perchlorates	Perchlorates[f]	e.g., $(Mg, Ca)(ClO_4)_2$

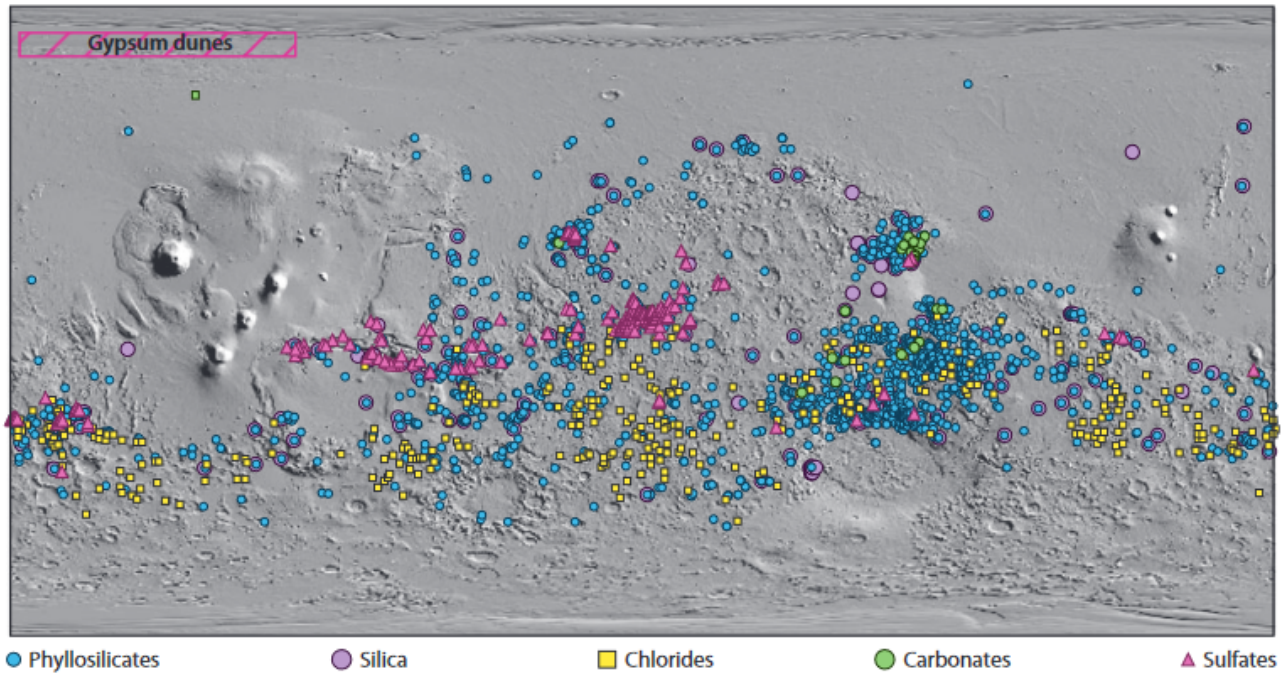

Figure 6.2: Global distribution of the major classes of aqueous minerals on Mars. Phyllosilicates occur in almost every region where Noachian crust is exposed. The distributions of other secondary minerals are more regional and/or patchy [Ehlmann and Edwards, 2014].

7 Location of interest on Mars

Several locations are potentially interesting for the scope of this master's thesis : locations where data are available like landing sites for Martian space mission or future Martian space mission, but also locations with specific features or interesting detections.

The models built in the next parts will have different depth in function of their composition. If there are 2 layers or more, the model will go up to 12m deep. If there is only 1 layer, the model will go up to 10m. Thus when there are 2 layers, their respective thickness is 6 m, when there are 3 layers, it's 4m and finally when there are 4 layers, each layer has a thickness of 3m.

It is mainly driven by the method used to run the model in Python (see Appendix). As the Crank-Nicolson method is formulated with a matrix form $AT^{t+1} = BT^t + C$ (see equation 8.2.9, 8.2.10 and 8.2.12 and that each matrix is a square matrix, it is easier to model symmetric layers and 12m is a multiple of 2,3 and 4.

Moreover, as this master's thesis focuses on small impactors a total depth of 10 or 12 m is enough to model the effect of those small impactors .

7.1 InSight

The first location of interest is the InSight landing site. It is located near the equator of Mars, more precisely at $4.5°N, 136.6°E$. As a landing site, several data are available. Moreover the InSight mission contains a seismometer and recent impacts are detected near its position, making it a very interesting location for the modelisation of impacts on Mars.

[Egea-Gonzalez et al., 2021] proposed a model (shown in Figure 7.1) where the InSight landing site was composed of several layers. A crust either basaltic or felsic, a mantle and for some cases Megaregolith as a surface layer. The properties of each component used are shown in the table 7.1.

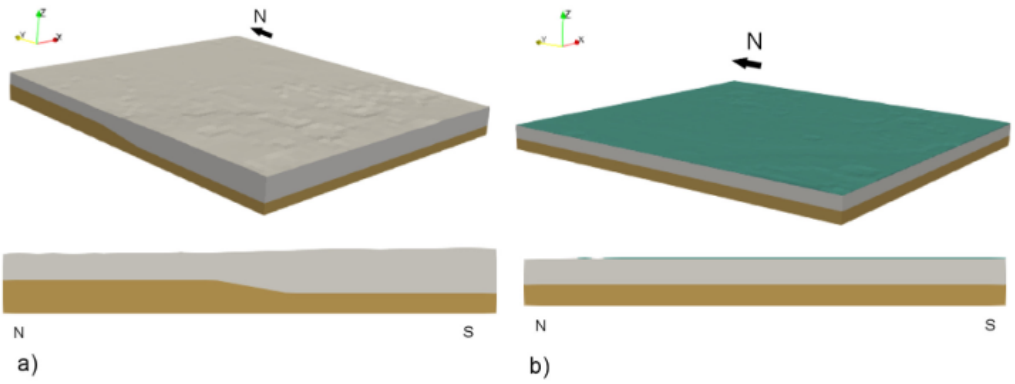

Figure 7.1: Model used to study the thermal state around the InSight landing site. The Gray block is the crust and the brown block is the mantle. The blue block represents the megaregolith [Egea-Gonzalez et al., 2021].

	Conductivity ($W\,m^{-1}\,K^{-1}$)	Density ($kg\,m^{-3}$)
Mantle	3.5	3500
Basaltic crust	2	2900
Felsic crust	2.5	2750
Megaregolith	0.8	1700

Table 7.1: Properties of the different layers that compose the models. [Egea-Gonzalez et al., 2021].

However, the model proposed in this paper uses a very deep model (it goes down to 90km) but in the scope of this master's thesis there is a focus on small impactors and the effect of small impacts are investigated up to 10 or 12m. For this reason the mantle component will not be used in a model in this master's thesis.

Based on [Egea-Gonzalez et al., 2021], 5 models are elaborated for the InSight landing site based of 3 components :

- Basaltic crust
- Felsic crust
- Megaregolith defined as "a porous, fragmentary layer formed by large com- pact and coherent blocks with regolith material filling the gaps between them" [Egea-Gonzalez et al., 2021].

The first model is composed of a 10m deep basaltic crust. The second model is composed of a 10m deep felsic crust. The third model is composed of a 10m deep Megaregolith layer. And finally Model 4 and 5 are respectively composed of a 6 m deep layer of megaregolith above a 6m deep layer of basaltic crust and of a 6m deep layer of megaregolith on top of 6m deep layer of felsic crust. The five models are showed in Figure 7.2.

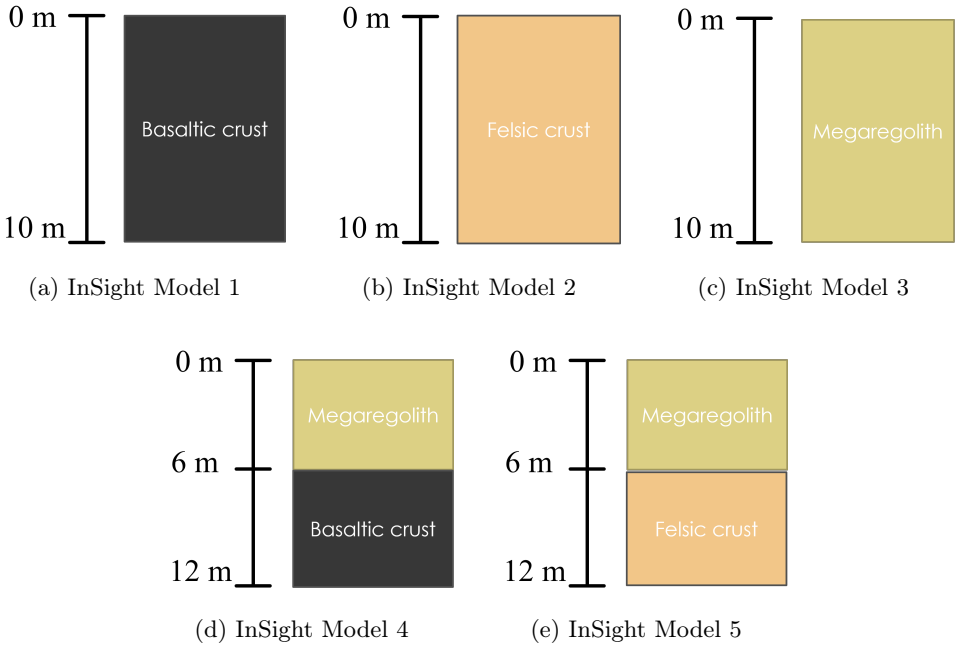

(a) InSight Model 1 (b) InSight Model 2 (c) InSight Model 3

(d) InSight Model 4 (e) InSight Model 5

Figure 7.2: Representation of the 5 models for the InSight landing site.

7.2 Jezero Crater

As a second location is the Jezero crater where Perseverance landed in. It is located at $18.4°N, 77.4°E$. As a Martian mission landing site and like the InSight landing site, several data were collected and are available.

Based on 2 papers [Ahern et al., 2021, Zastrow and Glotch, 2021], several characteristics were exploited to model the Jezero crater. First of all, based on spectral observation, it is known that there is 2 major minerals present in the Jezero crater. The abundance of those 2 minerals, olivine and carbonate, are shown in Figure 7.3. Moreover, three defined zone can be described in the Jezero crater, the marginal Carbonates, the olivine-rich sand and the molted terrain (see Figure 7.4. In detail, [Zastrow and Glotch, 2021] described the 3 zones as following :

- the Marginal Carbonates with high Mg-rich and Fe-rich carbonate and a lack of olivine and serpentine;
- the Mottled Terrain with Fe-rich carbonate and less significant amounts of olivine an serpentine;
- the olivine-rich sands enriched in finely particulate calcite and serpentine.

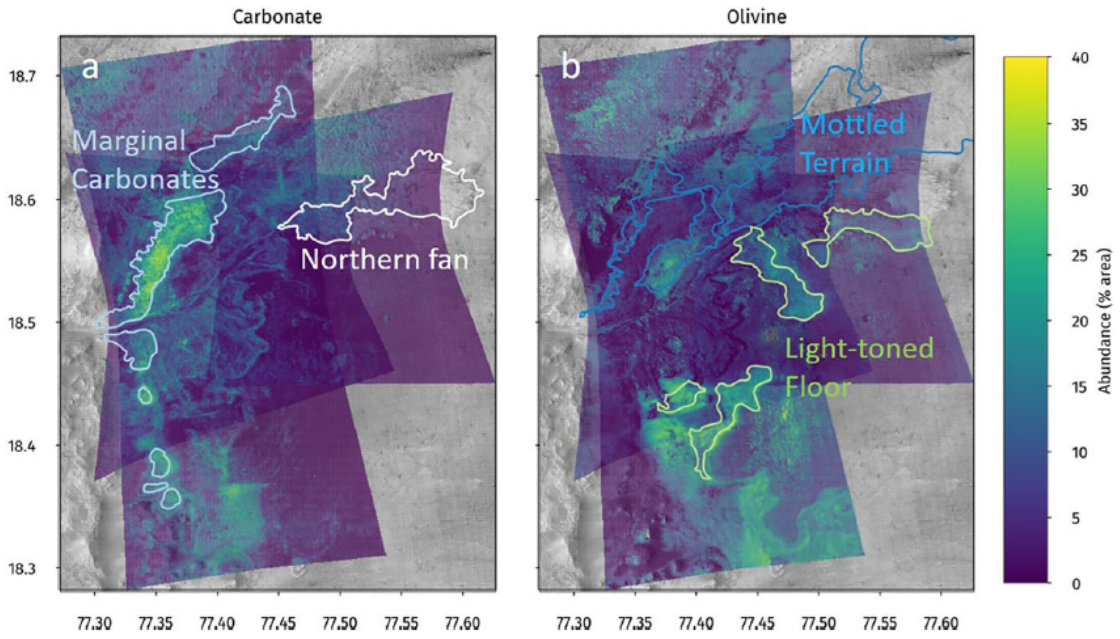

Figure 7.3: Jezero Crater regolith structure with the cumulative abundance maps for (a) carbonate and (b) olivine [Zastrow and Glotch, 2021].

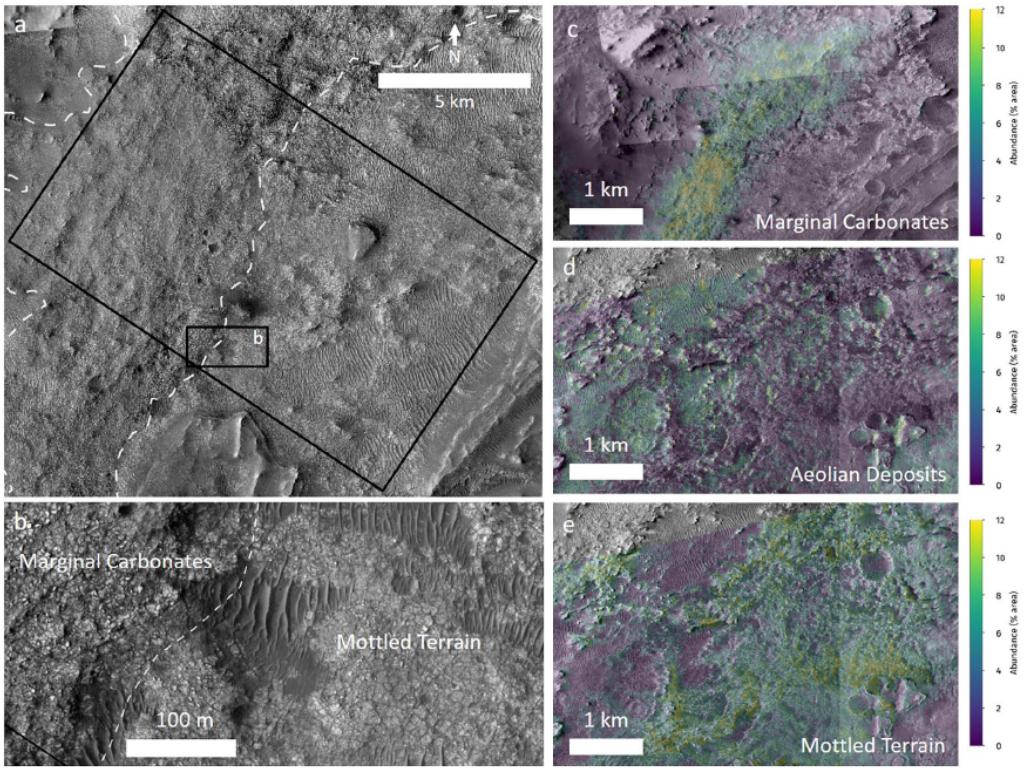

Figure 7.4: Zoom of the Region Of Interest. (b) Zoom to highlight contact between Marginal Carbonates and Mottled Terrain. (c–e) Abundance maps of the three main carbonate units. (c) Marginal Carbonates, (d) olivine-rich sand with calcite abundances overlain, and (e) Mottled Terrain. Base image is the Murray Lab HiRISE mosaic $E77 - 25 - N18 - 5.tif$ [Zastrow and Glotch, 2021].

From the available information of the mineralogy of the Jezero crater, 4 models were built. In addition, a symplifying hypothesis is made in this master's thesis: the carbonate unit are approximated with

the properties of Calcite . The first model is composed of a 10 m deep layer of olivine. The second model is composed of a 6 m deep carbonate (calcite) on top of a 6m deep layer of olivine. The third model is composed of a 10 m deep Carbonate(calcite) layer. And finally Model 4 is composed of a 4 m deep layer of carbonate (calcite) above a 4 m deep layer of serpentine on top of a 4 m deep layer of olivine. The 4 models are showed in Figure 7.5.

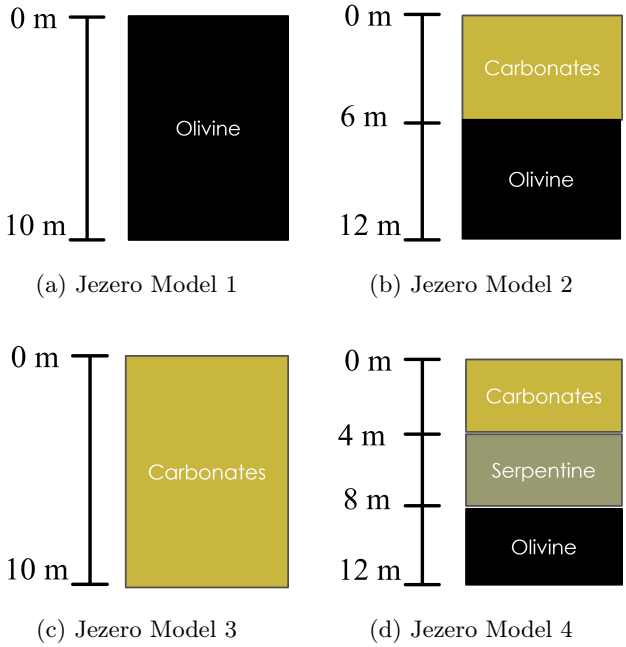

(a) Jezero Model 1 (b) Jezero Model 2

(c) Jezero Model 3 (d) Jezero Model 4

Figure 7.5: Representation of the 4 models for the Jezero crater.

7.3 Oxia Planum

Oxia Planum is located at $17.28°N, 334.29°E$. Oxia planum is an interesting loction because the ExoMars 2022 mission is planned to land there. Therefore, information will be collected and the landing site was well studied to prepare the incoming mission.

For Oxia Planum, models were build based on 2 papers [Formisano et al., 2021, Gary-Bicas and Rogers, 2021]. The first one, [Formisano et al., 2021], brings a different method and result than the other one. It builds a thermophysical model of Oxia Planum via a numerical model. A thermal conductivity of $0.045 W m^{-1} K^{-1}$ was obtained as a result for a dust/unconsolidated regolith present on the Oxia planum surface. This value is smaller than the one used for megaregoltih ($0.8 W m^{-1} K^{-1}$) or than the one used for basaltic crust ($2 W m^{-1} K^{-1}$). For this reason three models were built.

The first one is purely based on [Formisano et al., 2021] with a 10m deep layer of unconsolidated particles with a thermal conductivity of $0.045 W m^{-1} K^{-1}$. The rest of the properties (heat capacity, density, adiabatic bulk modulus at zero pressure and the pressure derivative of the bulk modulus) are unknown for the unconsolidated particles and thus the simplifying hyposthesis that those are similar than the properties of megaregolith from [Egea-Gonzalez et al., 2021] is made.

The second model is based of a 6m deep layer of megaregolith (with a thermal conductivity of $0.8 W m^{-1} K^{-1}$) from [Egea-Gonzalez et al., 2021] below a 6m deep layer of the dust/unconsolidated regolith from [Formisano et al., 2021]. And finally the third model is a 10m deep layer of megaregoltih (with a thermal conductivity of $0.8 W m^{-1} K^{-1}$). The three models are shown in Figure 7.6.

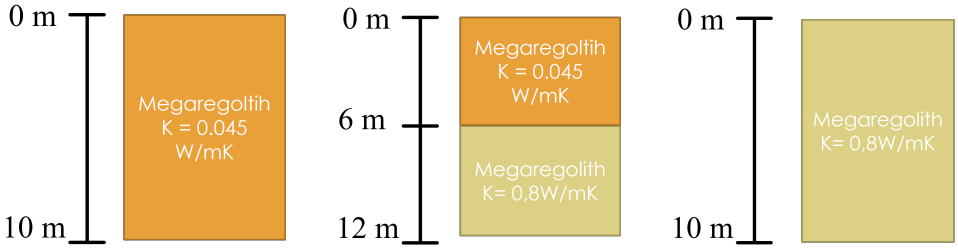

(a) Oxia Planum Model 1 (b) Oxia Planum Model 2 (c) Oxia Planum Model 3

Figure 7.6: Representation of the 3 models for Oxia Planum.

The second paper , [Gary-Bicas and Rogers, 2021] gives more information about the mineralogy of Oxia planum. As shown in Figure 7.7 and Figure 7.8, the ExoMars 2022 landing site is composed of several different "Units". Each unit is discrimined due to varying spectral, thermophysical, and textural properties thanks to combined Thermal Emission Imaging System (THEMIS) data (THEMSI is a thermal camera on board the 2001 Mars Odyssey orbiter) and Context Camera (CTX) imagery (camera on board the Mars Reconnaissance Orbiter (MRO)).

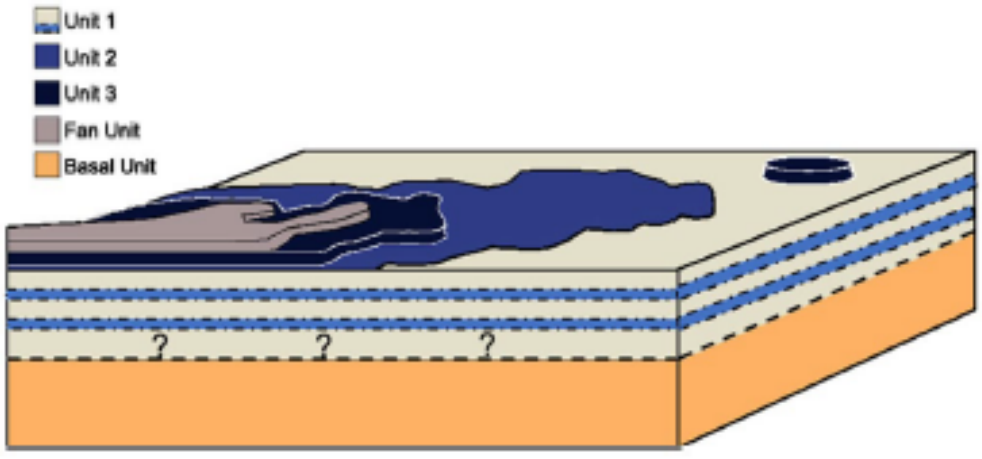

Figure 7.7: 3D stratigraphic model depicting different units found in Oxia Planum, looking south. At the very bottom is the basal unit or native bedrock for the region (not observed). It is overlain by a succession of light toned material with dark-toned layers, mapped together as Unit 1. The dark-toned layers may be the same material as Unit 2 but the relationship is uncertain. Depth of transition from basal unit to Unit 1 material is unknown (dashed line and question marks). At the top right, we depict an example of inverted craters found on Unit 1 infilled with Unit 3 material. At the bottom left corner of the model the stratigraphic relationship between units where the Fan unit overlies Unit 3, and Unit 3 overlies Units 1 and 2 is depicted [Gary-Bicas and Rogers, 2021].

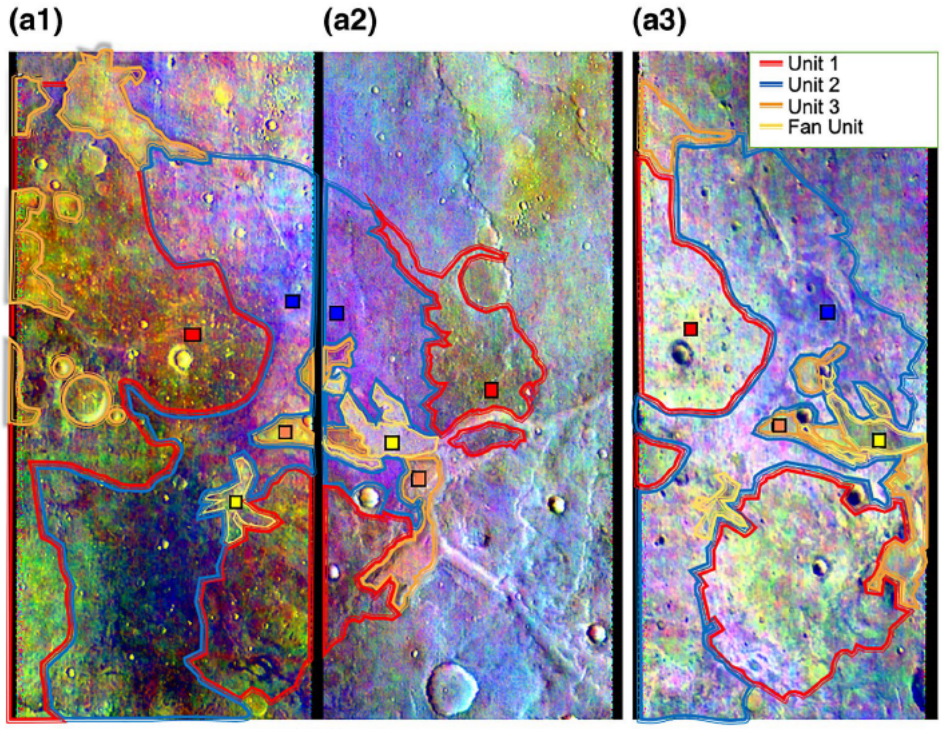

Figure 7.8: Regolith structure of the ExoMars 2022 landing site [Gary-Bicas and Rogers, 2021].

The first unit, Unit 1, is consistent with Mg-smectite clays, Unit 2 exhibits a stronger mafic signature and will be associated to Olivine. Unit 3 shows weak 1.9 and 2.3μm absorptions consistent with phyllosilicates therefore, it will be associated to kaolinite. And finally , the fan Unit, is spectrally similar to Units 1 and 3 in THEMIS data, but likely covered with unconsolidated materials. For this master's thesis and because no information were found for the properties of the unconsolidated materials, the simplifying hypothesis that the fan unit can be approximated with the megaregolith properties from [Egea-Gonzalez et al., 2021] was made.

Following the stratigraphic model of Oxia Planum (see Figure 7.7), 4 models were built. The first one is a 6m deep layer of olivine on top of a 6m deep layer of smectite. The second one is a 3m deep layer of olivine on top of a 3m deep layer of smectite which itself is on top of a 3m layer deep olivine with a 3m layer deep smectite at the base of the model. The third model is a 4m deep layer of kaolinte on top of a 4m deep layer of olivine with a 4m deep layer of smectite at the base of the model. Finally the last model is a a 3m deep layer of non-consolidated regolith on top of a 3m deep layer of kaolinite which itself is on top of a 3m layer deep olivine with a 3m layer deep smectite at the base of the model. These models are represented in Figure 7.9.

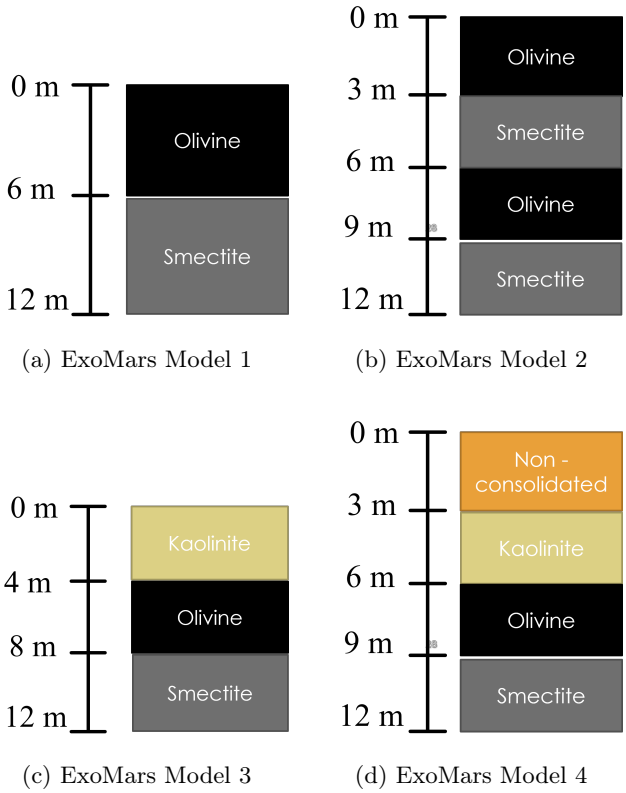

(a) ExoMars Model 1 (b) ExoMars Model 2

(c) ExoMars Model 3 (d) ExoMars Model 4

Figure 7.9: Representation of the 4 models for the ExoMars 2022 landing site.

7.4 Phoenix landing site

The Phoenix landing site , also a location where a Martian mission is occuring has another interesting feature. Located in the Northern Hemisphere, $68.21°N, 234.24°E$, it was shown that at this latitude the ice water table was very close to the surface and that there is a seasonal frost on the surface (on top of the regolith) and in the near-subsurfacen while the permanent ice table ($\approx 70\%$ volume fraction in pore spaces) is just a fex cm deep [Sizemore and Mellon, 2006, Putzig et al., 2014]. Moreover, at this latitude, it was shown that there are accumulation of carbonates[Ehlmann and Edwards, 2014]. Also, [Mellon et al., 2009] showed that the ice table was shallower at high latitude and deeper at lower latitude and that a the Phoenix landing site the ice table was present under a mean depth of 4.6 cm. From these collected data, 4 models were built for the Phoenix landing site.

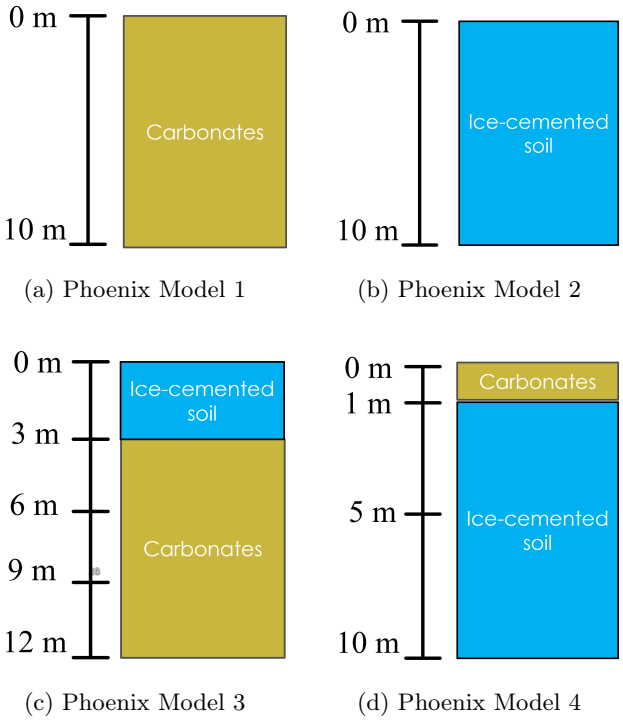

(a) Phoenix Model 1 (b) Phoenix Model 2

(c) Phoenix Model 3 (d) Phoenix Model 4

Figure 7.10: Representation of the 4 models for the Phoenix landing site.

The first model is composed of a 10m deep layer of Carbonate (Calcite). The second model is composed of a 10m deep layer of ice-cemented soil (characteristics from [Sizemore and Mellon, 2006]). The third model is composed of a 3m deep layer of ice-cemented soil on top of a 9m deep layer of Carbonates (Calcite). The last model, is composed of a 1m deep layer of Carbonate (Calcite) on top of a 9m deep layer of ice-cemented soil. The 4 models are shown in Figure 7.10.

7.5 Gale crater

The Gale crater located at $4.5°S, 137.4°E$, it is the landing location for the Curisity Rover. As a landing site, several datas are available but there is also a feature of interest : methane has been detected in the atmosphere at this location [Webster et al., 2015].

Methane detection sites are relevant for this master's thesis because it investigates the possible destabilization of methane clathrate by small impactors and thus the possible release of methane in the atmosphere caused by impacts. Thi is why it is important to know the depth of the methane clathrate at those sites.

From [Crumpler, 2021], it is known that at the Gale crater, there are at least 3 layers of different minerals. On top there is a layer of sulfate, with a layer of phyllosilicate in the middle and a layer of hematite beneath it. For this master's thesis, 2 simplifying hypotheses are made and are needed. First that the sulfate can be approximated with the properties of Gypsum (a mineral part of the sulfate family) and then that the phyllosilicate can be approximated with the properties of smectite (a mineral part of the phyllosilicate family). One model is then obtained for the Phoenix landing site: a 4m deep layer of gypsum on top of a 4m deep layer of smectite with a 4m deep layer of hematite at the base of

the model. This model is shown in Figure 7.11.

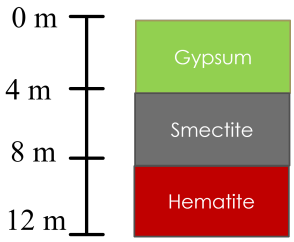

(a) Gale Crater Model 1

Figure 7.11: Representation of the model for Gale Crater.

7.6 Other methane detection site

In addition to Gale crater, three other locations were investigated due to the detection of methane in the atmosphere :

- Terra Sabae located at $2°N, 42°E$
- Nili Fossae located at $22°N, 75°E$
- Syrtis major located at $8.4°N, 69.5°E$

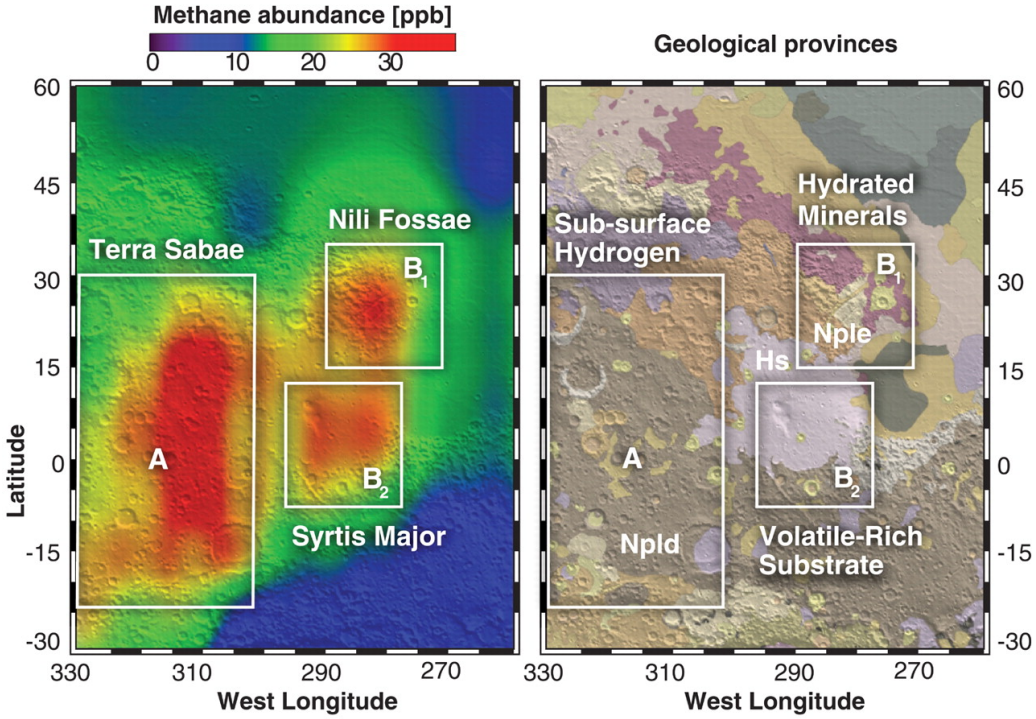

Figure 7.12: Syrtis major, Terra Sabae and Nili fossae location and methane detection [Mumma et al., 2009].

For Terra Sabae, no information about the mineralogy of this site was found. Thus the assumption was made that it was composed of only basalt following that basaltic crust is globally present on Mars

[Ehlmann and Edwards, 2014].

In function of the papers ([Egea-Gonzalez et al., 2021, Goossens et al., 2017, Joiret, 2020], several density of basalt can be found (see subsection 7.8). Two models were built to see the difference when pure basalt with a density of $2600 kgm^{-3}$ was used and when the porosity of 23% was taken in account. The density of porous basalt is $2000 kgm^{-3}$.

For Nili Fossae, one model was built from the information given in [Mangold et al., 2007]. The simplifying assumption was made that the clay present in Nili Fossae could be approximated with smectite as smectite is a minera part of the phyllosilicate family. Indeed the model is composed of a 10m deep layer of smectite.

For Syrtis Major, one model was built from the information given in [Ehlmann and Edwards, 2014]. Indeed the model is composed of a 10m deep layer of olivine.

The four models are shown in Figure 7.13.

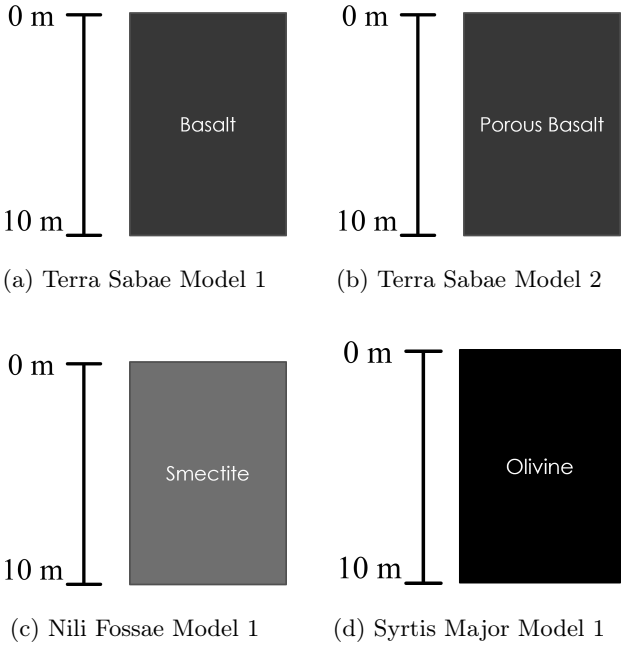

(a) Terra Sabae Model 1 (b) Terra Sabae Model 2

(c) Nili Fossae Model 1 (d) Syrtis Major Model 1

Figure 7.13: Representation of the 4 models for the other methane detection site.

Based on the Martian mineralogy (see 6 and on the diferrent models created for specific location of interest on Mars (see 7) , several parameters for specific minerals found on Mars were gathered and resumed in table 7.2.

Table 7.2: Parameters of several potential components of the Martian regolith

	C	ρ	**K0**	**n**	**k**
	Heat Capacity ($Jkg^{-1}K^{-1}$)	Density (kgm^{-3})	adiabatic bulk modulus at zero pressure (GPa)	pressure derivative [5] of the bulk modulus (unitless)	thermal conductivity at 250°C ($Wm^{-1}K^{-1}$)
Basalt	800[5]	2900[13]	19.3[7]	5.5[8]	2[9]
Olivine	600[5]	3222[6]	129[7]	4.5[8]	4[9]
Gypsum	900[5]	2317[6]	42[7]	3.3[8]	4[9]
Calcite	500 -620[5]	2711[6]	73.3[7]	5.7[8]	3[9]
Smectite	650[5]	2200[7]	70[7]	5.5[8]	0.8[9]
Kaolinite	650[5]	2669[5]	71.1[7]	5.5[8]	2.5[10]
Hematite	510[5]	5000[6]	161[7]	5.6[8]	6[11]
Serpentine	1000[5]	2600[6]	61[7]	4.1[8]	2.7[12]

7.7 Thermal conductivity

The thermal conductivity k in $Wm^{-1}K^{-1}$ is the ability of a regolith to conduct heat. k depends on :

- The conductivity of the solid
- The soil conductivity at the contact between grains
- Radiative heat transfer between grains through pores
- Interstitial gas conductivity (k_{gas})

Figure 7.14 shows the reprensetation of the thermal conductivity between two grains.

If the grains are ine a vacuum, the only contributing factors to the thermal conductivity is from the solid part and from the radiative transfer. To be noted, the radiative transfer is only dependant of the temperature and the grain size [Piqueux and Christensen, 2009, Watson, 1964].

As seen in the Figure 7.15, the case of the thermal conductivity on Mars is in the transitional regime and is thus dependant to grain size. For this master's thesis, the simplifying assumption that the thermal conductivity stays constant for a material with the evolution of temperature, porosity, grain size, etc. Thus, the variation of thermal conductivity for a material will not be taken in account in the analytical model

[5] From [Vu et al., 2019]
[6] From [Drozdovskiy et al., 2020]
[7] From [Hofmeister, 2019]
[8] From [Hofmeister, 1991]
[9] From [Cermak and Rybach, 1982]
[10] From [Michot et al., 2008]
[11] From [Mo/lgaard and Smeltzer, 1971]
[12] From [Osako et al., 2010]
[13] See part 7.8

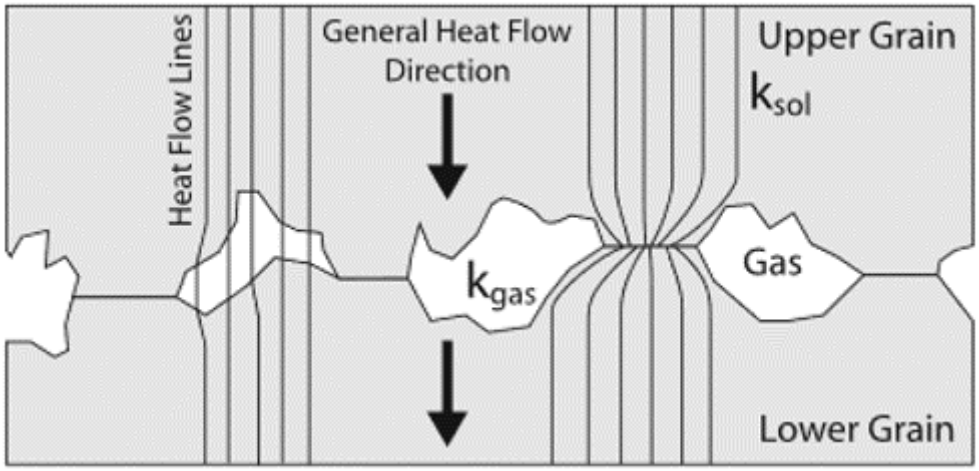

Figure 7.14: Shematic representation of a contact between two grains with k_{sol} the conductivity of the grains and k_{gas} for the conductivity of the gas [Piqueux and Christensen, 2009].

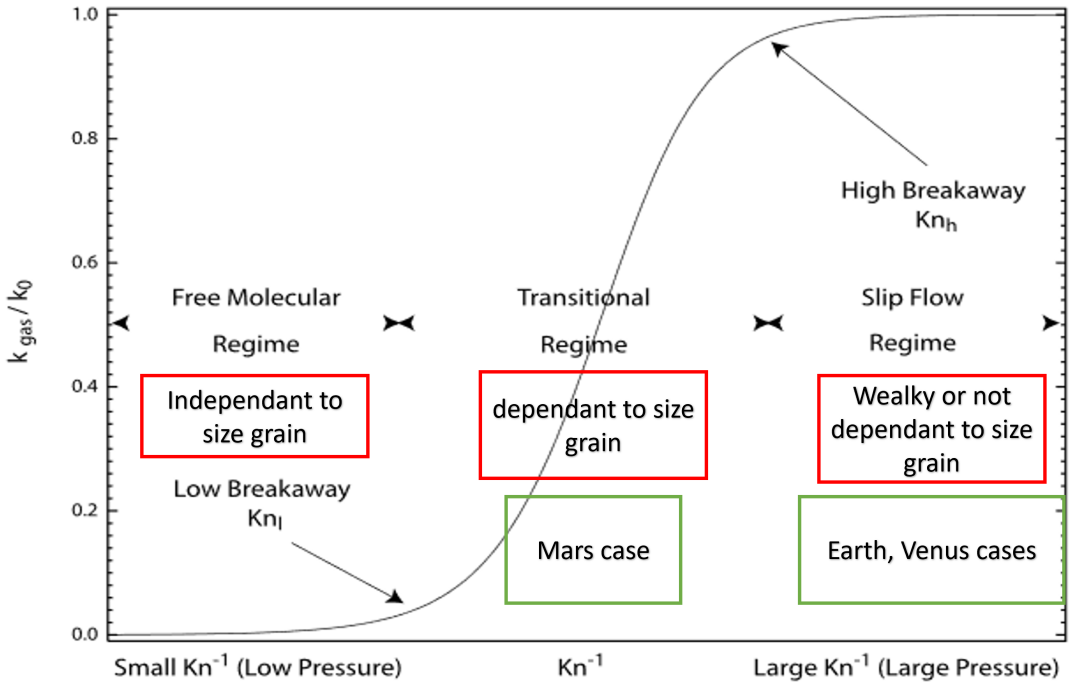

Figure 7.15: Normalized gas thermal conductivity in function of the pressure and temperature with the pressure expressedwith the Knudsen number. [Piqueux and Christensen, 2009].

7.8 Porosity

The porosity of the regolith is an important parameter as it plays a crucial role for the density but also for the thermal conductivity which are needed to run the model. For example, basalt is known to have a density around 3000 kgm^{-3} [Drozdovskiy et al., 2020] but as previously explained for some models a density of 2900 kgm^{-3} was picked for the InSight model for the basaltic crust [Egea-Gonzalez et al., 2021] and a density of 2600 kgm^{-3} was picked for the basalt used in [Joiret, 2020].

The discrimination has to be made between the basalt at 2900 kgm^{-3} and the basalt assumed in the crust with 2600 kgm^{-3} or 2000 kgm^{-3} if a porosity of 23% is taken in account. Based on [Goossens et al., 2017], the low average bulk crustal density for Mars is equal to $2582 \pm 209 kgm^{-3}$. Moreover, the crustal density has large lateral variations. For this master's thesis the density of the basalt will vary in function of the papers based for the model and thus in function of the locations. Thus, the variation of porosity for a material will not be taken in account in the analytical model

7.9 Regolith Structure

The structure of the regolith suggested for the specific locations are purely theoretical. Indeed some of them may not be stable with the assumed parameters (see Table 7.2). About the density, it is known that the density increases with the depth and that this increases of density in function with the depth is needed to have a stable regolith [Revil et al., 2002, Marfil et al., 1996]. However in certain models, a layer with high density is on top of a layer with lower density. The increase of the density with the depth and the stability of the regolith were not taken in account in the analytical model.

As presented in Section 6, there is a global coverage of reddish dust. Moreover several papers [Formisano et al., 2021, Gary-Bicas and Rogers, 2021] included the presence of a thin layer of unconsolidated regolith. More information are needed about its properties, coverage and thickness but one may assume a surface layer of dust/unconsolidated regolith. For this master's thesis, when this surface layer was not mentionned , it was assumed that this layer was not present or may be negligible.

8 Modeling the Martian subsurface temperature

8.1 Modeling the increase of temperature following an impact

To model the increase of temperature of a surface after the impact of a meteorite two methods are available :

1. The analytical method
2. The numerical method (more precisely, the simulation using a hydrocode[6], which is the iSALE-2D shock physics code [Amsden et al., 1980, Collins et al., 2004, Wünnemann et al., 2006].

The last-mentioned method might be more accurate to model large impacts for the reason that it takes into account the displacement of material away from the center as well as the strength and porosity of material. Nevertheless this master's thesis concentrate on small impacts and thus the displacement of material is less important than for big impactors. The small impactors commonly create craters of about few tens or possibly a few hundreds of meters in diameter [Melosh, 1989]. Hence analytical models are then good approximations.

Two analytical models are investigated here. The first one the Gault-Heitowit model [Abramov, 2006], expresses that the energy loss per kilogram of the target is given by :

$$\Delta E = \frac{1}{2}u^2\{1 - 2[\xi - \xi^2 \ln(1 + \frac{1}{\xi})]\} \tag{8.1.1}$$

where

$$\xi = \frac{C}{Su} \tag{8.1.2}$$

C and S are constants whose value depend on the surface composition. C=2600 m/s and S=1.62 considering a basaltic crust [Melosh, 1989]. And

$$u = \frac{v}{2}(\frac{R_p}{r})^{1.87} \tag{8.1.3}$$

with :

- v : the impactor velocity in m/s.
- R_p : the radius of the impactor in m
- r the distance from the center of impact in m

By dividing ΔE by the heat capacity the increase of temperature is obtained.

The second method is based on the Murnaghan equation of state. Here the energy loss per kilogram

[6] A hydrocode is a computer code for modeling fluid flow at all speeds. Hydrocodes can also be used to fine-tune analytical models [Pierazzo and Collins, 2004].

of the target - also called specific waste heat - is stated as :

$$\Delta E = \frac{1}{2}[PV_0 - \frac{2K_0V_0}{n}][1 - (\frac{Pn}{K_0} + 1)^{-\frac{1}{n}}] + \frac{K_0V_0}{n(1-n)}[1 - (\frac{Pn}{K_0} + 1)^{1-\frac{1}{n}}] \tag{8.1.4}$$

where :

- V_0 is the specific uncompressed volume ($V_0 = \frac{1}{\rho_0}$)
- ρ_0 the density
- K_0 : the adiabatic bulk modulus at zero pressure
- n : the pressure derivative of the bulk modulus
- P : the peak shock pressure, which follows the following power law:

$$P = A(\frac{r}{R_p})^{-k} \tag{8.1.5}$$

with :

- R_p : the radius of the projectile in m
- r : the distance from the impact center in m
- k : the decay exponent
- A : the pressure at $r = R_p$ in Pa

A is calculated on [51] :

$$A = \rho[C + Su0]u0 \tag{8.1.6}$$

and depends on the target and impactor properties. with :

- $C = 2600$ m/s
- $S = 1.62$ for basalt
- u_0 : the particle velocity behind the shock wave in m/s.

It is shown that in the case of a planar approximation and when the target density is roughly the same as the impactor density, $u_0 = \frac{v}{2}$ with v, the impact velocity. From that it is possible to approximate A on the order of

$$A = \frac{\rho v^2}{4} \tag{8.1.7}$$

with

- ρ the target and impactor density (approximated to $2600 kg/m^3$ for basaltic crust hitted by a rocky asteroid).

Still, the expression of the specific waste heat ΔE needs to be divided by the heat capacity (= $800 Jkg^{-1}K^{-1}$ for basalt) to obtain the increase of temperature. The two unknowns are the impactor velocity and radius for both models. [Pierazzo and Melosh, 2000] have shown that most impactors hit the surface with an impact angle of 45°. Thus, the impactor velocity (v) consistently needs to be

multiplied by sin(45°) in the expressions 8.1.7. About the projectile radius it can be determined from the crater diameter [Ivanov, 2001]. Indeed, the transient crater diameter can be expressed as

$$D_{tc} = 1.16(\frac{\delta}{\rho})^{1/3} D_P^{1.78} (v \times sin\alpha)^{0.43} g^{0.22} \tag{8.1.8}$$

with

- ∂/ρ : ratio of densities between target and projectile (≈ 1 for a rocky asteroid striking a basaltic crust)
- v : the impactor velocity in m/s
- α : the impact angle in degrees
- g : the acceleration of gravity on Mars ($\approx 3.721 m/s^2$)
- D_p : projectile diameter in m
- $D_{tc} = \frac{D_{tr}}{1.2}$ the rim-to-rim diameter of the transient crater in m and can be obtained from [Schwenzer et al., 2012]

$$D = 0.91 \frac{D_{tr}^{1.125}}{D_Q^{0.09}} \tag{8.1.9}$$

with

- D : the rim-to-rim diameter of the final crater
- D_Q : the simple-to-complex transition diameter. It is estimated to 8400 m for Mars.

As an illustration for small impactors, the rim-to-rim diameter of the final crater (D) of 100 m corresponds to a rim-to-rim diameter of the transient crater (D_{tr}) of 134.3 m and a transient crater diameter (D_{tc}) of 111.9 m. This leads to a projectile diameter of 3.42 m (radius of 1.71 m) if this impactor is hitting the surface of Mars with a velocity of 10 km/s and an impact angle of 45°C.

Temperature following the impact

For this section, several parameters will be used to model the temperature following an impact on Mars. Based on [Joiret, 2020], the analytical method used in this master's thesis is the Murnaghan equation of state (see 8.1.4). Indeed, it is easier to take in account the different composition of the Martian regolith with the Murnaghan equation of state than with the Gault-Heitowit.

Still based on [Joiret, 2020] and because this master's thesis focus on studying the effects of regolith heterogeinity the impactor radius will be fixed at 1.7m and the impactor will have a velocity of $10 km/s$. It will hit the surface with an angle of 45° and the decay exponent k (see 8.1.5) will be fixed at -1.025. Indeed, it is more suited to consider only one of the cases developped in [Joiret, 2020] to better understand the effect of regolith heterogeinity. Those parameters are resumed in table 8.1.

Table 8.1: Impact parameters considered for the following results

Impact parameter	
Impactor radius	1.7m
Impact velocity	10 km/s
Impact angle	45°
Decay exponent	-1.025

Figure 8.1 shows the increase of temperature for an impactor of a 1.7m radius which corresponds to a crater of 100m of diameter on a Basaltic surface.

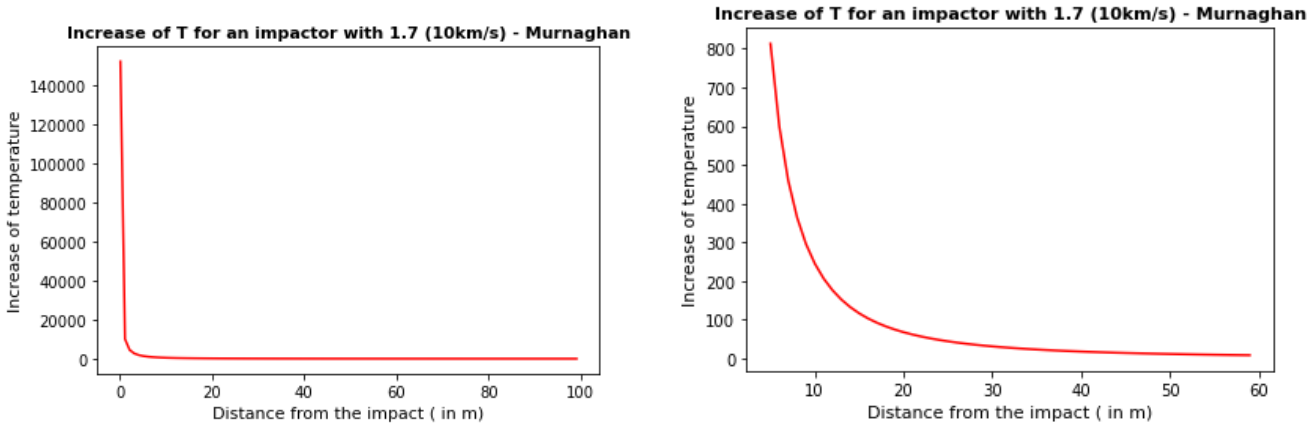

(a) Starting at the center of the crater

(b) starting at a distance of 5 meters from the impact

Figure 8.1: Temperature after an Impact of a 1,7 m radidus impactor with a velocity of 10 km/s and with an angle of 45° on surface composed of Basalt.

Figure 8.2 displays the increase of temperature and the shock pressure. To have a better visualization of the depths at which these increases of temperature occur, a third plot shows the increase of temperature between 0 and 500 °.

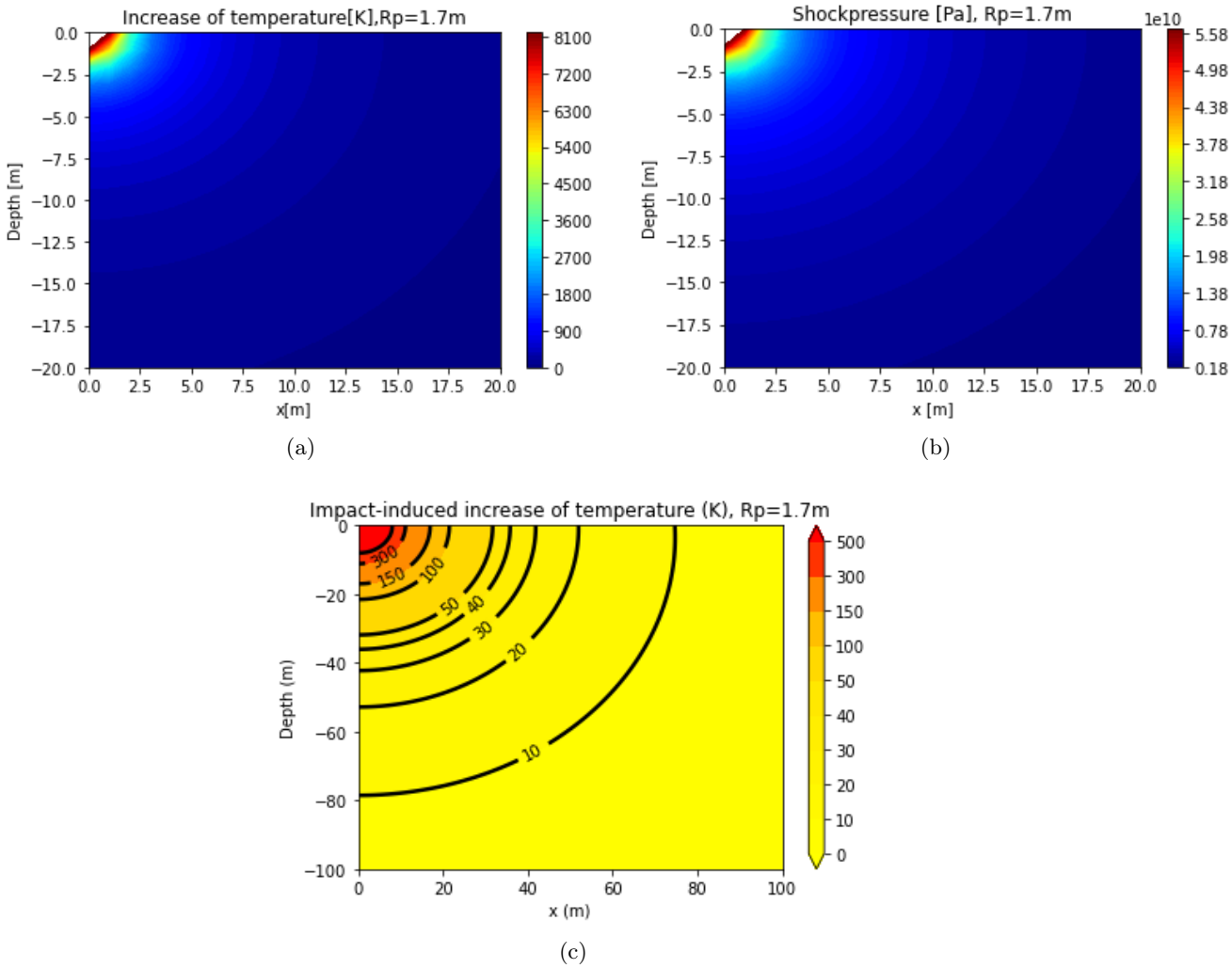

(a) (b) (c)

Figure 8.2: Temperature after an Impact of a 1,7 m radius impactor with a velocity of 10 km/s and with an angle of 45° on a basaltic regolith.

The graphs for the other type of minerals are similar but with some variation of their results according to the difference in their properties.

Comparison between the Analytical method and the Hydrocode method

First of all, it must be noted that for the comparison between the iSALE-2D hydrocode and the analytical method, an angle of 90°was considered. This is the reason why the results in Figure 8.3 are bigger than the one in Figure 8.2. Moreover, the comparison was made for a basaltic crust with a density of 2600 kgm^{-3}. Then, in the analytical method, the peak shock (see equation 8.1.5) is calculated by dividing r, the distance from the impact center, by R_p the radius of the impactor. Thus at the center of the crater, $r = 0$ and the analytical solution goes up to ∞. So one must treat carefully the results for the first meters near the impact.

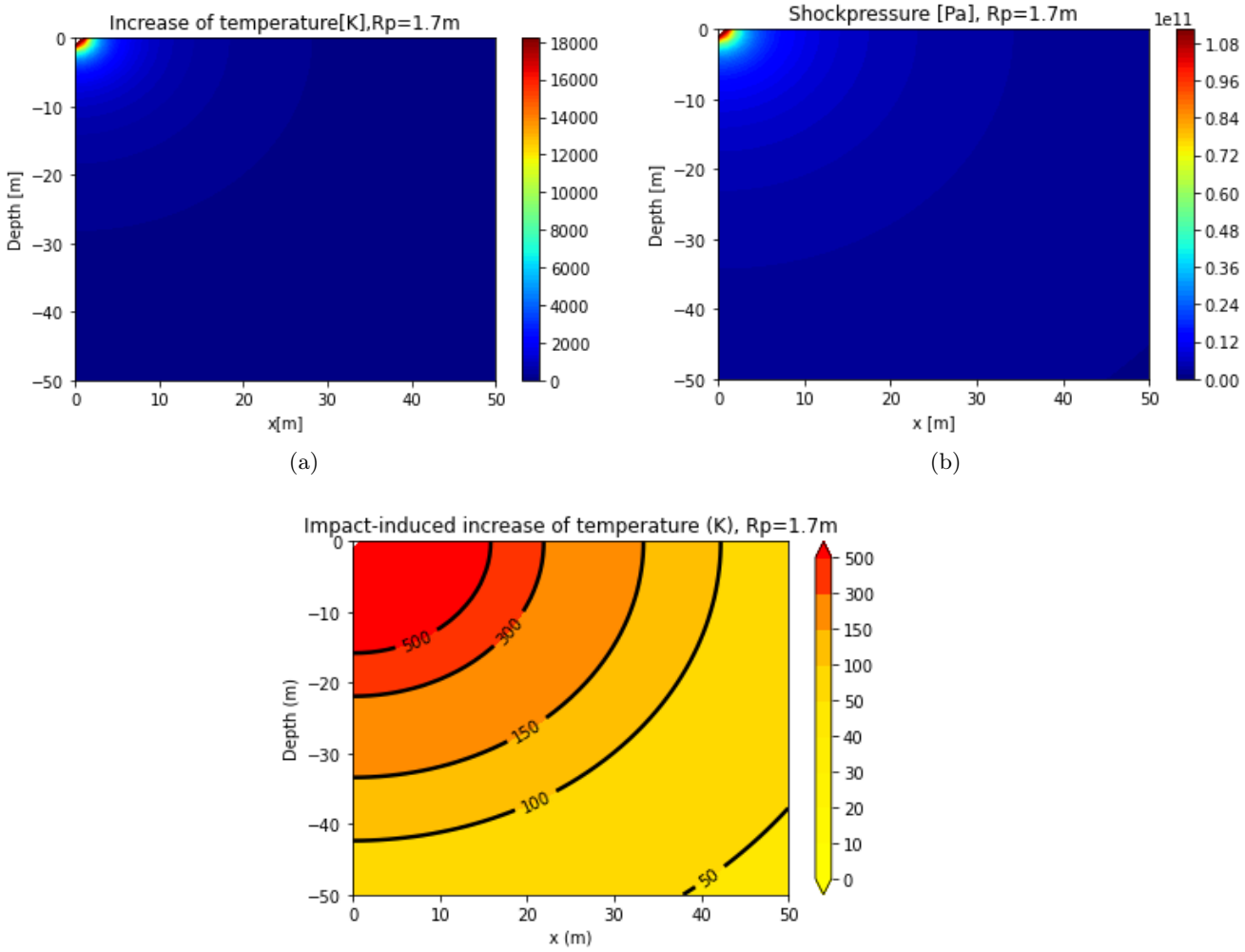

(a) (b)

(c)

Figure 8.3: Temperature after an impact of a 1,7 m radius impactor with a velocity of 10 km/s and with an angle of 90° on a basaltic regolith.

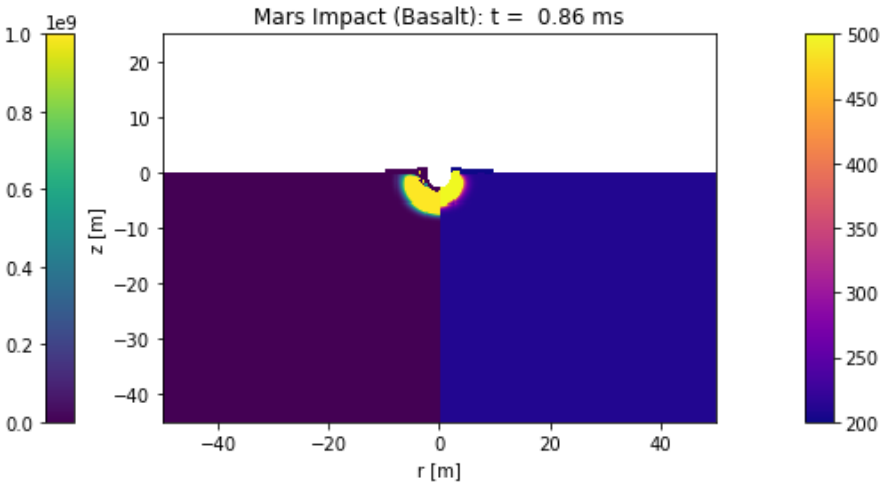

Figure 8.4: Temperature and shock pressure after 0.86s after an impact of a 1,7 m radius impactor with a velocity of 10 km/s and with an angle of 90° on a basaltic regolith. Credits: Cem Berk Senel iSALE-2D hydrocode

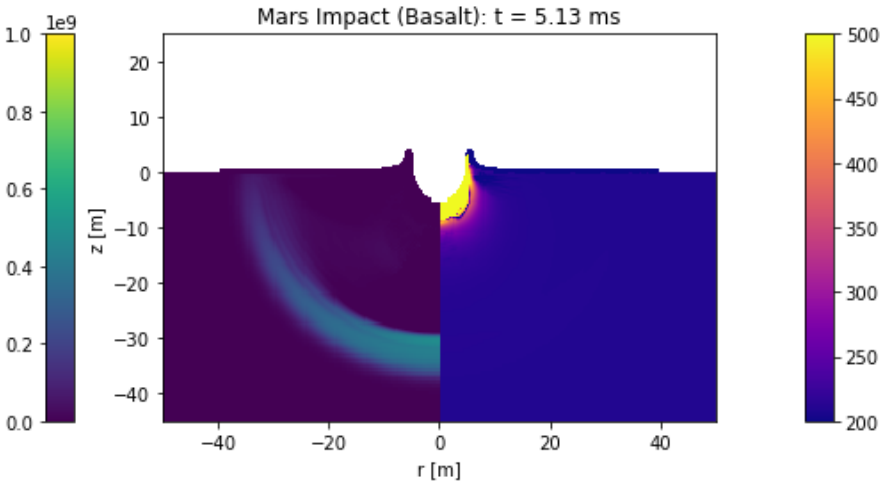

Figure 8.5: Temperature and shock pressure after 5.13s after an impact of a 1,7 m radius impactor with a velocity of 10 km/s and with an angle of 90° on a basaltic regolith. Credits: Cem Berk Senel iSALE-2D hydrocode

Table 8.2: Values of temperature from 1m to 15 of the impact center. Due to the displacement of material, the first few meters are not available for the hydrocode at 5.13ms from the impact. The temperature from the analytical method is an increase of temperature and thus the initial temperature must be added. The initial temperature was chosen as the initial temperature for the iSALE-2D hydrocode.

Distance in m from the impact center	**Temperature from hydrocode at 0.86ms**	**Temperature from hydrocode at 5.13ms**	**Increase of Temperature from analytical method**	**Temperature if Tinit = 211K**
1	3041	/	18025	18236
2	2709	/	7996	8206
3	2144	/	4874	5085
4	1578	/	3392	3603
5	1029	1801	2541	2752
6	427	1493	1996	2207
7	289	1490	1620	1831
8	243	1482	1348	1559
9	224	1462	1143	1354
10	215	1379	984	1005
11	211	1243	857	1068
12	210	1020	755	966
13	210	796	671	882
14	210	460	600	811
15	210	470	541	752
Distance till 211K	11m	70 m	100+	100+

Table 8.3: Values of Pressure from the analytical method and the hydrode. Due to the displacement of material, the first few meters are not available for the hydrocode at 5.13ms from the impact.

distance in m from the impact center	**Pressure from hydrocode at 0.86ms (GPa)**	**Pressure from hydrocode at 5.13ms (Pa)**	**Pressure from analytical method (GPa)**
1	18.07	/	112
2	16.99	/	55.0
3	20.21	/	36.3
4	16.77	/	27.0
5	9.66	/	21.5
6	6.87	37186.6	17.8
7	5.57	0.49	15.2
8	3.21	0.39	13.3
9	1.71	0.14	11.8
10	0.92	0.065	10.5
11	0.42	0.0026	9.6
12	0.15	3.84e-07	8.8
13	0.05	3.91e-12	8.1
14	0.01	-12500	7.5
15	0.003	-12500	6.9

The main goal of the analytical method is to model the evolution of post-impact temperature. Between both methods (analytical method and hydrocode at 5.13ms after the impact) with the addition of an initial temperature (as the data from the analytical methods are only an increase of temperature due to the impact), the values are close through the depths between 8 and 13m, as can be seen in Table 8.2.

For the pressure, both methods have close order of magnitudes between the depths of 3 and 5m, whereas the difference increases through deeper sublayers as seen in Table 8.3. This is due to the fact that the analytical method is very simplistic and does not take into account the material strength and porosity as well as as the displacement of material after the impact. It is worth noting that the column with the pressure from the hydrocode at 5.13ms is not comparable because the shock wave is already propagated from the cratering area through the deeper sublayers, in which very low pressure remains.

The first few meters are hard to compare as on one hand, the hydrocode values may be missing due to the displacement of material. And on the other hand, the analytical method has a bias for the first few meters.

Finally, even if the values may differ in the first few meters and in the last meters (where wave of temperature did not propagate enough for the hydrocode values) the temperature values are in the same ordre of magnitude for both methods.

8.2 Solving the heat equation for the Martian subsurface temperatures

The first step to solve the equation is to discretize both spatial and temporal coordinates on a grid. An equally spaced mesh points with 24 hours × 3698.96 s time-steps, which is the duration in seconds of a Martian solar day (sol[7]) and 10 × 10 m spatial-steps were first applied.

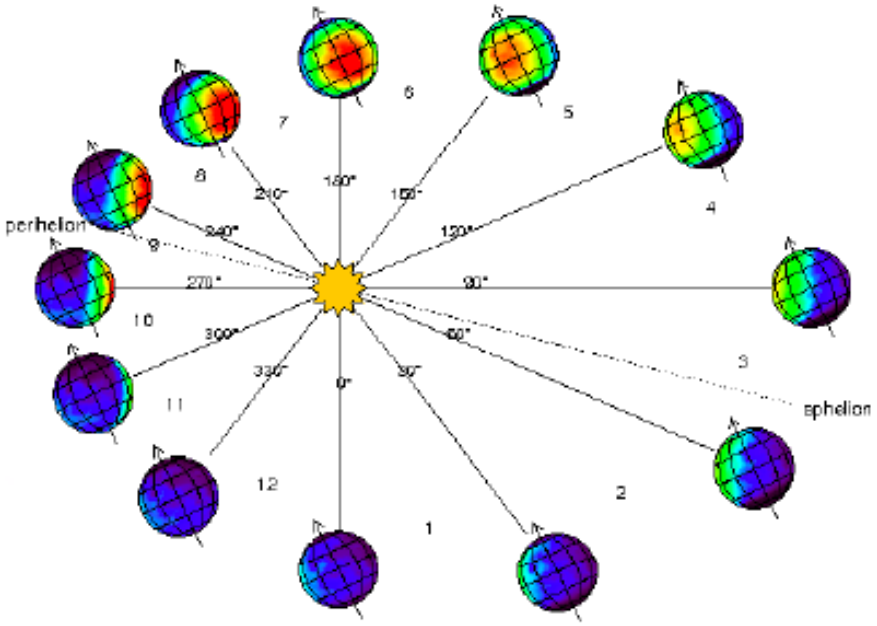

Figure 8.6: The solar longitude Ls is the Mars-Sun angle, measured from the Northern Hemisphere spring equinox where $Ls = 0°$. $Ls = 90°$ corresponds to northern summer solstice, $Ls = 180°$marks the northern autumn equinox and $Ls = 270°$ is the northern winter solstice. Credits: Mars Climate Database.

Once the modelisation of the temperature after an impact is done, the following step is to model the evolution of the Martian subsurface temperature over time. For that the heat equation must be solved using a numerical method. The Crank-Nicolson method was selected, since its solution is independent from the time or spatial step.

The heat equation is given by:

$$\rho c \frac{\partial T}{\partial t} = \frac{\partial}{\partial z}(k \frac{\partial T}{\partial z}) + \rho H \tag{8.2.1}$$

with

$$k \frac{\partial T}{\partial z} = F \tag{8.2.2}$$

where

- ρ : the density in kg/m^3
- c : the specific heat capacity in $Jkg^{-1}K^{-1}$

[7]A sol lasts for 24 Martian hours which is equal to 24h39 terrestrial hours.A year lasts 12 Martian months (669 sols or 687 terrestrial days). The largest month on Mars lasts 66.7 sols at the aphelion and the shortest month lasts 46.1 sols at the perihelion.

- T : the temperature in K
- t : the time in s
- z : the depth in me eu
- k : the thermal conductivity in $Wm^{-1}K^{)1}$
- H : the radiogenic heat production in Wkg^{-1}
- F : the heat flux in Wm^{-2}

The thermal conductivity depends on the type of minerals present in the regolith but also of the respective volume fractions of soil and igneous rock. For each type of minerals a fixed thermal conductivity will be used (see 7.2).
The heat flux is varying accros all longitude and latitute. As seen in figure 8.7, the variation ranges from $0.014W/m^2$ to $0.025W/m^2$. The average radiogenic heat production (H) is predicted to be equal to $5 * 10^{-11}$ but at shallow depths it could be neglected [Hahn et al., 2011].

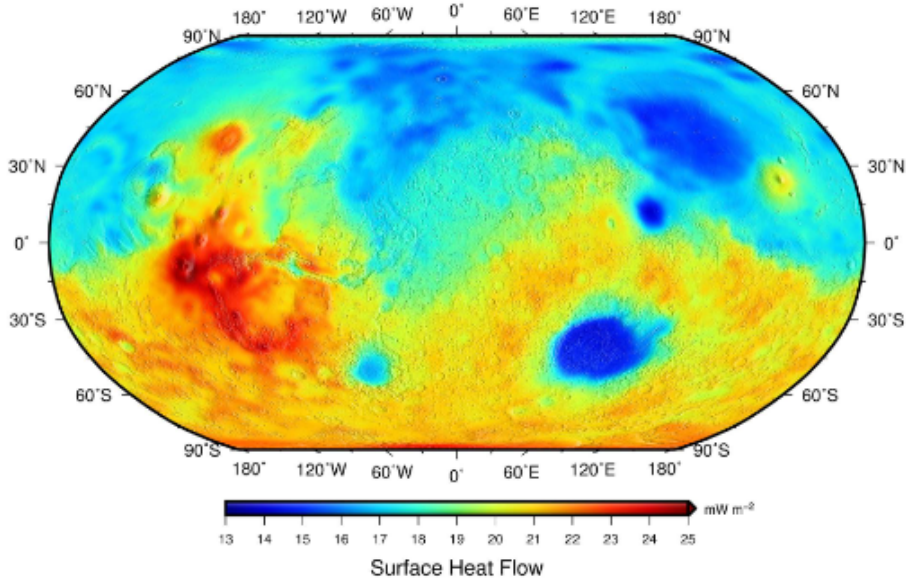

Figure 8.7: Surface heat flow [Parro et al., 2017]

$$\frac{\partial}{\partial z}F_j = \frac{F_{j+1/2} - F_{j-1/2}}{(z_{j+1} - z_{j-1})/2} = 2\frac{k_{j+1/2}\frac{T_{j+1}-T_j}{z_{j+1}-Z_j} - k_{j-1/2}\frac{T_j-T_{j-1}}{z_j-z_{j-1}}}{z_{j+1} - z_{j-1}} \tag{8.2.3}$$

With

- j : the layer index

Taking into account that T and the other specifed regolith parameters of different layers (see table 7.2) is varying with depth and that the spatial steps Δz are constant, it is possible to symplify the heat equation so that it becomes :

$$\rho c\frac{\partial T_j}{\partial t} = \frac{k}{(\Delta z)^2}T_{j+1} - \frac{2k}{(\Delta z)^2}T_j + \frac{k}{(\Delta z)^2}T_{j-1} + \rho H \tag{8.2.4}$$

By introducing $\alpha = \frac{k}{2(\Delta z)^2}\frac{\Delta t}{\rho c}$ the heat equation becomes :

$$\Delta t \frac{\partial T_j}{\partial t} = 2\alpha T_{j+1} - 4\alpha T_j + 2\alpha T_{j-1} + \frac{\Delta t H}{c} \tag{8.2.5}$$

Then, Crank-Nicolson scheme gives :

$$T_j^{t+1} - T_j^t = \alpha T_{j+1}^{t+1} - 2\alpha T_j^{t+1} + \alpha T_{j-1}^{t+1} + \alpha T_{j+1}^t - 2\alpha T_j^t + \alpha T_{j-1}^t + \frac{\Delta t H}{c} \tag{8.2.6}$$

With

- t : the time index

After isolating the different time-variables Crank-Nicolson become :

$$-\alpha T_{j+1}^{t+1} + (1+2\alpha) T_j^{t+1} - \alpha T_{j-1}^{t+1} = \alpha T_{j+1}^t + (1-2\alpha) T_j^t + \alpha T_{j-1}^t + \frac{\Delta t H}{c} \tag{8.2.7}$$

The lower the boundary condition is given by :

$$(1+\alpha) T_N^{t+1} - \alpha T_{N_1}^{t+1} = (1-\alpha) T_N^t + \alpha T_{N_1}^t + \frac{\Delta t F}{\rho c \Delta z} + \frac{\Delta t H}{c} \tag{8.2.8}$$

with

- N : the total number of subsurface layers

It is possible to formulate this system of linear expression with a matrix form as $AT^{t+1} = BT^t + C$ with T^{t+1} and T^t the column matrices of the temperatures at each layer at time $t+1$ and t respectively. Thus the Crank-Nicolson equation gives :

$$A = \begin{pmatrix} 1 & 0 & 0 & 0 & \cdots & 0 \\ -\alpha & 1+2\alpha & -\alpha & 0 & \cdots & 0 \\ 0 & -\alpha & 1+2\alpha & -\alpha & \cdots & 0 \\ \vdots & \ddots & \ddots & \ddots & \ddots & \vdots \\ 0 & \cdots & 0 & -\alpha & 1+2\alpha & -\alpha \\ 0 & \cdots & \cdots & 0 & -\alpha & 1+\alpha \end{pmatrix} \tag{8.2.9}$$

$$B = \begin{pmatrix} 1 & 0 & 0 & 0 & \cdots & 0 \\ \alpha & 1-2\alpha & \alpha & 0 & \cdots & 0 \\ 0 & \alpha & 1-2\alpha & \alpha & \cdots & 0 \\ \vdots & \ddots & \ddots & \ddots & \ddots & \vdots \\ 0 & \cdots & 0 & \alpha & 1-2\alpha & \alpha \\ 0 & \cdots & \cdots & 0 & \alpha & 1-\alpha \end{pmatrix} \tag{8.2.10}$$

and

$$C = \begin{pmatrix} T[t+1,0] - T[t,0] \\ \frac{\Delta t H}{c} \\ \vdots \\ \frac{\Delta t H}{c} \\ \frac{\Delta t H}{c} + \frac{\Delta t F}{\rho c \Delta z} \end{pmatrix} \tag{8.2.11}$$

From that, the temperatures in $t+1$ are easily obtained inverting the matrix A:

$$T^{t+1} = A^{-1}(BT^t + C) \tag{8.2.12}$$

Figure 8.8 shows important temperature variations over a sol: a difference of 90° between the day and the night. It comes from the very thin atmosphere, and the absence of greenhouse effect on Mars. However, deeper than 1 m and at least down to 100 m, the temperature stabilizes at a value of 226 K. The initial temperature come from Global Circulation Model (Credits : Orkun Temel).

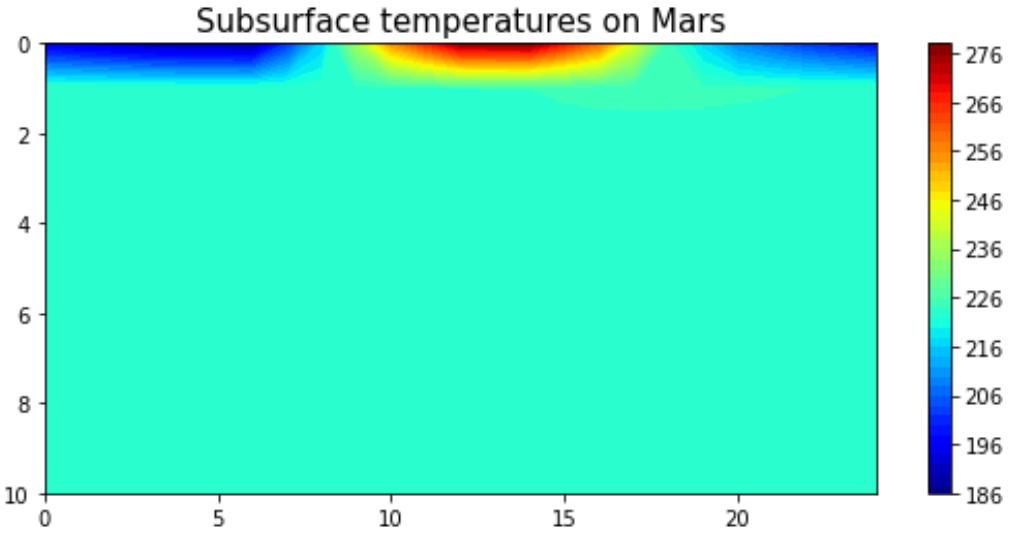

Figure 8.8: Martian subsurface temperatures with 10 × 0.1 m spatial discretization, throughout a sol , k=1.5 W/mK. The surface temperatures are for a latitude of 30°N and a longitude of 60°W and a solar longitude of 178.3°.

Figure 8.9 shows the evolution of temperature over 1 whole martian year. The time step is still fixed at 1 martian hour (= 3698.96 s) but the upper boundary condition for the surface temperatures is now an array of size 24 hours × 669 sols (instead of 24 hours ×1 sol). The range of variation of temperature over 1 year is greater than over 1 sol. Indeed the temperature range over 1 year goes from 160 °in winter to a maximum of 256K in summer. The surface temperatures come from General Circulation Model (GCM) simulations. As methane has been detected at equatorial latitude, the temperature of Figure 8.9 corresponds to a latitude of 30°N and a longitude of 60°W.

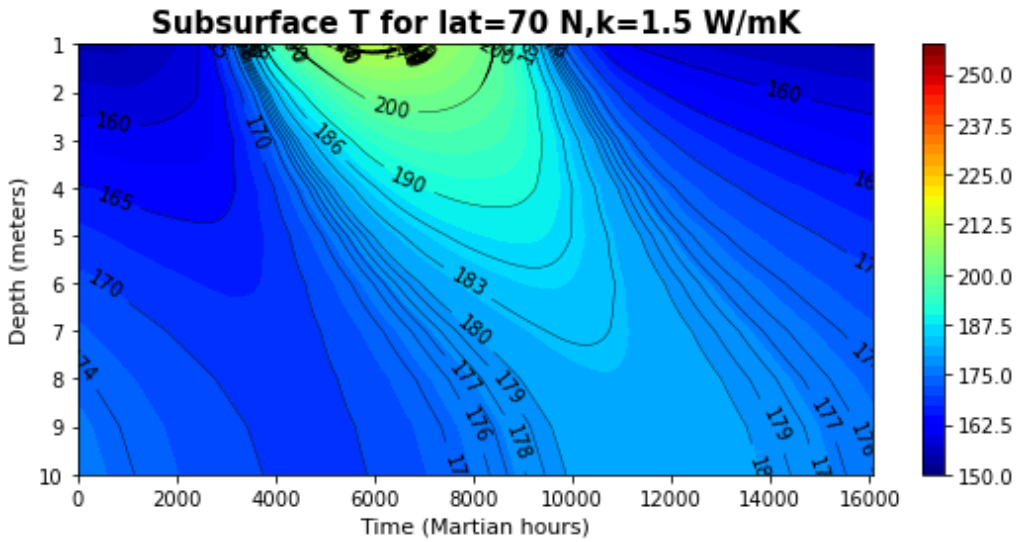

Figure 8.9: Martian subsurface temperatures throughout a Martian year for a latitude of $30°N$ and a longitude of $60°W$ and a solar longitude of 178.3°., considering a thermal conductivity of $k = 1.5W/mK$. The time is expressed in Martian hours and is shown beginning with northern spring (Time=0), then northern summer (Time=4639), northern autumn (Time=8926) and finally northern winter (Time=12350).

8.3 Adding the impact-induced temperatures to the initial subsurface temperatures

After modelling the evolution of temperature over time, the increase of temperature following a small impact will be considered. For that a source term needs to be added to the heat equation 8.2.1.

$$\rho c \frac{\partial T}{\partial t} = \frac{\partial}{\partial z}(k \frac{\partial T}{\partial z}) + \rho H + \rho c S_{impact} \tag{8.3.1}$$

with

$$S_{impact} = f \frac{\Delta T_{increase}}{\Delta t} \tag{8.3.2}$$

The Crank-Nicolson scheme developed in section 8.2 (equation 8.2.6) now gives:

$$T_j^{t+1} - T_j^t = \alpha T_{j+1}^{t+1} - 2\alpha T_j^{t+1} + \alpha T_{j-1}^{t+1} + \alpha T_{j+1}^t - 2\alpha T_j^t + \alpha T_{j-1}^t + \frac{\Delta t H}{c} + \Delta t S_{impact} \tag{8.3.3}$$

In practice, $\Delta t S_{impact}[i] = f T_{increase}[i]$ (with i the depth in meter) needs to be added to the C matrix (from section 8.2) as follows:

$$C = \begin{pmatrix} T[t+1,0] - T[t,0] \\ \frac{\Delta t H}{c} + f T_{increase}[i] \\ \vdots \\ \frac{\Delta t H}{c} + f T_{increase}[i] \\ \frac{\Delta t H}{c} + \frac{\Delta t F}{\rho c \Delta z} + f T_{increase}[i] \end{pmatrix} \tag{8.3.4}$$

With $f = 1$ only between the time of impact and the time of impact plus the numerical time step, otherwise $f = 0$.

About the matrix C, each line of the matrix corresponds to a certain depth, therefore the index i must be suitable for the corresponding layer. Due to a limitation of the analytical method there is no increase of temperature added to the first line which corresponds to the surface layer. Indeed the analytical method for the increase of temperature as a function of distance from the impact produces a vertical asymptote in $z = 0$ and thus $T_{increase}[0] = \infty$. Therefore it is not realistic and not possible to take into account the increase of temperature at the surface. The first finite value given by the analytical model is $T_{increase}[1]$, so the increase of temperature can only be added starting from the depth of the first layer (which is 1 m in this case). Thus, the following plots will only show the subsurface temperatures deeper than 1 m, as the temperatures at shallower depths are not incremented with the effect of the meteorite impact.

Figure 8.10 shows the evolution of temperature in the Martian subsurface following an impact of 1.7 on a basaltic surface with a velocity of 10 km/s and impact angle of 45°. The time of the impact was arbitrarily chosen just before the fourth month of the year and the northern summer solstice,in other words at t=4000 h after the start of the Martian year, A thermal conductivity of 1.5 W/mK was considered.
It can be seen that the impact affect the temperature of the surface up to 8m and lasts ≈ 8000 Martians hours which is ≈ 324 sols ≈ 6 − 7 Martian months. However, the increase of temperature is still too high to be realistic. Indeed with an increase of more than 7000K the regolith will melt. Indeed, it is known that basalt has a melting temperature of 1450 - 1500 °[Chen et al., 2017].

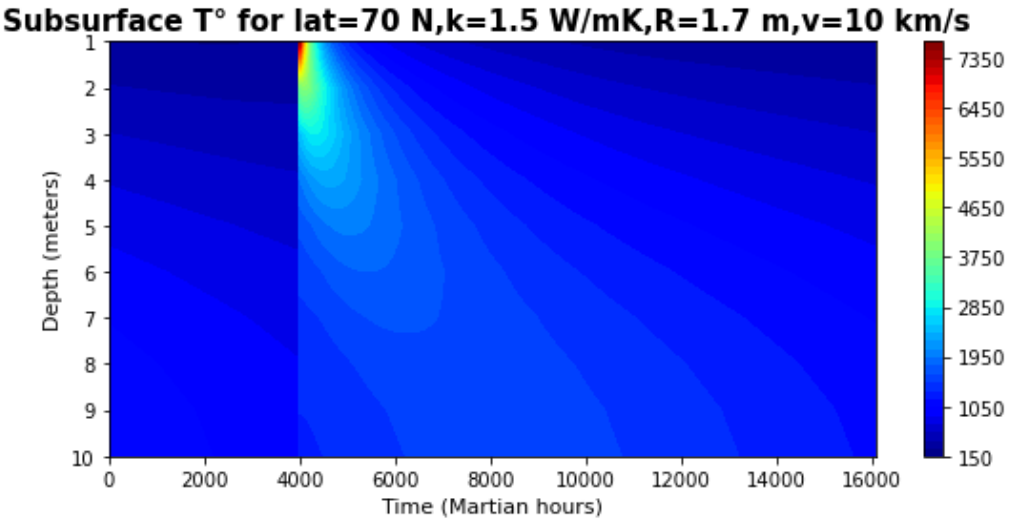

Figure 8.10: Martian subsurface temperatures throughout a Martian year considering an impact of 1.7 m is hitting the surface at a velocity of 10 km/s with an angle of 45° at Time = 4000. The initial subsurface temperatures are for a latitude of 70°N and a longitude of 2.5°E, and a thermal conductivity of k=1.5 W/mK.

8.4 Modeling Subsurface Temperature for 1 martian year for different scenarii

Evolution of subsurface temperature for the Exomars landing site

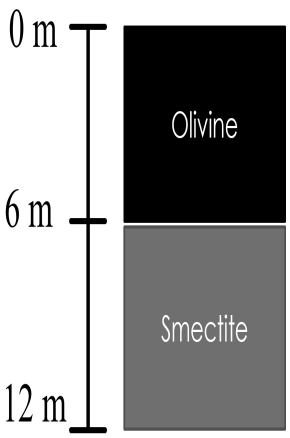

(a) Exomars Model 1

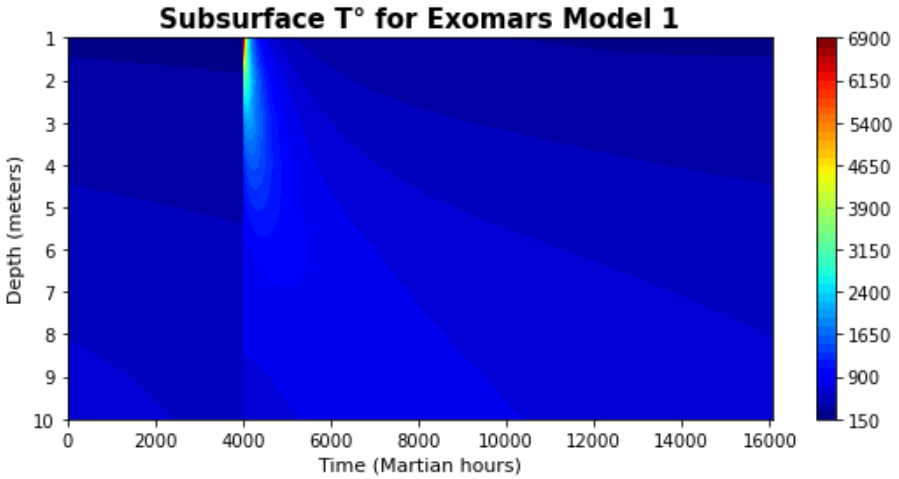

(b) Subsurface temperatures considering an impactor of 1.7 m hitting the surface at Time = 4000 with a velocity of 10 km/s and an impact angle of 45°. The initial subsurface temperatures are for a latitude of ExoMars.

Figure 8.11: First model and results for the ExoMars 2022 landing site.

In Figure 8.11 the maximum of temperature is 6722K following the impact and an effect of the impact lasts for at least ≈ 10000 hours. The impact has a strong effect up to 5 m deep and a increase of temperature up to at least 10 m deep.The impact has a strong effect up to 6 m deep and a increase of temperature up to at least 10 m deep. The smectite layer between 3 and 6 m deep seems to propagate the increase of temperature further than the olivine layer.

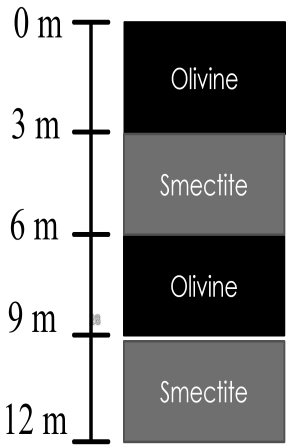

(a) Exomars Model 2

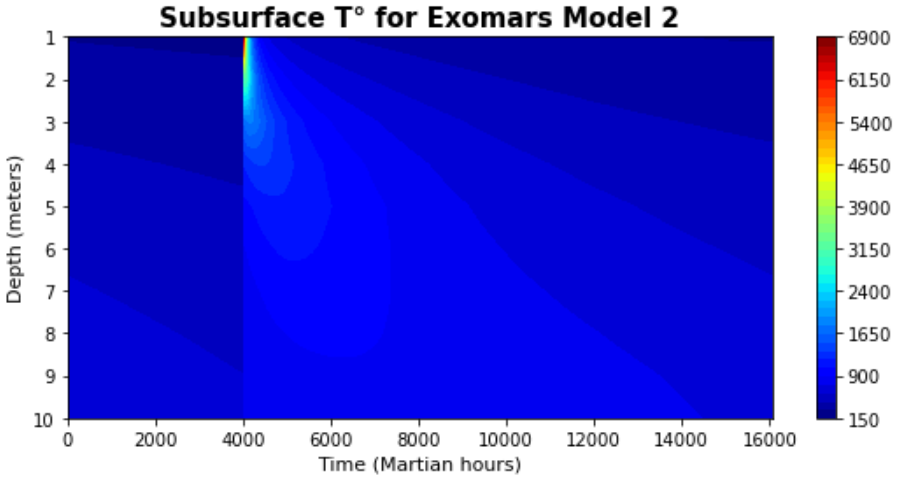

(b) Subsurface temperatures considering an impactor of 1.7 m hitting the surface at Time = 4000 with a velocity of 10 km/s and an impact angle of 45°. The initial subsurface temperatures are for a latitude of ExoMars.

Figure 8.12: Second model and results for the ExoMars 2022 landing site.

In Figure 8.12 the maximum of temperature is 6722K following the impact and an effect of the impact lasts for at least ≈ 8000 hours.The impact has a strong effect ($> 1000K$ up to 7 m deep and a increase

of temperature up to at least 10 m deep. The smectite layer between 3 and 6 m deep seems to propagate the increase of temperature further than the olivine layer.

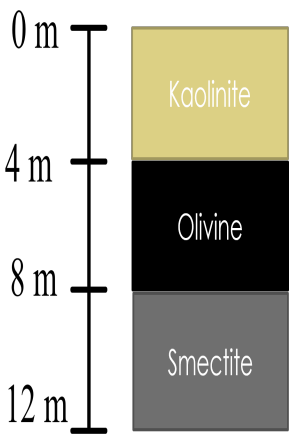

(a) Exomars Model 3

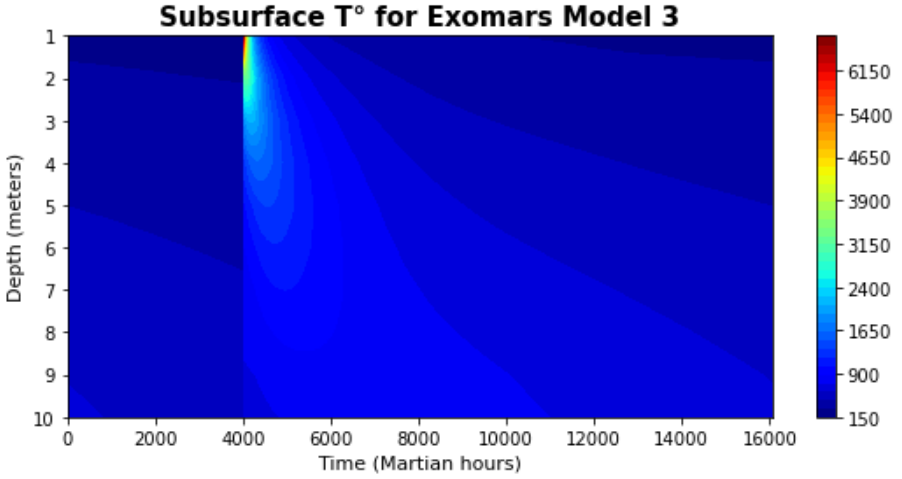

(b) Subsurface temperatures considering an impactor of 1.7 m hitting the surface at Time = 4000 with a velocity of 10 km/s and an impact angle of 45°. The initial subsurface temperatures are for a latitude of ExoMars.

Figure 8.13: Third model and results for the ExoMars 2022 landing site.

In Figure 8.13 the maximum of temperature is 6712K following the impact and an effect of the impact lasts for at least $\approx$ 10000 hours. The impact has a strong effect ($> 1000K$) up to 7 m deep and a increase of temperature up to at least 10 m deep. The smectite layer between 8 and 12 m deep seems to propagate the increase of temperature further than the olivine layer.

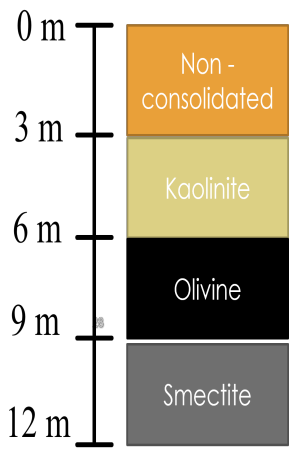

(a) Exomars Model 4

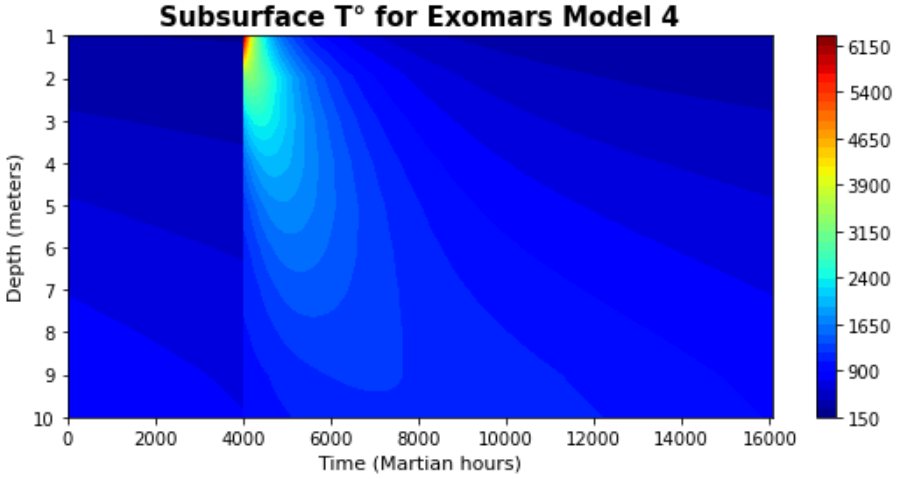

(b) Subsurface temperatures considering an impactor of 1.7 m hitting the surface at Time = 4000 with a velocity of 10 km/s and an impact angle of 45°. The initial subsurface temperatures are for a latitude of ExoMars.

Figure 8.14: Fourth model and results for the ExoMars 2022 landing site.

In Figure 8.14 the maximum of temperature is 6220K following the impact and an effect of the impact lasts for at least $>$ 12000 hours. The impact has a strong effect ($> 1000K$) up to 10 m deep.

The Olivine layer, if present on top seems to get a bigger increase of temperature following an impact but it looks like olivine reduces more the conduction of heat through the regolith and over time than the non-consolidated layer which is coherent regarding their respective thermal conductivity.

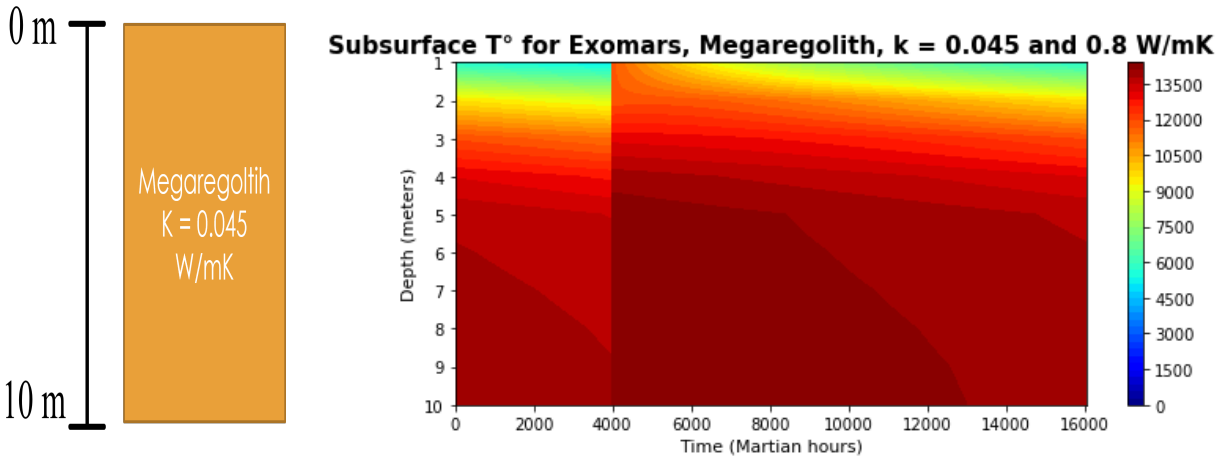

(a) Exomars Model formisano 1

(b) Subsurface temperatures considering an impactor of 1.7 m hitting the surface at Time = 4000 with a velocity of 10 km/s and an impact angle of 45°. The initial subsurface temperatures are for a latitude of ExoMars.

Figure 8.15: First model based on [Formisano et al., 2021] and results for the ExoMars 2022 landing site.

In Figure 8.15 the maximum of temperature is 13000 following the impact. This scenario is unlikely and it seems that with this thermal conductivity, a layer this thick (10m) would not be realisable.

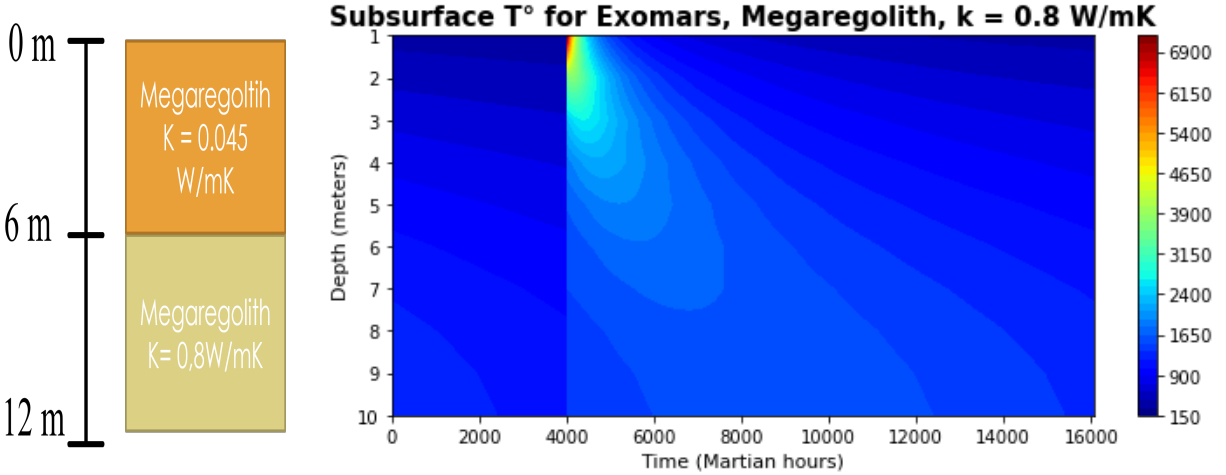

(a) Exomars Model formisano 2

(b) Subsurface temperatures considering an impactor of 1.7 m hitting the surface at Time = 4000 with a velocity of 10 km/s and an impact angle of 45°. The initial subsurface temperatures are for a latitude of ExoMars.

Figure 8.16: Second model based on [Formisano et al., 2021] and results for the ExoMars 2022 landing site.

In Figure 8.16 the maximum of temperature is 6722K following the impact and an effect of the impact lasts for at least ≈ 12000 hours. The impact has a strong effect ($> 1000K$) up to 10 m deep.

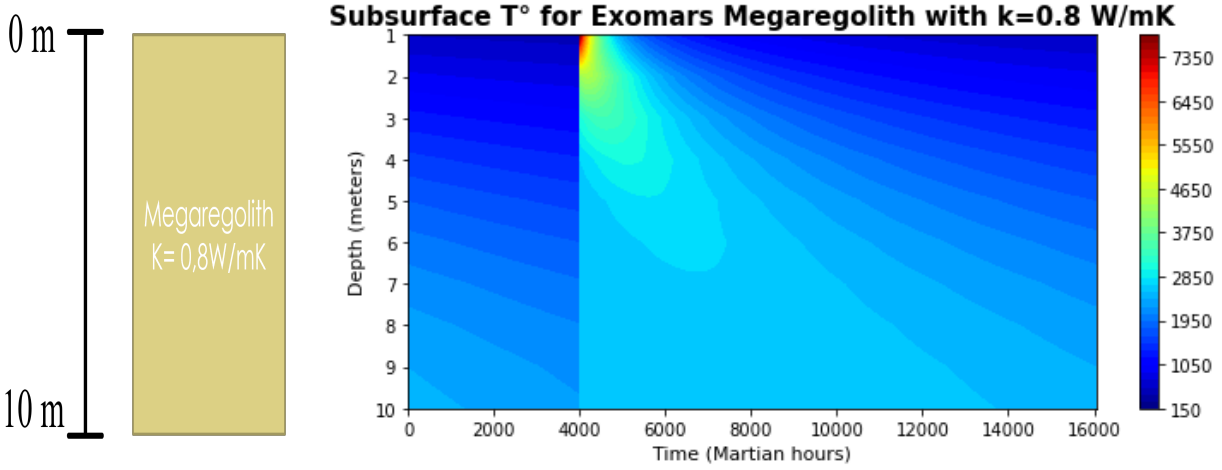

(a) Exomars Model formisano 3

(b) Subsurface temperatures considering an impactor of 1.7 m hitting the surface at Time = 4000 with a velocity of 10 km/s and an impact angle of 45°. The initial subsurface temperatures are for a latitude of ExoMars.

Figure 8.17: Third model based on [Formisano et al., 2021] and results for the ExoMars 2022 landing site.

In Figure 8.17 the maximum of temperature is 7791K following the impact and an strong effect (2400K) of the impact lasts for at least > than 12000 hour and up at least 10m.

Evolution of subsurface temperature for the Insight landing site

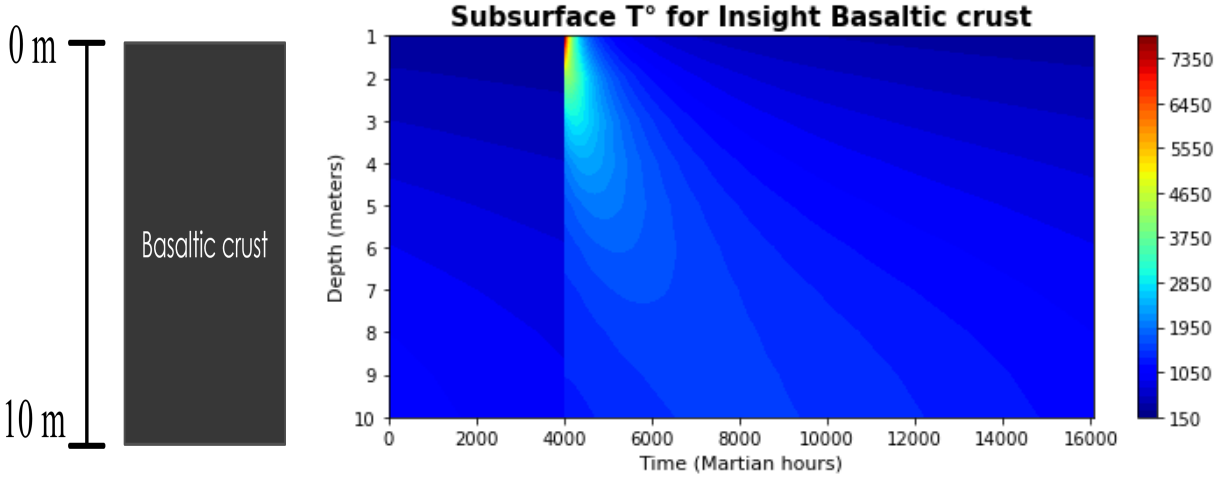

(a) Insight Model 1

(b) Subsurface temperatures considering an impactor of 1.7 m hitting the surface at Time = 4000 with a velocity of 10 km/s and an impact angle of 45°. The initial subsurface temperatures are for a latitude of InSight.

Figure 8.18: First model and results for the InSight landing site.

In Figure 8.18 the maximum of temperature is 7709K following the impact and an effect of the impact lasts for at least ≈ 8000 hours.The impact has a strong effect ($> 1000K$) up to at least 10 m deep.

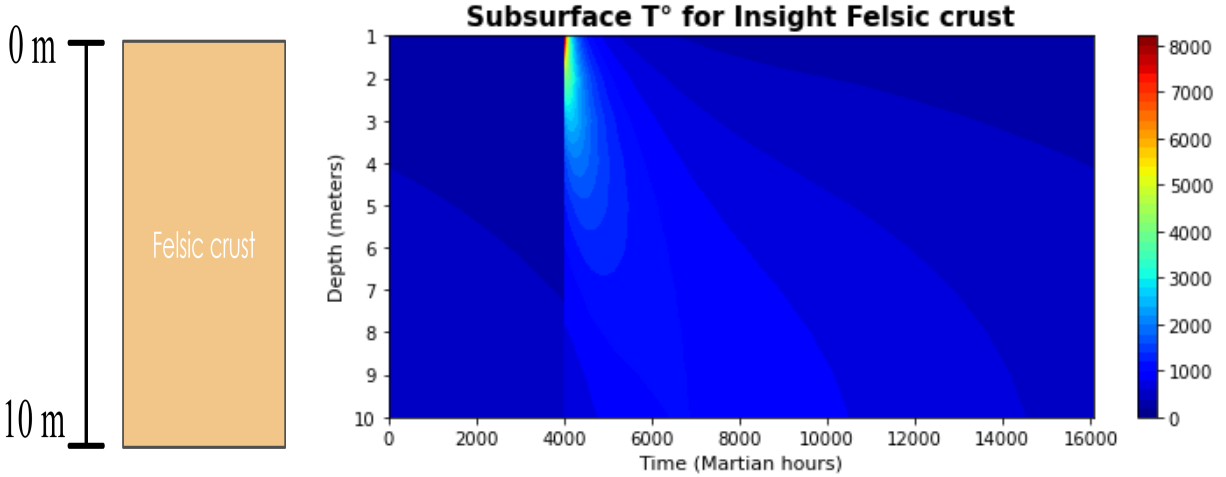

(a) Insight Model 2

(b) Subsurface temperatures considering an impactor of 1.7 m hitting the surface at Time = 4000 with a velocity of 10 km/s and an impact angle of 45°. The initial subsurface temperatures are for a latitude of InSight.

Figure 8.19: Second model and results for the InSight landing site.

In Figure 8.19 the maximum of temperature is 8163K following the impact and an effect of the impact lasts for at least $\approx$ 6000 hours. The impact has a strong effect ($> 1000K$) up to 7 m deep and a increase of temperature up to at least 10 m deep.

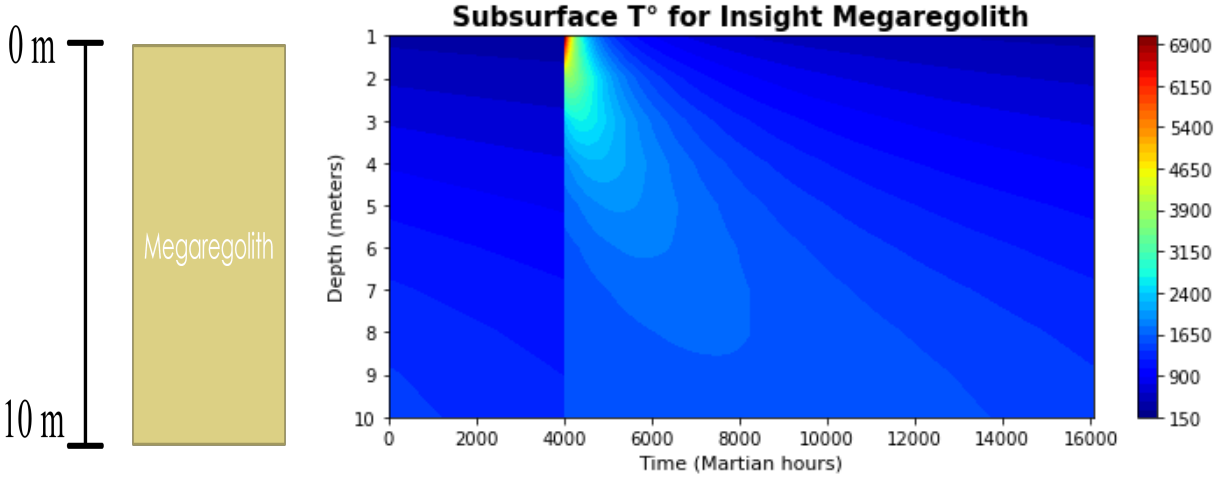

(a) Insight Model 3

(b) Subsurface temperatures considering an impactor of 1.7 m hitting the surface at Time = 4000 with a velocity of 10 km/s and an impact angle of 45°. The initial subsurface temperatures are for a latitude of InSight.

Figure 8.20: Third model and results for the InSight landing site.

In Figure 8.20 the maximum of temperature is 7030K following the impact and an effect of the impact lasts for at least $>$ 12000 hours. The impact has a strong effect ($> 1000K$) up to at least 10 m deep.

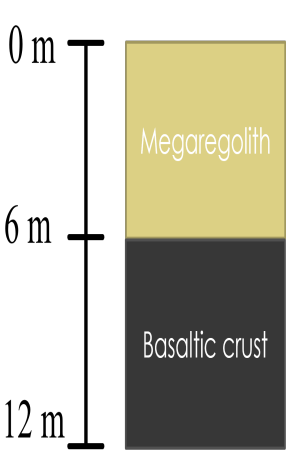

(a) Insight Model 4

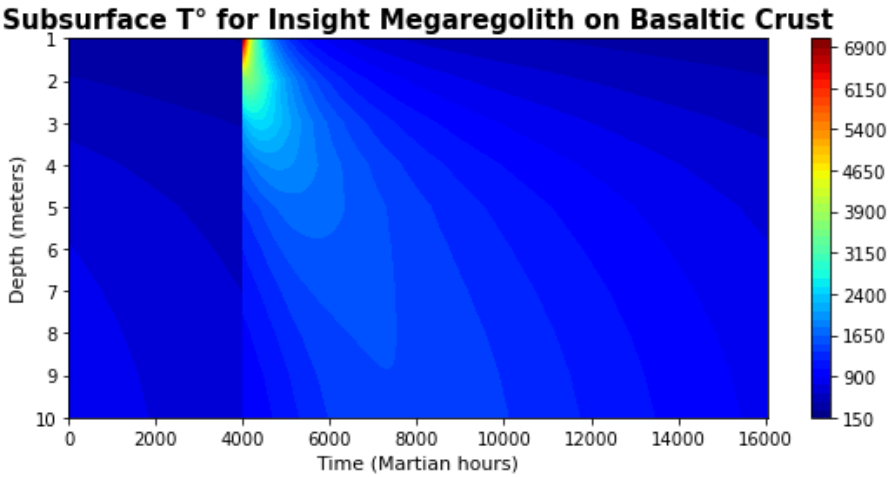

(b) Subsurface temperatures considering an impactor of 1.7 m hitting the surface at Time = 4000 with a velocity of 10 km/s and an impact angle of 45°. The initial subsurface temperatures are for a latitude of InSight.

Figure 8.21: Fourth model and results for the InSight landing site.

In Figure 8.21 the maximum of temperature is 6966K following the impact and an effect of the impact lasts for at least $\approx$ 8000 hours. The impact has a strong effect ($> 1000K$) up to at least 10 m deep.

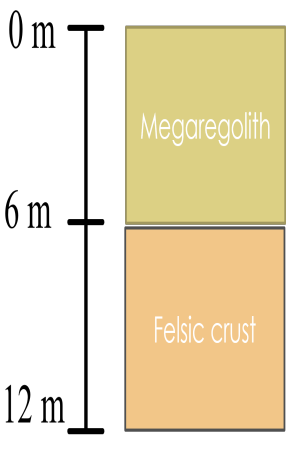

(a) Insight Model 5

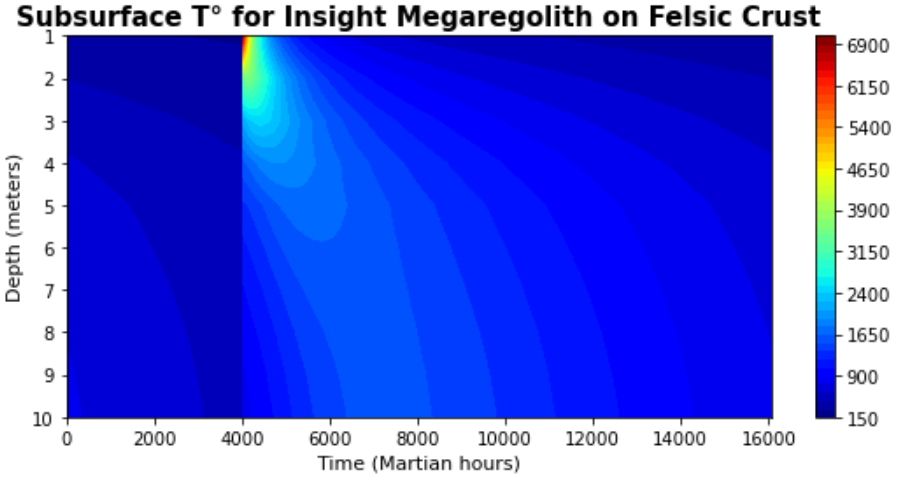

(b) Subsurface temperatures considering an impactor of 1.7 m hitting the surface at Time = 4000 with a velocity of 10 km/s and an impact angle of 45°. The initial subsurface temperatures are for a latitude of InSight.

Figure 8.22: Fifth model and results for the InSight landing site.

In Figure 8.22 the maximum of temperature is 6956K following the impact and an effect of the impact lasts for at least $\approx$ 8000 hours. The impact has a strong effect ($> 1000K$) up to 10 m deep. The felsic crust layer seems to reduce more the propagation of temperature than the megaregolith layer.

Evolution of subsurface temperature for the Jezero Crater

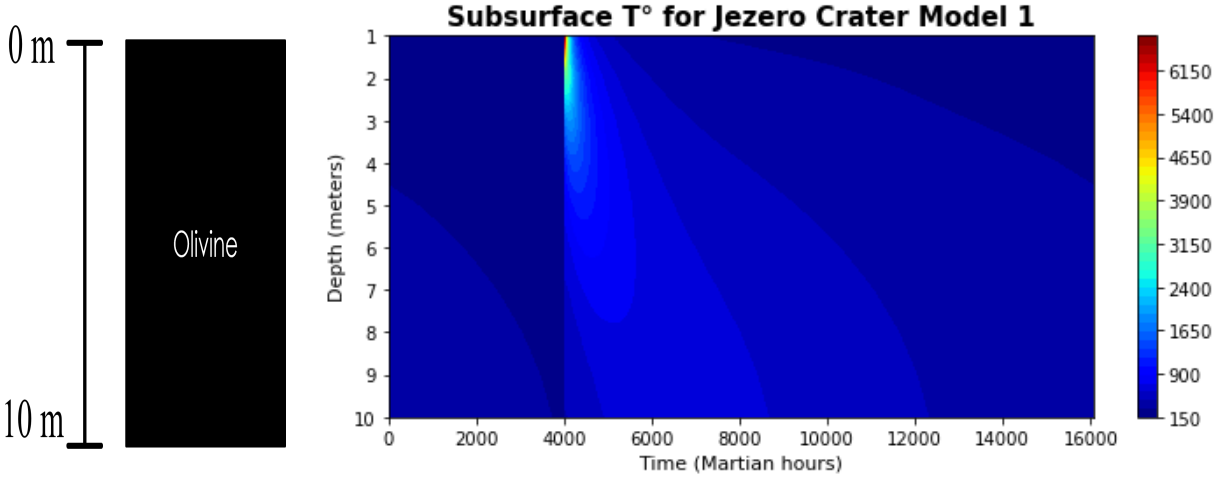

(a) Jezero Model 1

(b) Subsurface temperatures considering an impactor of 1.7 m hitting the surface at Time = 4000 with a velocity of 10 km/s and an impact angle of 45°. The initial subsurface temperatures are for a latitude of Jezero crater.

Figure 8.23: First model and results for the Jezero Crater.

In Figure 8.23 the maximum of temperature is 6740K following the impact and an effect of the impact lasts for at least ≈ 4000 hours. The impact has a strong effect ($> 1000K$) up to 5 m deep and a increase of temperature up to at least 10 m deep.

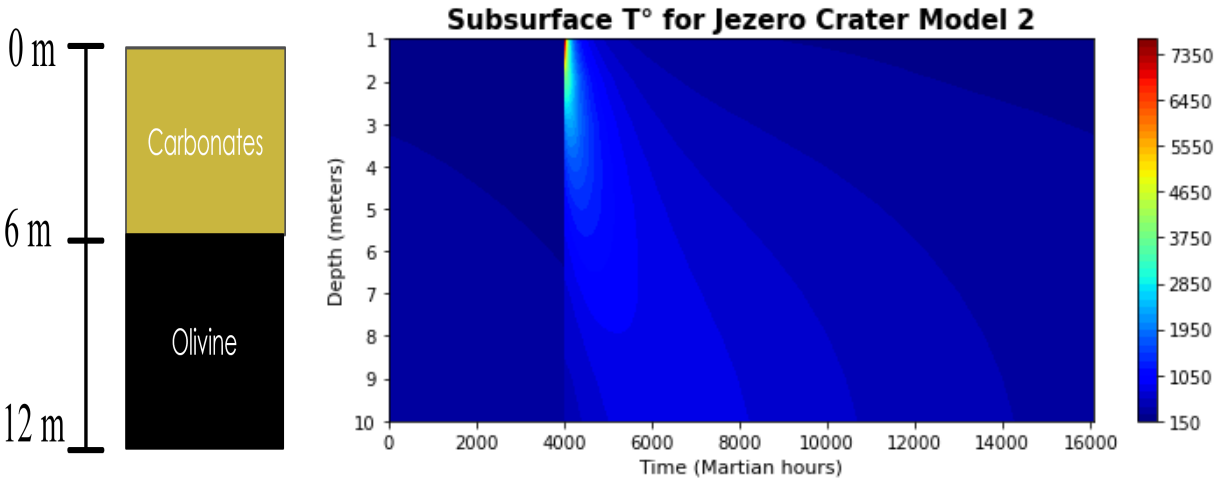

(a) Jezero Model 2

(b) Subsurface temperatures considering an impactor of 1.7 m hitting the surface at Time = 4000 with a velocity of 10 km/s and an impact angle of 45°. The initial subsurface temperatures are for a latitude of Jezero crater.

Figure 8.24: Second model and results for the Jezero Crater.

In Figure 8.24 the maximum of temperature is 7548K following the impact and an effect of the impact lasts for at least ≈ 6000 hours. The impact has a strong effect ($> 1000K$) up to 9 m deep and a increase of temperature up to at least 10 m deep.

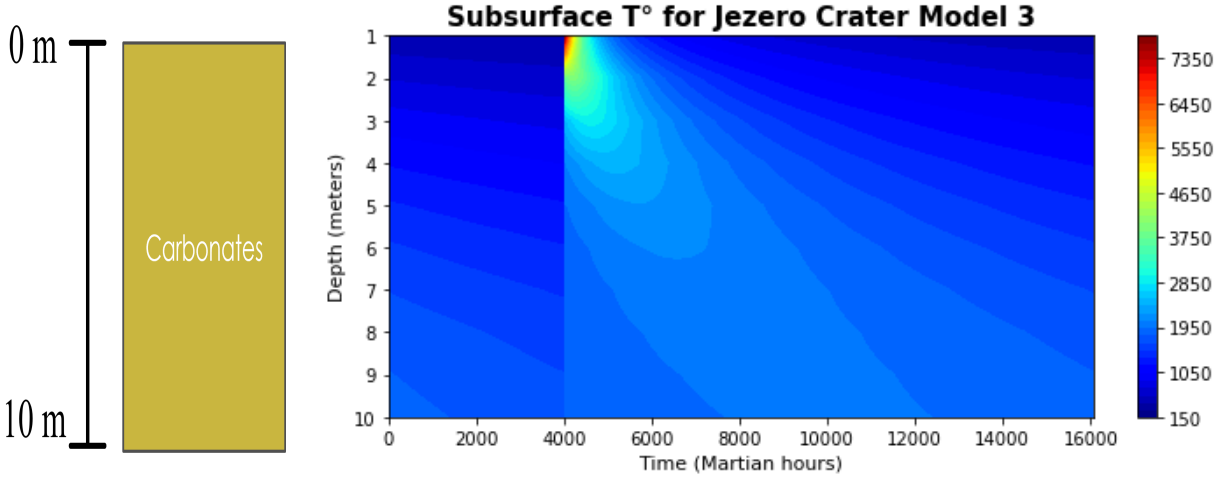

(a) Jezero Model 3

(b) Subsurface temperatures considering an impactor of 1.7 m hitting the surface at Time = 4000 with a velocity of 10 km/s and an impact angle of 45°. The initial subsurface temperatures are for a latitude of Jezero crater.

Figure 8.25: Third model and results for the Jezero Crater.

In Figure 8.25 the maximum of temperature is 7699K following the impact and an effect of the impact lasts for at least $\approx$ 12000 hours. The impact has a strong effect ($> 1000K$) up to at least 10 m deep.

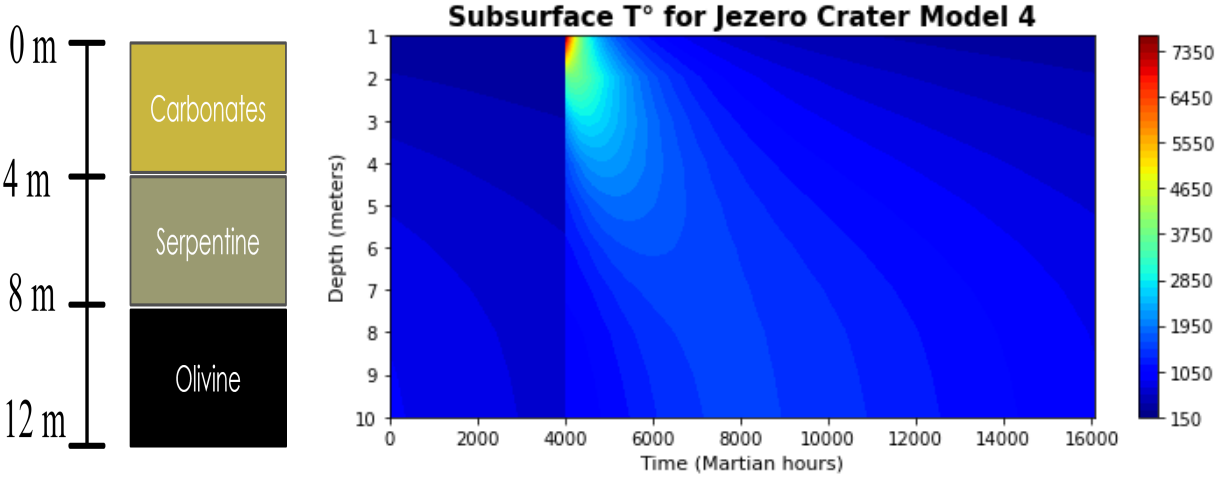

(a) Jezero Model 4

(b) Subsurface temperatures considering an impactor of 1.7 m hitting the surface at Time = 4000 with a velocity of 10 km/s and an impact angle of 45°. The initial subsurface temperatures are for a latitude of Jezero crater.

Figure 8.26: Fourth model and results for the Jezero Crater.

In Figure 8.26 the maximum of temperature is 7564K following the impact and an effect of the impact lasts for at least $\approx$ 8000 hours. The impact has a strong effect ($> 1000K$) up to at least 10 m deep.

The Carbonate layer seems to have in greater increase of temperature following an impact ($\approx 6700K$ for the olivine layer at the surface in model 1, $\approx 7500 to 7700K$ for the other models).

Evolution of subsurface temperature for the MSL landing site

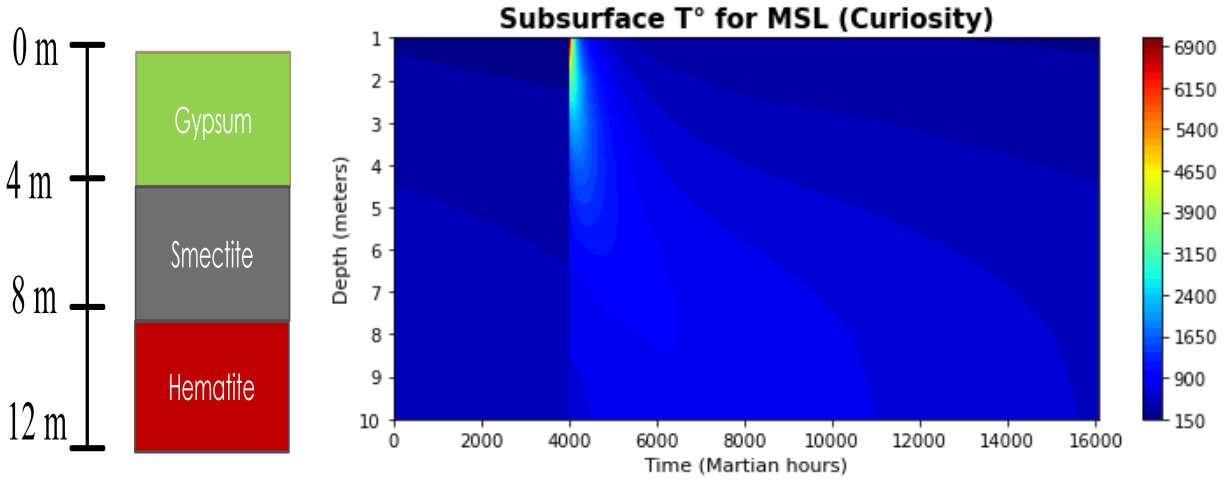

(a) Gale crater/ MSL Model 1

(b) Subsurface temperatures considering an impactor of 1.7 m hitting the surface at Time = 4000 with a velocity of 10 km/s and an impact angle of 45°. The initial subsurface temperatures are for a latitude of Gale crater/MSL.

Figure 8.27: First model and results for the Gale Crater/MSL.

In Figure 8.27 the maximum of temperature is 6941K following the impact and an effect of the impact lasts for at least ≈ 6000 hours. The impact has a strong effect ($> 1000K$) up to 6 m deep and a increase of temperature up to at least 10 m deep.

Evolution of subsurface temperature for the Phoenix landing site

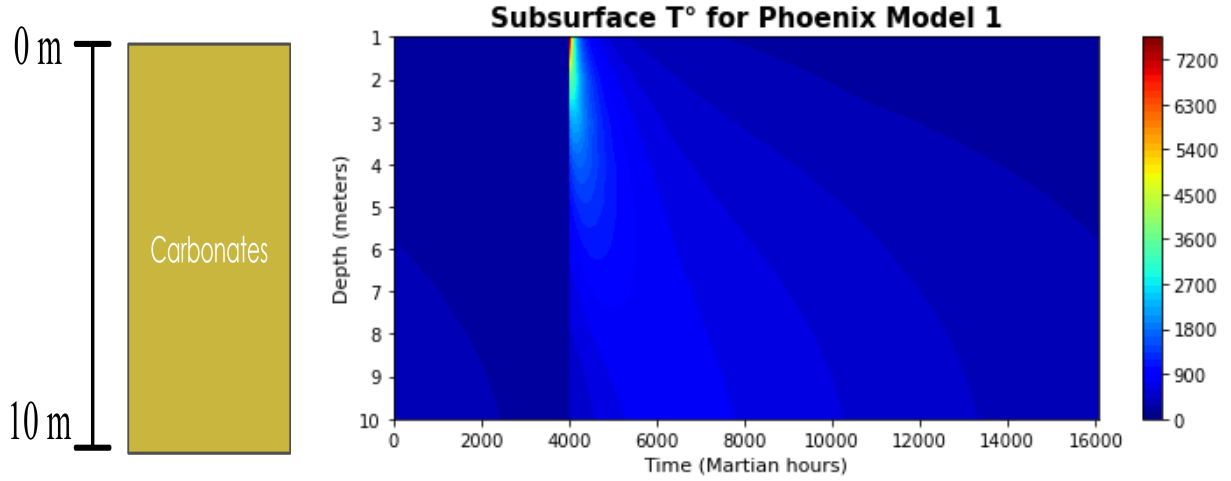

(a) Phoenix Model 1

(b) Subsurface temperatures considering an impactor of 1.7 m hitting the surface at Time = 4000 with a velocity of 10 km/s and an impact angle of 45°. The initial subsurface temperatures are for a latitude of Phoenix.

Figure 8.28: First model and results for the Pheonix landing site.

In Figure 8.28 the maximum of temperature is 7538K following the impact and an effect of the impact lasts for at least ≈ 4000 hours. The impact has a strong effect ($> 1000K$) up to 6 m deep and a increase of temperature up to at least 10 m deep.

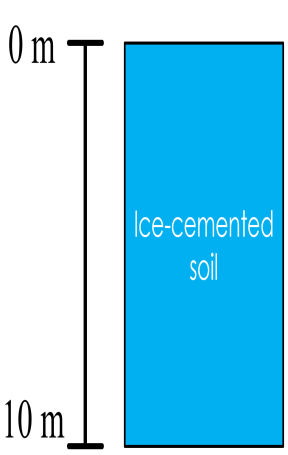

(a) Phoenix Model 2

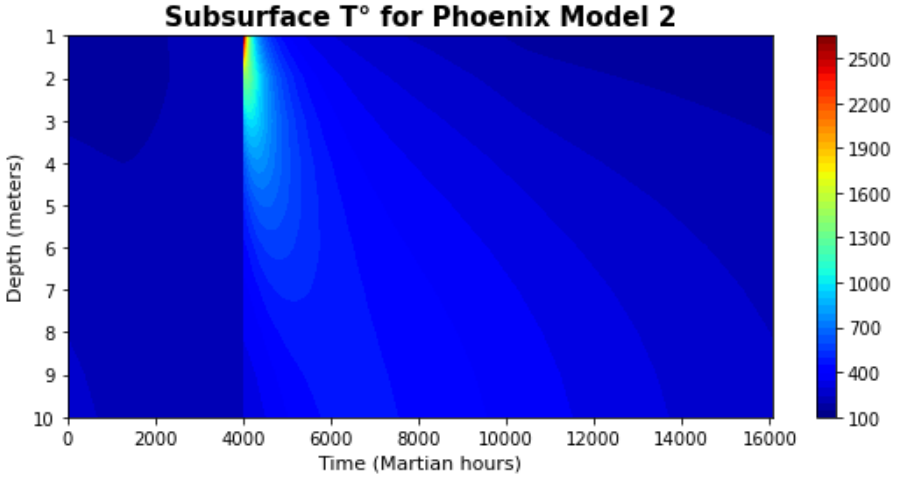

(b) Subsurface temperatures considering an impactor of 1.7 m hitting the surface at Time = 4000 with a velocity of 10 km/s and an impact angle of 45°. The initial subsurface temperatures are for a latitude of Phoenix.

Figure 8.29: Second model and results for the Pheonix landing site.

In Figure 8.29 the maximum of temperature is 2627K following the impact and an effect of the impact lasts for at least $>$ 12000 hours. The impact has a strong effect ($> 1000K$) up to at least 10 m deep.

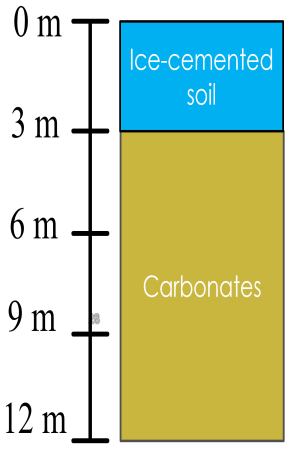

(a) Phoenix Model 3

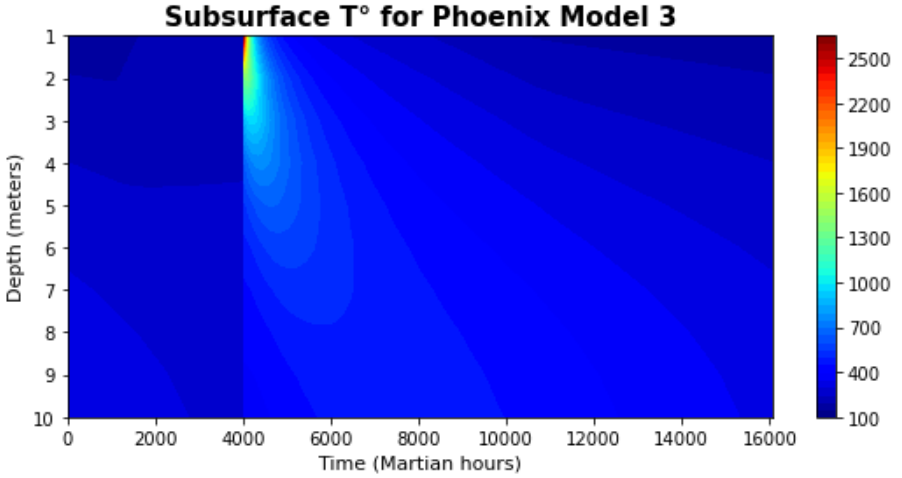

(b) Subsurface temperatures considering an impactor of 1.7 m hitting the surface at Time = 4000 with a velocity of 10 km/s and an impact angle of 45°. The initial subsurface temperatures are for a latitude of Phoenix.

Figure 8.30: Third model and results for the Pheonix landing site.

In Figure 8.30 the maximum of temperature is 2635K following the impact and an effect of the impact lasts for at least $>$ 12000 hours. The impact has a strong effect ($> 1000K$) up to at least 10 m deep.

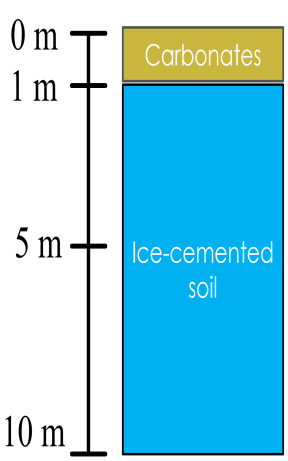

(a) Phoenix Model 4

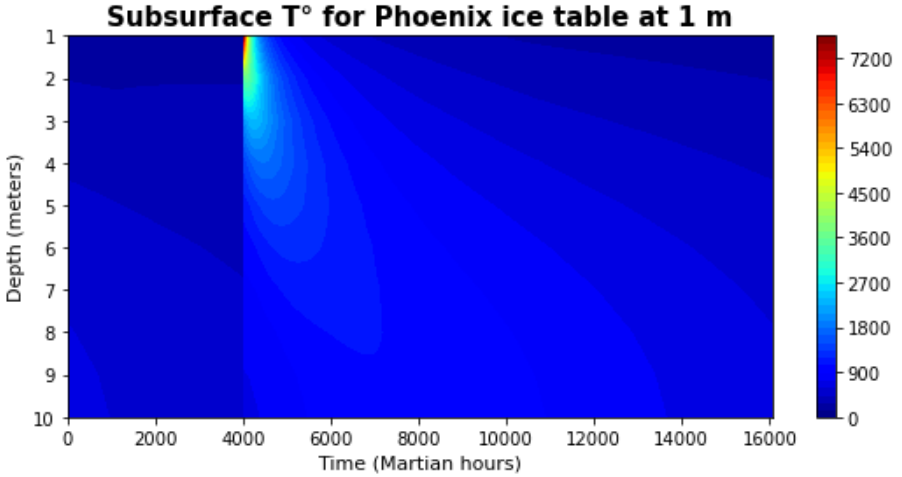

(b) Phoenix Model 4 Max temp K

Figure 8.31: Fourth model and results for the Pheonix landing site.

In Figure 8.31 the maximum of temperature is 7538K following the impact and an effect of the impact lasts for at least $\approx$ 10000 hours. The impact has a strong effect ($> 1000K$) up to 8 m deep and a increase of temperature up to at least 10 m deep.

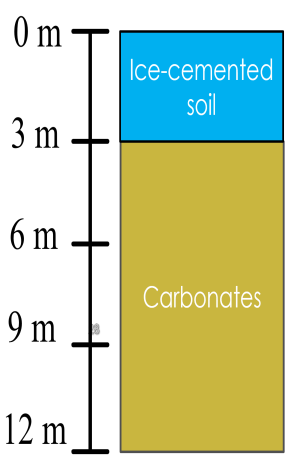

(a) Phoenix Model 5

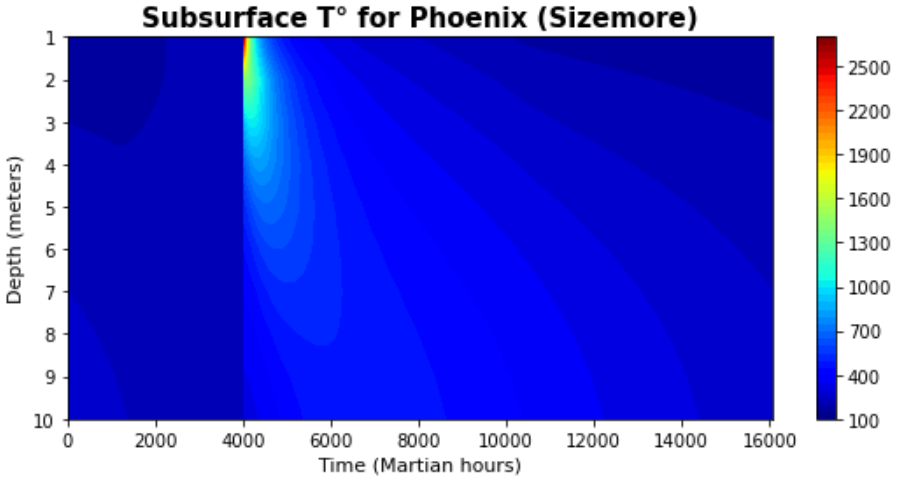

(b) Subsurface temperatures considering an impactor of 1.7 m hitting the surface at Time = 4000 with a velocity of 10 km/s and an impact angle of 45°. The initial subsurface temperatures are for a latitude of Phoenix.

Figure 8.32: Fifth model and results for the Pheonix landing site.

In Figure 8.32 the maximum of temperature is 2635K following the impact and an effect of the impact lasts for at least $\approx$ 10000 hours. The impact has a strong effect ($> 1000K$) up to at least 10 m deep.

The ice-cemented layer if present at the top, prevent an high increase of temperature following an impact in comparison with the carbonate layer ($\approx 2600K$ and $\approx 7500K$ respectively for the ice-cemented layer and for the carbonate layer). However, the carbonate seems to retain more the heat than the ice-cemented layer and thus it could lead to a greater effect deeper in the regolith.

Evolution of subsurface temperature for Nili Fossae

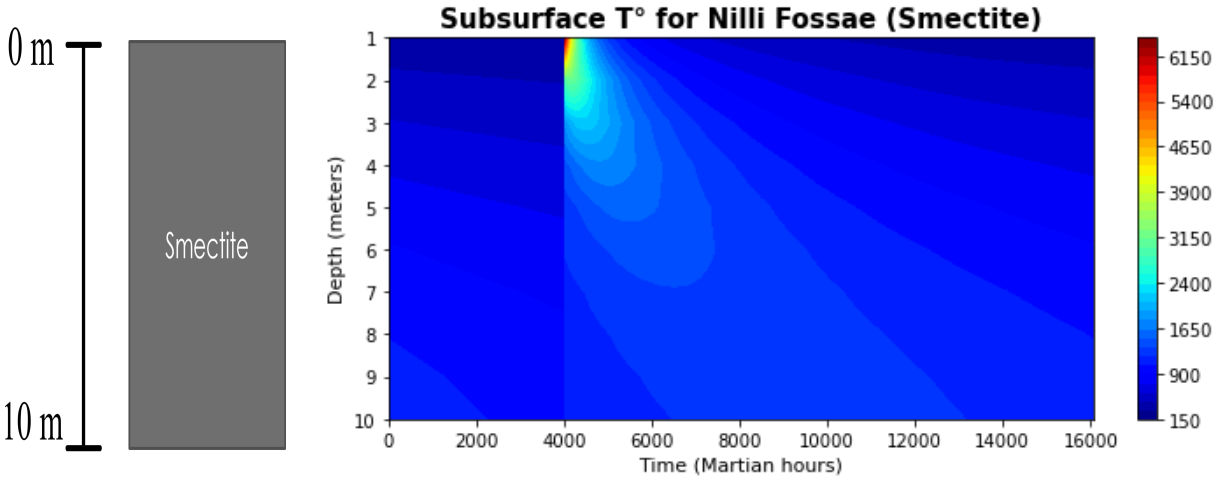

(a) Nili Fossae Model

(b) Subsurface temperatures considering an impactor of 1.7 m hitting the surface at Time = 4000 with a velocity of 10 km/s and an impact angle of 45°. The initial subsurface temperatures are for a latitude of Nili Fossae.

Figure 8.33: First model and results for the Nili Fossae location.

In Figure 8.33 the maximum of temperature is 6401K following the impact and an effect of the impact lasts for at least $\approx$ 12000 hours. The impact has a strong effect ($> 1000K$) up to at least 10 m deep.

Evolution of subsurface temperature for Syrtis major

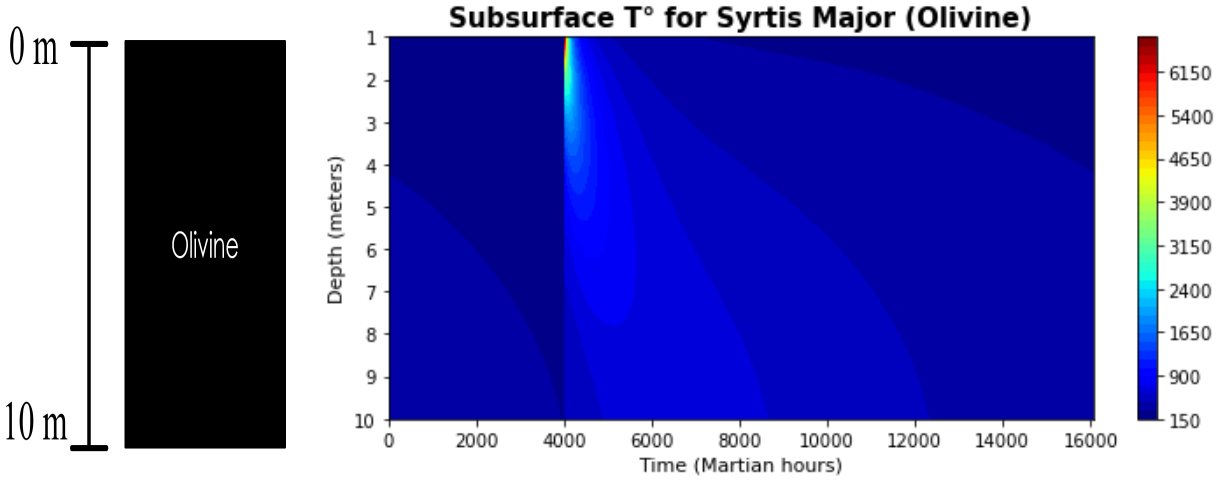

(a) Syrtis Major Model

(b) Subsurface temperatures considering an impactor of 1.7 m hitting the surface at Time = 4000 with a velocity of 10 km/s and an impact angle of 45°. The initial subsurface temperatures are for a latitude of Syrtis Major.

Figure 8.34: First model and results for the Syrtis Major location.

In Figure 8.34 the maximum of temperature is 6736K following the impact and an effect of the impact lasts for at least $\approx$ 4000 hours. The impact has a strong effect ($> 1000K$) up to 6 m deep and a increase of temperature up to at least 10 m deep.

Evolution of subsurface temperature for Terra Sabae

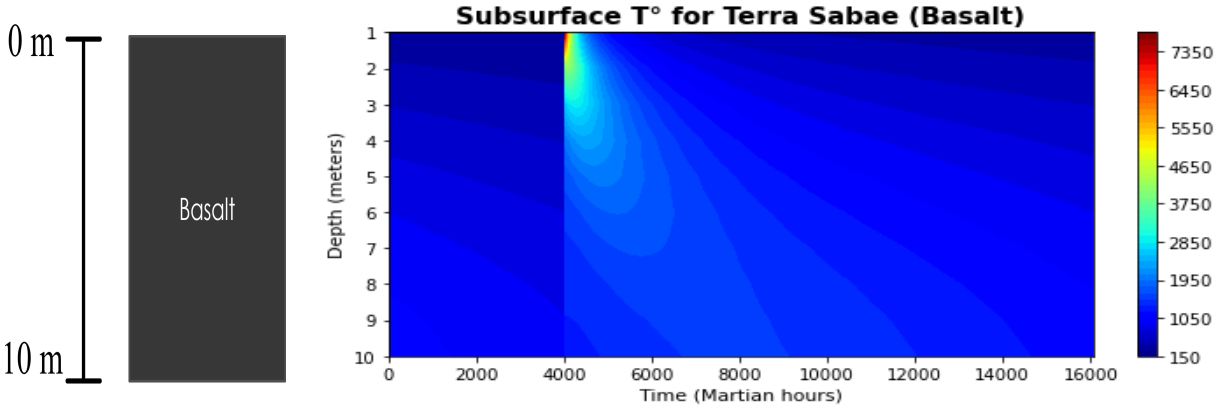

(a) Terra Sabae Model 1. Basalt density = $2600 kgm^{-3}$

(b) Subsurface temperatures considering an impactor of 1.7 m hitting the surface at Time = 4000 with a velocity of 10 km/s and an impact angle of 45°. The initial subsurface temperatures are for a latitude of Terra Sabae.

Figure 8.35: First model and results for the Terra Sabae location.

In Figure 8.35 the maximum of temperature is 7700K following the impact and an effect of the impact lasts for at least ≈ 8000 hours. The impact has a strong effect ($> 1000K$) up to at least 10 m deep.

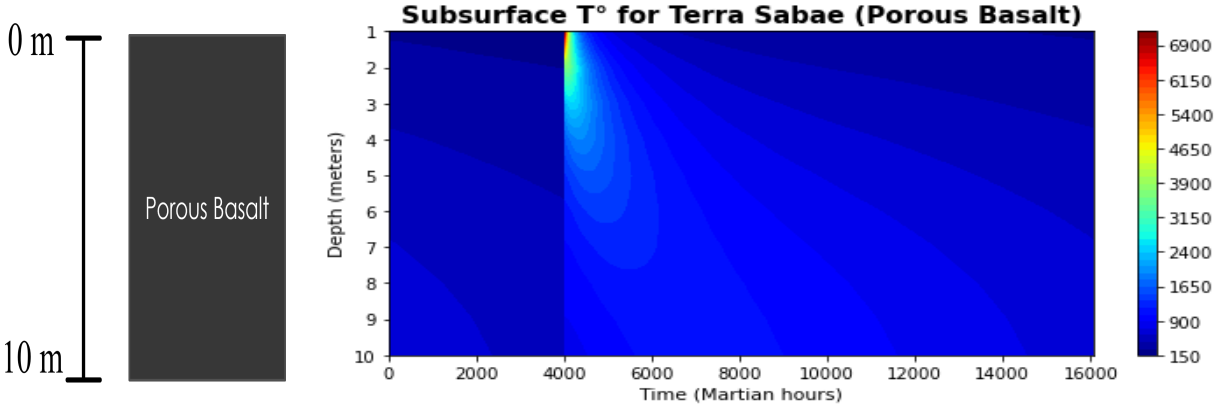

(a) Terra Sabae Model 2. Basalt density = $2000 kgm^{-3}$

(b) Subsurface temperatures considering an impactor of 1.7 m hitting the surface at Time = 4000 with a velocity of 10 km/s and an impact angle of 45°. The initial subsurface temperatures are for a latitude of Terra Sabae.

Figure 8.36: Second model and results for the Terra Sabae location.

In Figure 8.36 the maximum of temperature is 7145K following the impact and an effect of the impact lasts for at least ≈ 4000 hours. The impact has a strong effect ($> 1000K$) up to 8 m deep and a increase of temperature up to at least 10 m deep.

The increase of porosity seems to reducde the increase of temperature following an impact (7700K for the denser basalt and 7145K for the porous Basalt), leading to a reduced effect in the deeper layer of the regolith.

9 Environmental effects of small impactors

9.1 Destabilization of ice table

In this master's thesis, one location is likely to have a destabilization of the ice table and it is the Phoenix landing site. Indeed, it is known that the ice water table is very close to the surface (10cm under the surface) [Sizemore and Mellon, 2006].

All the results presented in section 8.4 shows a strong increase of temperature ($>$ 1000K) over the first few meters and following different regolith's compositions. Thus It is likely that if a small impactor hit the surface at the latitude, a destabilization of the ice table occurs over a few meters deep.

However in function of the composition of the top layer, a difference of 5000K was noticed in the increase of temperature. It may have an impact on how the destabilization occurs and propagates.

9.2 Destabilization of methane clathrates

To study the potential effect of the heterogeneity of the regolith on the destabilization of methane clathrate following a collision with a small impactor, it is required to know the depth of the top of the stability zone of the methane clathrate.

From [Gloesener et al., 2021] its known that the clathrate stability zone is larger for higher thermal conductivity. Thus we could potentially link the effect of the reglith's heterogeneity. Moreover it is known that the clathrates stability zone is closer to the surface at higher latitude [Gloesener et al., 2013]. Still, it is needed to verify this with the locations of interest. The depth of the clathrate stability zone for the specific locations of interest are visible in table 9.1.

Table 9.1: Methane clathrate stability depths for location of interest. Credits : Élodie Gloesener.

	methane clathrate stability depths (m)
Near-equator	a few tens of meters deep
Gale Crater/ MSL landing site	55
Nili Fossae	62
Syrtis Major	59
Terra Sabae	34
Phoenix	6

For the Gale crater /MSL landing site, the clathrate stability zone is present at 55 m under the surface. It is unlikely that the increase of temperature following the impact of a 1.7m radius destabilize the clathrate. Indeed, even if the model does not go below 10 m, The maximum of temperature at max depth is 892K at time = 6559 (2559 hours after the impact) and it decreases slowly up to 590K, the base value.

For the Phoenix landing site, the clathrate stability zone is present at 6 m under the surface. It is

likely that the increase of temperature following the impact of a 1.7m radius destabilize the clathrate. Indeed, The maximum of temperature for at 6m deep:

- Model 1 and 4 : $\approx 1100K$ at time = 4609 (609 hours after the impact) with a base temperature around 300 K
- Model 2,3 and 5 : $\approx 570K$ at time = 4757 (757 hours after the impact) with a base temperature around 250 K

For Nili Fossae, the clathrate stability zone is present at 62 m under the surface. It is unlikely that the increase of temperature following the impact of a 1.7m radius destabilize the clathrate. Indeed, even if the model does not go below 10 m, The maximum of temperature at max depth is 1255K at time = 10027 (6027 hours after the impact) and it decreases slowly up to 1131K, the base temperature.

For Syrtis Major , the clathrate stability zone is present at 59 m under the surface. It is unlikely that the increase of temperature following the impact of a 1.7m radius destabilize the clathrate. Indeed, even if the model does not go below 10 m, The maximum of temperature at max depth is 703K at time = 6290 (2290 hours after the impact) and it decreases slowly up to 360K, the base value.

For Terra Sabae, the clathrate stability zone is present at 34 m under the surface. More information are needed to determine if the increase of temperature following the impact of a 1.7m radius may destabilize the clathrate. Indeed, even if the model does not go below 10 m, The maximum of temperature at max depth is :

- for mode 1 :1523K at time = 8175 (4175 hours after the impact) and it decreases slowly up to 1139K, the base.
- for model 2 : 1117K at time = 7228 (3228 hours after the impact) and it decreases slowly up to 693K, the base value.

For the Near equator locations, where methane have been detected, the clathrate stability zone is present at a few tens of meters deep below the surface (see 4.1).

For the ExoMars 2022 landing site, it is unlikely that for models 1, 2 and 3 the increase of temperature following the impact of a 1.7m radius destabilize the clathrate. However, more information need the be collected to dertermine the potential for model 4, Formisano 2 and formisano 3. Indeed it is unclear with the limited depth of the simulation, the potential depth of the clathrate stability zone, the low thermal conductivity and the high increase of temperature following the impact if it will destabilize the clathrates.

For the InSight landing site, it is unlikely that for model 2 the increase of temperature following the impact of a 1.7m radius destabilize the clathrate. However, more information need the be collected to dertermine the potential for models 1,3,4 and 5. Indeed it is unclear with the limited depth of the simulation, the potential depth of the clathrate stability zone, the low thermal conductivity of megaregoltih and the high increase of temperature following the impact if it will destabilize the clathrates.

For the Jezero crater, it is unlikely that for models 1 and 2 the increase of temperature following the impact of a 1.7m radius destabilize the clathrate. However, more information need the be collected to dertermine the potential for models 3 and 4. Indeed it is unclear with the limited depth of the simulation, the potential depth of the clathrate stability zone, the low thermal conductivity of carbonates and the high increase of temperature following the impact on carbonates if it will destabilize the clathrates.

10 Conclusions and perspectives

To conclude this master's thesis, a subsurface structure was developped for different locations of interest based on available observations. Then an analytical model (Murnaghan equation of state) was used to simulate the effect of small impactors and its evolution over one martian years. The increase of temperature following an impact was compared to the iSALE-2D shock physics hydrocode.

It was found that the regolith's heterogeneity leads to a different behavior to an impact of a small comets or meteroites on the surface of Mars. Ice table and clathrate stability zone may be destabilized by impacts and volatile may be released in the atmosphere. Some locations, especially the Phoenix landing site, are very likely to see the destabilization of methane clathrates or ice table. Other locations near the equator (InSight landing site, Jezero crater and the ExoMars 2022) may need more information to determine accurately if a destabilization is possible or not.

Methane clathrates are a possible solution to the variability of the methane concentration in the martian atmosphere. For now proof still need to be found for the presence of methane clathrates on Mars but it is a good lead to help to the understanding of the red planet. Even if the detection of methan happened near the equator and that the clathrate stability zone is the deepest there, viable solutions exist to explain the presence of methane and possibly the destabilization of the methane clathrates.

It is however not a fully understood process. There are still unknown parts and the heterogeneity of the martian subsurface adds more complexity to the problem. Nevertheless, the stability zone could be closer to the surface due to the effect of slope or regolith's composition altering the subsurface temperature. Again the regolith's composition may also lead to a greater propagation of the increase of temperature following an impact and thus leading to the releasing of gas.

Another possibility may come from the base of the clathrate stability zone, where it can be closer to the surface on the condition that eutectic $NaCl$, $Mg(ClO4)_2$ and $CaCl_2$ brines are present [Gloesener et al., 2021]. The base of the clathrate zone could also be decomposed by being in contact with high salinity fluids leading to the release of volatile [Madden et al., 2007].

The first results are encouraging but there are still a need for confirmation and improvement to go further in their development.

First of all, the model in itself is improvable to produce more accurate results and a complementary use of the analytical method and hydrocode could help to improve the final result. Indeed taking into account the displacement of material after the impact, the shock wave as well as the strength and porosity of material would be an great impovement. However analytical model are easier and faster but may lead to unrealistic results like the initial increase of temperature following an impact or when the thermal conductivity is low (see ExoMars Model Formisano 1). If ressources (time and computation power) are not limited, hydrocode would offer better results. However analytical model

could be used complementary to select the more pertinent simulation to run. If ressources are limited, few hydrocode simulation could bring better initial condition to obtain more accurate analytical model.

To be noted, the analytical method used in this master's thesis contain a vertical asymptote at the impact center leading to an infinite value for the first result of the increase of temperature. However, as the ice table and the clathrate stability zone are deeper than the surface, it is acceptable for the range of this master's thesis. Nevertheless some cases need verification to be sure results are realistic.

Also, it would be interesting to add other locations if new information would become available or near other detections of methane or when the ice table is close to the surface.

Obviously, the depth of the model needs to be increased in order to check for the influence of the depth of some stability zone. And the lack of information about the impact rate of small impactors as well as their diameter sizes will limit our results. A broader range of diameter could be added for future work.

Moreover, several parameters (thermal conductivity, density, porosity) were approximated or assumed and could be more fine tuned. For example the thermal conductivity which is a crucial parameter is not constant with the evolution of temperature, pressure, grain size , etc. Linked to the thermal conductivity, the porosity and the density are also important parameters for the modelisation of the subsurface and more information would be needed in order to have a more accurate model.

Then the regoltih's composition was aslo approximated based on the available data of the different locations. But some model of the regolith's structure may not be stable. Therefore, additionnal information are needed and will become availabe for locations already present in this master's thesis (after the landing of ExoMars 2022 in Oxia Planum, or other future mission). An update of the regoltih structure and properties would be interesting according to new information. The result could be more accurate if this composition was also more precise (ype of minerals, layer thickness).

Finally, future work could implement an estimate of the volume of clathrates or ice table destabilized by small impacts in order to quantify the environmental effect it could have. It could also give more weight to the clathrate hypothesis as a sink mechanism for the methane mystery on Mars.

Appendix A

Python code

Module containing needed variables and constant for 1D and 2D modelisation

```
import numpy as py
from Models import *
#
# Some default initialisations
#



# Initial surface temperature
v0 = np.array( [ 196.5, 194.5, 192.5, 190.9, 189.3
               , 188.4, 187.4, 201.8, 216.1, 235.5
               , 254.9, 265.4, 276.0, 276.5, 277.0
               , 267.7, 258.5, 241.7, 224.9 ,217.1
               , 209.4, 205.6, 201.8, 199.2, 196.5]
               , dtype=float)

impact = Impact( v         = 10000
               , angle     = 45
               , radius    = 0.12
               , distances = (0, 100, 1)
               , cdiam     = 100
               , de        = 1.62)

basalt = Layer(
           heat_capacity = 800
         , density       = 2600
         , bulk          = 19.3*(10**9)
         , p             = 5.5
         , S             = float(1.025)
         , rh            = 5 / np.power(10,11)
         , F             = 0.019
         , k             = 1.5 # thermal conductivity
         )

def_params = Parameters(
           v0        = v0
         , t0        = 200 # default temperature
         , zlims     = (0, 10, 1)
         , dz        = 1
         , dt        = 3698.96
```

```
        , threshold = 0.01
        , steps     = 5000
        , isot      = [ 150,160,165,170,174,176,177,178,179,180,183
                      , 186,190 , 200,210]
        )
```

Modeling the increase of temperature after an impact (as a function of distance from the impact) using Murnaghan equation of state

```
import numpy as np
import matplotlib.pyplot as plt
import scipy.constants


def plot_murnaghan(v=10000):
    # v: impact velocity
    D = 100. #rim-to-rim diameter of the final crater in m
    R = D/2.
    # distances from the impact in m: max=crater
    rs = np.arange(0.1 ,100, 1)
    sin_alpha = np.sin(np.deg2rad(45))
    A = 2600* (( v * sin_alpha )**2 ) / 4.0
    decay = 1.025 #decay exponent
    R_p = 0.12
    V0 = 1.0/2600.
    K0 = 19.3* (10**9)
    P = A * np.power(rs / R_p, -decay)
    n = 5.5
    delta_E=(0.5*(P*V0-(2*K0*V0/n))*(1-np.power((P*n/K0)+1,-1./n))) + \
            (K0*V0/(n*(1-n)))*(1-np.power((P*n/K0)+1.,1.- 1./n))
    plt.plot(rs, delta_E/800.0, '-', color='red')
    plt.title("Increase of T for an impactor with " + str(R_p) + " (10km/s) "
              "- Murnaghan"
             , fontsize=11
             , fontweight='bold')
    plt.xlabel('Distance from the impact ( in m)',fontsize=11)
    plt.ylabel('Increase of temperature',fontsize=11)
    plt.show()
plot_murnaghan(v=10000)

def plot_murn5(v=10000):
    # v: impact velocity
    D = 100. #rim-to-rim diameter of the final crater in m
    R = D/2.
```

```
    # distances from the impact in m: max=crater
    rs = np.arange( 5 ,60, 1)
    sin_alpha = np.sin(np.deg2rad(45))
    A = 2610 * (( v * sin_alpha )**2 ) / 4.0
    decay = 1.025 #decay exponent
    R_p = 0.12
    V0 = 1.0/2610.
    K0 = 56.9 * (10**9)
    P = A * np.power(rs / R_p, -decay)
    n = 5.4
    delta_E=(0.5*(P*V0-(2*K0*V0/n))*(1-np.power((P*n/K0)+1,-1./n))) + \
            (K0*V0/(n*(1-n)))*(1-np.power((P*n/K0)+1.,1.- 1./n))
    plt.plot(rs, delta_E/580.0, '-', color='red')
    plt.title("Increase of T for an impactor with " + str(R_p) + " (10km/s) "
              "- Murnaghan"
             , fontsize=11
             , fontweight='bold')
    plt.xlabel('Distance from the impact ( in m)',fontsize=11)
    plt.ylabel('Increase of temperature',fontsize=11)
    plt.show()
plot_murn5(v=10000)
```

Modeling in 2D the increase of temperature and pressure following an impact

```
import numpy as np
import matplotlib.pyplot as plt
import scipy.constants

#graphe pour increase of T, Shock pressure and impact-induced increase of temperatu
v = 10000.
rho = 2600 # basaltic crust
Heat_C= 800 # J/kg/K
K0 = 19.3 *(10**9) #adiabatic bulk modulus at zero pressure
n = 5.5 # pressure derivative of the bulk modulus basalt
V0=1./rho
Rp = 1.7 # radius of impactor
pcoef=-1.025
ui =10000. #impact velocity in m/s
#sin_alpha = np.sin(np.deg2rad(45))
#ui_sin = ui*sin_alpha
#P_A= rho * (( v * sin_alpha )**2 ) / 4.0
P_A= rho * (( v  )**2 ) / 4.0 #angle de 90
x = np.zeros((101,101))
y = np.zeros((101,101))
```

```
d = np.zeros((101,101))
P = np.zeros((101,101))
dE = np.zeros((101,101))
dT = np.zeros((101,101))



xrange = 100 #m
yrange = 100 #m

xlim = 101
ylim = 101
xres = xrange /(xlim)
yres = yrange / (ylim)

Dtdz = 12 #thermal gradient in K/km
T0 = np.zeros((xlim,ylim))
T0 [:,0] = 0
for j in range (0,ylim):
    T0[:,j]=T0[:,j-1]+Dtdz*yres/1000.

for i in range (0,101):
  for j in range (0,101):
   x[i,j]=i
   y[i,j]=-j
   d[i,j]=np.sqrt(np.power(x[i,j],2)+np.power(y[i,j],2))/Rp
   # terms for impact-induced energy
   P[i,j]=P_A*np.power(d[i,j],pcoef)
   A=0.5*(P[i,j]*V0-2*K0*V0/n)
   B=1-np.power((P[i,j]*n/K0+1),-1/n)
   C=(K0*V0)/(n*(1-n))
   D=1-np.power(P[i,j]*n/K0+1,1-(1/n))
   dE[i,j]=A*B+C*D
   dT[i,j]=dE[i,j]/Heat_C

f=plt.figure()
ax=f.add_subplot(1,1,1)
ax.set_title('Increase of temperature[K],Rp=1.7m')
ax.set_xlabel('x[m]')
ax.set_ylabel('Depth [m]')
colorinterpolation=1000
colourMap=plt.cm.jet
plt.contourf(x,y,dT,colorinterpolation,cmap=colourMap)
plt.colorbar()
```

```
plt.show()

f2=plt.figure()
ax=f2.add_subplot(1,1,1)
ax.set_title('Shockpressure [Pa], Rp=1.7m')
ax.set_xlabel('x [m]')
ax.set_ylabel('Depth [m]')
colorinterpolation= 100
colourMap = plt.cm.jet
plt.contourf(x , y , P, colorinterpolation , cmap=colourMap )
plt.colorbar()
f3=plt.figure()
ax=f3.add_subplot( 1 , 1 , 1 )
ax.set_title('Increase of temperature only considering the termal gradient [K]')
ax.set_xlabel('x [m]')
ax.set_ylabel('Depth [m]')
colorinterpolation= 50
colourMap =plt.cm.jet
plt.contourf (x, y, T0, colorinterpolation , cmap=colourMap )
plt.colorbar()
plt.show()

#Murnaghan small crater
levels=np.array([0, 10, 20, 30, 40, 50, 100, 150, 300, 500])
f4=plt.figure()
ax=f4.add_subplot ( 1 , 1 , 1 )
ax.set_title('Impact-induced increase of temperature (K), Rp=1.7m')
ax.set_xlabel('x (m)')
ax.set_ylabel( 'Depth (m)' )
colorinterpolation= 100
CS1=plt.contourf(x, y, dT+T0, levels , cmap='autumn_r', origin= 'lower',extend='both
cbar=plt.colorbar()
CS=plt.contour(x, y, dT+T0, levels , colors='black', origin='lower', extend='both',
plt.clabel(CS, inline=True, colors='black', fontsize=10, fmt='%1.f')
plt.show()
#print(dT+T0)
```

Functions used for Crank-Nicolson matrix

```
"""Tridiagonal Crank-Nicolson matrix.
"""
import numpy as np

def triDiagonalMatrix(n, v):
```

```
    # Matrix A (Crank Nicolson)
    # n: the size of the square matrix
    # v: value on the diagonal 1 + 2 * v
    #          on the snd diag : -v or +v
    # v is typically the alpha constant
    M = np.zeros((n,n), float)
    for i in range(1, n-1): # diagonal except the coins
        M[i,i] = 1 + 2 * v
        M[i,i-1] = M[i,i+1] = -v
    M[0,0] = 1
    M[0,1] = 1 # ??? !! (p. 28) Should be 0
    M[n-1,n-2] = -v
    M[n-1,n-1] = 1 + 2 * v
    return (M)

def tridiagonal(n,v):
    # n: dimension of matrix
    # v: value of alpha

    v = float(v)
    # left diagonal
    ld = np.diagflat([ -v for i in range(n-1)], -1)
    # diagonal
    cd = np.diagflat( [ float (1) ] +
                      [ float(1.0) + float(2.0) * v for i in range(n-2) ] +
                      [ float(1.0) + v ])
    # Right diagonal
    rd = np.diagflat( [ float(0) ] + [ -v for i in range(n-2)], 1)

    return (ld + cd + rd)

def tridiagonal_sum_property (n, v):
    # The sum of elements of this type of tridiagonal matrix equal its
    # dimension, whatever the value is
    # n : dimension
    # v : value of alpha
    return (tridiagonal(n,v).sum() == n)

def tridiagonal_sum_inverse_property(n,v):
    # The sum of elements of this type of tridiagonal matrix equal its
    # dimension, whatever the value is
    return (np.linalg.inv(tridiagonal(n,v)).sum() == n)
```

```
def tridiagonal_random_sum_property():
    # run 10 times
    ps = []
    for i in range(10):
        n = random.randrange(2, 100, 1) # dimension from 2 to 25
        v = random.random()             # random value
        ps.append((n,v,tridiagonal_sum_property(n,v)))

    return(ps)
```

Heat equation (Crank-Nicolson) without impact

```
import numpy as np
import matplotlib.pyplot as plt
import scipy.constants

import random # check of propoerties purposes

from Models import *
from Defaults import *
from Tridiagonal import *
from loaddata import *

tab=np.loadtxt("/1.Documents/AGO/1.Thesis/Code_Python/Ts_lat70.dat")
new_tab=np.transpose(tab)
T_surf=new_tab[4]

zs = np.array(range(0,14+1))  # solar longitude
ts = np.array(range(0,len(v0))) # time steps

# Constant properties
k = 1.5                       # thermal conductivity
c  = 800.                     # heat capacity in J/kgK
p  = 2000.0                   # density of basalt in kg/m3
F  = 0.019                    # heat flux in W/m^2
dz = 1                        # spatial step in meters
dt = 3698.96                  # time step in sec (a little more than one hour

# Some helpers constants to build C matrix
alpha = dt * k / (2 * dz * dz * p * c)
                              # layer interval is constant and alpha=gamma
H = 5 / np.power(10, 11)  # radiogenic heat production in W/kg
c1 = dt * F / (dz*p*c )
d1 = H * dt / c
```

```
def initTemperature(v=float(200), nt=len(ts), nz=len(zs), t0=v0):
    # define a matrix of nt x nz temperatures
    # prepend the column t0
    # nt: number of time steps
    # nz: number of solar longitude
    T = np.zeros((nt,nz))
    T[:,:] = v
    # prepend the column of initial temperatures
    T[:,0] = t0
    return T

def rowi (mt, i) :
  return(mt[i-1,:])

def mkC (v0, t, d1, c1):
    return np.array( [v0[t+1]-v0[t]
                    , d1, d1, d1, d1, d1, d1, d1, d1,d1,d1,d1,d1,d1, d1+c1])

def inner_loop(T) :
    (nt, nz) = T.shape
    A = np.linalg.inv (tridiagonal(nz,alpha)) # diag for time + 1
    B = tridiagonal(nz, -alpha)               # diag for time
    for t in range (0, nt-1): # range doesn't include right bound
        cm = mkC(v0, t, d1, c1)
        operation(A, B, cm, t, T)
    return(T)

def operation(am, bm, cm, t, tm):
        pm = np.dot(bm, rowi(tm, t+1))
        qm = np.add(cm, pm)
        tm[t+1,:] = np.dot (am, qm) # produit matriciel
        tm[t,:]   = tm[t+1,:]
        return tm

def swap(M, v0=v0):
    # first line get the last one
    # first column get initial temperature
    (nt, nz) = M.shape
    M[0,:]   = M[nt-1,:]
    M[:,0]   = v0
    return M
```

```
def under_flow(tm, precision):
    (nt,nz) = tm.shape
    return (np.abs(rowi(tm, nt) - rowi(tm,1)) / rowi(tm,1) > precision).all()


def not_boundary_conditions(tm, step, threshold=0.01):
    "Have we reached the boundary conditions (precision and step) ?"
    return (not(under_flow(tm, threshold)) and (step > 0))

def loopBis(step = 10000, threshold = 0.01):
    #LOOP
    T0 = v0
    T = initTemperature(200)
    (nt,nz) = T.shape
    while not_boundary_conditions(T, threshold=threshold, step=step):
        T = swap(inner_loop(T), T0)
        step -= 1
    return(T)

def crank_nicolson(tm=initTemperature(200), step=10000):
    # TODO attempt
    # us, vs: the initial condition
    (nt,nz) = tm.shape
    T_record = []
    am = np.linalg.inv(tridiagonal(nt, alpha))
    bm = tridiagonal(nt,-alpha)
    ts = v0 # initial condition
    for ti in range(1,step):
        fvec = 0
        tnew = np.linalg.solve(am, bm.dot(ts) + fvec)
        ts = tnew
        T_record.append(tnew)
    return tm


def plt_crank_nicolson(tm):
    time  = np.array(range(0,25))
    zs    = np.array(range(0,15)) #layer depths in m
    xs,ys = np.meshgrid(zs, ts)
    f     = plt.figure(figsize=(9,4))
    # Configure the contour
    plt.title("Contour of Temperature")
    colorinterpolation = 50
```

```
    plt.contourf(ys, xs, tm, colorinterpolation, cmap = plt.cm.jet)
    # Set Colorbar
    plt.colorbar()
    # Show the result in the plot window
    plt.gca().invert_yaxis()

    plt.title("Subsurface temperatures on Mars",fontsize=15,
        fontweight="bold")
    plt.xlabel("Time (in hours)",fontsize=11)
    plt.ylabel("Depth (in meters)",fontsize=11)
    labels=['0', '1','2','3','4','5','6','7','8','9','10','11','12','13','14',
        '15','16','17','18','19','20','21','22','23','24']
    plt.xticks(time,labels)
    plt.show()

#To produce subsurface Temperature of mars for 24h
tm = loopBis(step = 10000, threshold = 0.01)
plt_crank_nicolson(tm)

#-----------------------------------------------------
#Now for 1 Martian year
#-----------------------------------------------------

time= np.arange(16056)
#number of second from the start of the year at the start of each month
nh= len(time)
T0= T_surf
#Surface temperature during a martian year (12 martian months ) for
#lat=60N, lon=60W (   60E   ) solar longitude : 190 deg

def initTempYears(ini=float(200), nh=len(time), nz=len(zs), T0=T_surf):
    # define a matrix of nh x nz temperatures
    # prepend the column t0
    # nh: number of time steps
    # nz: number of solar longitude
    H = np.zeros((nh,nz))
    H[:,:] = ini
    # prepend the column of initial temperatures
    H[:,0] = T0
    return H

def rowiYears (mt, i) :
  return(mt[i-1,:])
```

```
def mkCYears (T0, t, d1, c1):
    return np.array( [T0[t+1]-T0[t]
                    , d1, d1,d1,d1,d1,d1, d1, d1, d1, d1, d1, d1, d1+c1])

def inner_loopYears(H) :
    (nh, nz) = H.shape
    A = np.linalg.inv (tridiagonal(nz,alpha)) # diag for time + 1
    B = tridiagonal(nz, -alpha)               # diag for time
    for t in range (0, nh-1): # range doesn't include right bound
        cm = mkCYears(T0, t, d1, c1)
        operationYears(A, B, cm, t, H)
    return(H)

def operationYears(am, bm, cm, t, tmY):
        pm = np.dot(bm, rowiYears(tmY, t+1))
        qm = np.add(cm, pm)
        tmY[t+1,:] = np.dot (am, qm) # produit matriciel
        tmY[t,:]   = tmY[t+1,:]
        return tmY

def swapYears(H, T0=T0):
    # first line get the last one
    # first column get initial temperature
    (nh, nz) = H.shape
    H[0,:]   = H[nh-1,:]
    H[:,0]   = T0
    return H

def under_flowYears(tmY, precision):
    (nh,nz) = tmY.shape
    return (np.abs(rowiYears(tmY, nh) - rowiYears(tmY,1)) / rowiYears(tmY,1) > prec


def not_boundary_conditions(tmY, step, threshold=0.01):
    "Have we reached the boundary conditions (precision and step) ?"
    return (not(under_flowYears(tmY, threshold)) and (step > 0))

def loopTerYears(step = 1000, threshold = 0.01):
    T0 = T_surf #T_surf viens de ls.dat
    H  = initTempYears(ini=float(200), nh=len(time), nz=len(zs), T0=T_surf)
    (nh,nz) = H.shape
    while not_boundary_conditions( H
```

```
                                    , threshold= threshold
                                    , step = step):
            H = swapYears(inner_loopYears(H), T0)
            step -= 1
        return(H)


def plt_crank_nicolsonYears(tmY):
    time  = np.arange(16056)
    zs    = np.array(range(0,15)) #layer depths in m
    xs,ys = np.meshgrid(zs, time)
    f     = plt.figure(figsize=(9,4))
    # Configure the contour
    plt.title("Contour of Temperature")
    colorinterpolation = 50
    plt.contourf(ys, xs, tmY, colorinterpolation, cmap = plt.cm.jet)
    # Set Colorbar
    plt.colorbar()
    #isotherms
    levels=np.array([150,160,165,170,174,176,177,178,179,180,183,186, \
    190,200,210])
    # Show the result in the plot window
    plt.gca().invert_yaxis()
    CS=plt.contour(ys, xs,tmY,levels,colors='black',origin='lower',extend='both', l
    plt.clabel(CS,inline=True,colors='black' ,fontsize=10,fmt='%1.f')
    # Show the result in the plot window
    plt.gca().invert_yaxis()
    plt.title('Subsurface T for lat=70 N,k=1.5 W/mK',fontsize=15, fontweight="bold"
    plt.xlabel('Time (Martian hours)',fontsize=11)
    plt.ylabel('Depth (meters)',fontsize=11)
    plt.ylim(15,1)
    plt.show()

#same plot but without isotherms
def plt_wthout_iso(tmY):
    time  = np.arange(16056)
    zs    = np.array(range(0,15)) #layer depths in m
    xs,ys = np.meshgrid(zs, time)
    f     = plt.figure(figsize=(9,4))
    # Configure the contour
    plt.title("Contour of Temperature")
    colorinterpolation = 50
    plt.contourf(ys, xs, tmY, colorinterpolation, cmap = plt.cm.jet)
```

```
    # Set Colorbar
    plt.colorbar()
    levels=np.array([150,160,165,170,174,176,177,178,179,180,183,186, \
    190,200,210])
    # Show the result in the plot window
    plt.gca().invert_yaxis()
    # Show the result in the plot window
    plt.gca().invert_yaxis()
    plt.title('Subsurface T for lat=70 N,k=1.5 W/mK ',fontsize=15, fontweight="bold
    plt.xlabel('Time (Martian hours)',fontsize=11)
    plt.ylabel('Depth (meters)',fontsize=11)
    plt.ylim(15,1)
    plt.show()

#To produce subsurface Temperature of mars for 16 000h
tmY =  loopTerYears(step = 1000, threshold = 0.01)
plt_crank_nicolsonYears(tmY)
plt_wthout_iso(tmY)
```

Module to load data for specific locations

```
import scipy.io
mat = scipy.io.loadmat('/1.Documents/AGO/1.Thesis/SurfaceTempData/marswrfrob_ts.mat
t_surface = mat['t_surface'] #array de (72,36,16056) => (lon,lat, hours)


#Select Surface temperature for Phoenix (68.21 N , 234.24 E )
Phoen = t_surface[11,31,:]

#Select Surface temperature for MSL (Curiosity/Gale crater) (4.5 S , 137.4 E )
MSL = t_surface[63,17,:]

#Select Surface temperature for Insight (4.5 N , 136.6 E )
Insight = t_surface[63,18,:]

#Select Surface temperature for Jezero Crater (Perseverance) (18.4 N , 77.4 E )
Perse = t_surface[51,21,:]

#Select Surface temperature for Terra Sabae (2 N , 42 E )
Terra = t_surface[44,18,:]

#Select Surface temperature for Nilli Fossae (22 N , 75 E )
Nilli = t_surface[50,22,:]
```

```
#Select Surface temperature for Syrtis Major (8.4 N , 69.5 E )
Syrtis = t_surface[49,19,:]

#Select Surface temperature for Oxia Planum(ExoMars2022) (17.28 N , 334.29 E )
Exomars = t_surface[31,21,:]
```

Heat equation with impact at t= 4000

```
import numpy as np
import matplotlib.pyplot as plt
import scipy.constants

import random # check of propoerties purposes

from Models import *
from Defaults import *
from Tridiagonal import *
from loaddata import *


tab=np.loadtxt("/1.Documents/AGO/1.Thesis/Code_Python/Ts_lat70.dat")
new_tab=np.transpose(tab)
#T_surf=new_tab[4]
T_surf = Phoen

zs = np.array(range(0,10+1))  # solar longitude
ts = np.array(range(0,len(v0))) # time steps

# Constant properties
k  = 3.                    # thermal conductivity
c  = 560.                  # heat capacity in J/kgK
p  = 2711.0                # density of basalt in kg/m3
F  = 0.019                 # heat flux in W/m^2
dz = 1                     # spatial step in meters
dt = 3698.96               # time step in sec (a little more than one hour

# Some helpers constants to build C matrix
alpha = dt * k / (2 * dz * dz * p * c)
                           # layer interval is constant and alpha=gamma
H = 5 / np.power(10, 11)  # radiogenic heat production in W/kg
c1 = dt * F / (dz*p*c )
d1 = H * dt / c

#-----------------------------------------------------------
```

```
#Now for 1 Martian year
#-------------------------------------------------------

time= np.arange(16056)
#number of second from the start of the year at the start of each month
nh= len(time)
T0= T_surf
#Surface temperature during a martian year (12 martian months ) for
#lat=60N, lon=60W (   60E   ) solar longitude : 190 deg

D = 100. #rim-to-rim diameter of the final crater in m
R = D/2.
v = 10000
# distances from the impact in m: max=crater
rs = np.arange(0.1 ,100, 1)
sin_alpha = np.sin(np.deg2rad(45))
A = p* (( v * sin_alpha )**2 ) / 4.0
decay = 1.025 #decay exponent
R_p = 1.7
V0 = 1.0/p
K0 = 161.* (10**9)
P = A * np.power(rs / R_p, -decay)
n = 5.6
delta_E=(0.5*(P*V0-(2*K0*V0/n))*(1-np.power((P*n/K0)+1,-1./n))) + \
(K0*V0/(n*(1-n)))*(1-np.power((P*n/K0)+1.,1.- 1./n))
T_increase = delta_E/c

def initTempYears(ini=float(200), nh=len(time), nz=len(zs), T0=T_surf):
    # define a matrix of nh x nz temperatures
    # prepend the column t0
    # nh: number of time steps
    # nz: number of solar longitude
    H = np.zeros((nh,nz))
    H[:,:] = ini
    # prepend the column of initial temperatures
    H[:,0] = T0
    return H

def rowiYears (mt, i) :
  return(mt[i-1,:])

def mkCYears (T0, t, d1, c1):
        return np.array( [T0[t+1] - T0[t]
```

```
    , d1
    , d1
    , d1  , d1  , d1
    , d1  , d1  , d1
    , d1  , d1 + c1 ])

def mkCWithImpact(T0, t, d1, c1, T_increase):

    if t == 4000:
        C = np.array( [T0[t+1] - T0[t]
    , d1 + T_increase[1]
    , d1 + T_increase[2]
    , d1 + T_increase[3], d1 + T_increase[4], d1 + T_increase[5]
    , d1 + T_increase[6], d1 + T_increase[7], d1 + T_increase[8]
    , d1 + T_increase[9], d1 + c1 + T_increase[10]])
    else:
        C = mkCYears(T0,t,d1,c1)

    return C


def inner_loopYears(H) :
    (nh, nz) = H.shape
    A = np.linalg.inv (tridiagonal(nz,alpha)) # diag for time + 1
    B = tridiagonal(nz, -alpha)               # diag for time

    for t in range (0, nh-1): # range doesn't include right bound
        cm = mkCWithImpact(T0, t, d1, c1, T_increase)
        operationYears(A, B, cm, t, H)
    return(H)

def operationYears(am, bm, cm, t, tmY):
        pm = np.dot(bm, rowiYears(tmY, t+1))
        qm = np.add(cm, pm)
        tmY[t+1,:] = np.dot (am, qm) # produit matriciel
        tmY[t,:]   = tmY[t+1,:]
        return tmY

def swapYears(H, T0=T0):
    # first line get the last one
    # first column get initial temperature
    (nh, nz) = H.shape
    H[0,:]   = H[nh-1,:]
```

```
    H[:,0]    = T0
    return H

def under_flowYears(tmY, precision):
    (nh,nz) = tmY.shape
    return (np.abs(rowiYears(tmY, nh) - rowiYears(tmY,1)) / rowiYears(tmY,1) > prec


def not_boundary_conditions(tmY, step, threshold=0.01):
    "Have we reached the boundary conditions (precision and step) ?"
    return (not(under_flowYears(tmY, threshold)) and (step > 0))

def loopTerYears( step = 1000, threshold = 0.01):
    T0 = T_surf #T_surf viens de ls.dat
    H  = initTempYears(ini=float(200), nh=len(time), nz=len(zs), T0=T_surf)
    (nh,nz) = H.shape
    while not_boundary_conditions( H
                                  , threshold= threshold
                                  , step = step):
        H = swapYears(inner_loopYears(H), T0)
        step -= 1

    return(H)


def plt_crank_nicolsonYears(tmY):
    time  = np.arange(16056)
    zs    = np.array(range(0,11)) #layer depths in m
    xs,ys = np.meshgrid(zs, time)
    f     = plt.figure(figsize=(9,4))
    # Configure the contour
    plt.title("Contour of Temperature")
    colorinterpolation = 50
    plt.contourf(ys, xs, tmY, colorinterpolation, cmap = plt.cm.jet)
    # Set Colorbar
    plt.colorbar()
    #isotherms
    #levels=np.array([150,160,165,170,174,176,177,178,179,180,183,186, \
    #190,200,210])
    # Show the result in the plot window
    plt.gca().invert_yaxis()
    CS=plt.contour(ys, xs,tmY, \
                   #levels
```

```
                    colors='black',origin='lower',extend='both', linewidths=0.4)
    plt.clabel(CS,inline=True,colors='black' ,fontsize=10,fmt='%1.f')
    # Show the result in the plot window
    plt.gca().invert_yaxis()
    plt.title('Subsurface T for Pheonix (Carbonate)', \
            # k=3 W/mK,R=1.7 m,v=10 km/s ', \
                fontsize=15, fontweight="bold")
    plt.xlabel('Time (Martian hours)',fontsize=11)
    plt.ylabel('Depth (meters)',fontsize=11)
    plt.ylim(10,1)
    plt.show()


#To produce subsurface Temperature of mars for 16 000h
tmY =  loopTerYears(step = 1000, threshold = 0.01)
plt_crank_nicolsonYears(tmY)
```

Models for different scenarii with paramaters for each layers

```
#Heat equation (Crank-Nicolson and fully implicit method)vwithout impact
import numpy as np
import matplotlib.pyplot as plt
import scipy.constants

import random # check of propoerties purposes

from Models import *
from Defaults import *
from Tridiagonal import *
from loaddata import *
#Surface temperature different for each location
#Heat flux different for each location
#To find max of a TmY (matrix of Temp) : print (max(map(max, tmY)))


"""
Layer 1 : top
...
...
Layer 4 : down

a : indice for layer 1 (ex : ka,ca, etc.)
b : indice for layer 2 (ex : kb,cb, etc.)
```

```
c : indice for layer 3 (ex : kc,cc, etc.)
d : indice for layer 4 (ex : kd,cd, etc.)

"""
#-----------------------------------------------------------------

"""
Insight : 5 models
"""
"""
#Model 1 : Basalt crust
# Constant properties
T_surf = Insight
n   = 5.5                   # pressure derivative of the bulk modulus for impact
K0  = 19.3 * (10**9)        # adiabatic bulk modulus at zero pressure (Pa)
ka  = 2.                    # thermal conductivity
ca  = 800.                  # heat capacity in J/kgK
pa  = 2900.0                # density in kg/m3
kb  = ka                    # thermal conductivity
cb  = ca                    # heat capacity in J/kgK
pb  = pa                    # density  in kg/m3
kc  = ka                    # thermal conductivity
cc  = ca                    # heat capacity in J/kgK
pc  = pa                    # density o in kg/m3
kd  = ka                    # thermal conductivity
cd  = ca                    # heat capacity in J/kgK
pd  = pa                    # density  in kg/m3
F   = 0.0173                # heat flux in W/m^2
dz  = 1                     # spatial step in meters
dt  = 3698.96               # time step in sec (a little more than one hour)
"""

"""
#Model 2 : Felsic crust
# Constant properties
T_surf = Insight
n   = 5.4                   # pressure derivative of the bulk modulus for impact
K0  = 56.9 * (10**9)        # adiabatic bulk modulus at zero pressure (Pa)
ka  = 2.5                   # thermal conductivity
ca  = 580.                  # heat capacity in J/kgK
pa  = 2750.0                # density  in kg/m3
kb  = ka                    # thermal conductivity
cb  = ca                    # heat capacity in J/kgK
```

```
pb  = pa                    # density  in kg/m3
kc  = ka                    # thermal conductivity
cc  = ca                    # heat capacity in J/kgK
pc  = pa                    # density o in kg/m3
kd  = ka                    # thermal conductivity
cd  = ca                    # heat capacity in J/kgK
pd  = pa                    # density  in kg/m3
F   = 0.0173                # heat flux in W/m^2
dz  = 1                     # spatial step in meters
dt  = 3698.96               # time step in sec (a little more than one hour)
"""

"""
#Model 3 : Megaregoltih
# Constant properties
T_surf = Insight
n   = 5.5                   # pressure derivative of the bulk modulus for impact
K0  = 19.3 * (10**9)        # adiabatic bulk modulus at zero pressure (Pa)
ka  = 0.8                    # thermal conductivity
ca  = 800.                  # heat capacity in J/kgK
pa  = 1700.0                # density in kg/m3
kb  = ka                    # thermal conductivity
cb  = ca                    # heat capacity in J/kgK
pb  = pa                    # density  in kg/m3
kc  = ka                    # thermal conductivity
cc  = ca                    # heat capacity in J/kgK
pc  = pa                    # density o in kg/m3
kd  = ka                    # thermal conductivity
cd  = ca                    # heat capacity in J/kgK
pd  = pa                    # density  in kg/m3
F   = 0.0173                # heat flux in W/m^2
dz  = 1                     # spatial step in meters
dt  = 3698.96               # time step in sec (a little more than one hour)
"""

"""
#Model 4 : Megaregoltih on Basalt crust
# Constant properties
T_surf = Insight
n   = 5.5                   # pressure derivative of the bulk modulus for impact
K0  = 19.3 * (10**9)        # adiabatic bulk modulus at zero pressure (Pa)
ka  = 0.8                    # thermal conductivity
ca  = 800.                  # heat capacity in J/kgK
```

```
pa  = 1700.0                # density in kg/m3
kb  = ka                    # thermal conductivity
cb  = ca                    # heat capacity in J/kgK
pb  = pa                    # density  in kg/m3
kc  = 5.5                   # thermal conductivity
cc  = 800.                  # heat capacity in J/kgK
pc  = 2900.                 # density o in kg/m3
kd  = kc                    # thermal conductivity
cd  = cc                    # heat capacity in J/kgK
pd  = pc                    # density  in kg/m3
F   = 0.0173                # heat flux in W/m^2
dz  = 1                     # spatial step in meters
dt  = 3698.96               # time step in sec (a little more than one hour)
"""

"""
#Model 5 : Megaregoltih on Felsic crust
# Constant properties
T_surf = Insight
n   = 5.5                   # pressure derivative of the bulk modulus for impact
K0  = 19.3 * (10**9)        # adiabatic bulk modulus at zero pressure (Pa)
ka  = 0.8                    # thermal conductivity
ca  = 800.                  # heat capacity in J/kgK
pa  = 1700.0                # density in kg/m3
kb  = ka                    # thermal conductivity
cb  = ca                    # heat capacity in J/kgK
pb  = pa                    # density  in kg/m3
kc  = 5.4                   # thermal conductivity
cc  = 580.                  # heat capacity in J/kgK
pc  = 2750.                 # density o in kg/m3
kd  = kc                    # thermal conductivity
cd  = cc                    # heat capacity in J/kgK
pd  = pc                    # density  in kg/m3
F   = 0.0173                # heat flux in W/m^2
dz  = 1                     # spatial step in meters
dt  = 3698.96               # time step in sec (a little more than one hour)
"""
#-----------------------------------------------------------------
"""
4layers for  Gale crater (Curiosity/MSL)
1 layer : gypsum/anhydrite (top)
2 layer : gypsum/anhydrite
3 layer : smectite
```

```
4 layer : Hematite (down)
"""

"""
# Constant properties
T_surf = MSL
n    = 3.3                  # pressure derivative of the bulk modulus for impact
K0   = 42. * (10**9)        # adiabatic bulk modulus at zero pressure (Pa)
ka   = 4.                   # thermal conductivity
ca   = 900.                 # heat capacity in J/kgK
pa   = 2317.0               # density in kg/m3
kb   = 4.                   # thermal conductivity
cb   = 900.                 # heat capacity in J/kgK g
pb   = 2317.0               # density in kg/m3
kc   = 0.8                  # thermal conductivity smectite
cc   = 650.                 # heat capacity in J/kgK smectite
pc   = 2200.0               # density of smectite in kg/m3
kd   = 6.                   # thermal conductivity Hematite
cd   = 510.                 # heat capacity in J/kgK Hematite
pd   = 5000.0               # density of Hematite crust in kg/m3
F    = 0.0185               # heat flux in W/m^2
dz   = 1                    # spatial step in meters
dt   = 3698.96              # time step in sec (a little more than one hour)
"""
#-----------------------------------------------------------------
"""
For Oxia planum (Exomars, other article)
layer 1 : Megaregolith
Layer 2 : Kaolinite
Layer 3 : Olivine
Layer 4 : Mg smectite
different models :
Model 1 : 3/4
Model 2 : 3/4/3/4
Model 3 : 2/3/4
Model 4 : 1/2/3/4
"""
"""
#Model 4
# Constant properties
T_surf = Exomars
n    = 5.5                  # pressure derivative of the bulk modulus for impact
K0   = 19.3 * (10**9)       # adiabatic bulk modulus at zero pressure (Pa)
```

```
ka   = 0.8                    # thermal conductivity
ca   = 900.                   # heat capacity in J/kgK
pa   = 1700.0                 # density  in kg/m3
kb   = 2.5                    # thermal conductivity
cb   = 650.                   # heat capacity in J/kgK
pb   = 2669.0                 # density  in kg/m3
kc   = 4.                     # thermal conductivity
cc   = 600.                   # heat capacity in J/kgK
pc   = 3222.0                 # density  in kg/m3
kd   = 0.8                    # thermal conductivity
cd   = 650.                   # heat capacity in J/kgK
pd   = 2200.0                 # density in kg/m3
F    = 0.0175                 # heat flux in W/m^2
dz   = 1                      # spatial step in meters
dt   = 3698.96                # time step in sec (a little more than one hour)
"""
"""
#Model 3
# Constant properties
T_surf = Exomars
n    = 5.5                    # pressure derivative of the bulk modulus for impact
K0   = 71.1 * (10**9)         # adiabatic bulk modulus at zero pressure (Pa)
ka   = 2.5                    # thermal conductivity
ca   = 650.                   # heat capacity in J/kgK
pa   = 2669.0                 # density in kg/m3
kb   = 2.5                    # thermal conductivity
cb   = 650.                   # heat capacity in J/kgK
pb   = 2669.0                 # density  in kg/m3
kc   = 4.                     # thermal conductivity
cc   = 600.                   # heat capacity in J/kgK
pc   = 3222.0                 # density in kg/m3
kd   = 0.8                    # thermal conductivity
cd   = 650.                   # heat capacity in J/kgK
pd   = 2200.0                 # density o in kg/m3
F    = 0.0175                 # heat flux in W/m^2
dz   = 1                      # spatial step in meters
dt   = 3698.96                # time step in sec (a little more than one hour)
"""
"""
#Model 2
# Constant properties
T_surf = Exomars
n    = 4.5                    # pressure derivative of the bulk modulus for impact
```

```
K0  = 129  * (10**9)        # adiabatic bulk modulus at zero pressure (Pa)
ka  = 4.                    # thermal conductivity
ca  = 600.                  # heat capacity in J/kgK
pa  = 3222.0                # density  in kg/m3
kb  = 0.8                   # thermal conductivity
cb  = 650.                  # heat capacity in J/kgK
pb  = 2200.0                # density crust in kg/m3
kc  = 4.                    # thermal conductivity
cc  = 600.                  # heat capacity in J/kgK
pc  = 3222.0                # density in kg/m3
kd  = 0.8                   # thermal conductivity
cd  = 650.                  # heat capacity in J/kgK
pd  = 2200.0                # density in kg/m3
F   = 0.0175                # heat flux in W/m^2
dz  = 1                     # spatial step in meters
dt  = 3698.96               # time step in sec (a little more than one hour)
"""
"""
#Model 1
T_surf = Exomars
n   = 4.5                   # pressure derivative of the bulk modulus for impact
K0  = 129  * (10**9)        # adiabatic bulk modulus at zero pressure (Pa)
ka  = 4.                    # thermal conductivity
ca  = 600.                  # heat capacity in J/kgK
pa  = 3222.0                # density  in kg/m3
kb  = 4.                    # thermal conductivity
cb  = 600.                  # heat capacity in J/kgK
pb  = 3222.0                # density  in kg/m3
kc  = 0.8                   # thermal conductivity
cc  = 650.                  # heat capacity in J/kgK
pc  = 2200.0                # density o in kg/m3
kd  = 0.8                   # thermal conductivity
cd  = 650.                  # heat capacity in J/kgK
pd  = 2200.0                # density  in kg/m3
F   = 0.0175                # heat flux in W/m^2
dz  = 1                     # spatial step in meters
dt  = 3698.96               # time step in sec (a little more than one hour)
"""
"""
Exomars
Formisano 3, only megaregoltih with k=0.8
pa = 2000 vs pa = 2900
"""
```

```
T_surf = Exomars
n   = 5.5                  # pressure derivative of the bulk modulus for impact
K0  = 19.3 * (10**9)       # adiabatic bulk modulus at zero pressure (Pa)
ka  = 0.8                  # thermal conductivity
ca  = 800.                 # heat capacity in J/kgK
pa  = 2600.0               # density  in kg/m3
kb  = ka                   # thermal conductivity
cb  = ca                   # heat capacity in J/kgK
pb  = pa                   # density  in kg/m3
kc  = ka                   # thermal conductivity
cc  = ca                   # heat capacity in J/kgK
pc  = pa                   # density o in kg/m3
kd  = ka                   # thermal conductivity
cd  = ca                   # heat capacity in J/kgK
pd  = pa                   # density  in kg/m3
F   = 0.0175               # heat flux in W/m^2
dz  = 1                    # spatial step in meters
dt  = 3698.96              # time step in sec (a little more than one hour)



#-------------------------------------------------------------------------

"""
Jezero Crater (Perseverance)
4 Models :
Model 1 : Olivine sands
Model 2 : Olivine with carbonate on top
Model 3 : Carbonate
Model 4 : Carbo on serpentine on oli
"""
"""
#Model 1
T_surf = Perse
n   = 4.5                  # pressure derivative of the bulk modulus for impact
K0  = 129  * (10**9)       # adiabatic bulk modulus at zero pressure (Pa)
ka  = 4.                   # thermal conductivity
ca  = 600.                 # heat capacity in J/kgK
pa  = 3222.0               # density  in kg/m3
kb  = 4.                   # thermal conductivity
cb  = 600.                 # heat capacity in J/kgK
pb  = 3222.0               # density  in kg/m3
```

```
kc   = 4.                    # thermal conductivity
cc   = 600.                  # heat capacity in J/kgK
pc   = 3222.0                # density o in kg/m3
kd   = 4.                    # thermal conductivity
cd   = 600.                  # heat capacity in J/kgK
pd   = 3222.0                # density  in kg/m3
F    = 0.01855               # heat flux in W/m^2
dz   = 1                     # spatial step in meters
dt   = 3698.96               # time step in sec (a little more than one hour)
"""
"""
#Model 2
T_surf = Perse
n    = 5.7                   # pressure derivative of the bulk modulus for impact
K0   = 73.3 * (10**9)        # adiabatic bulk modulus at zero pressure (Pa)
ka   = 3.                    # thermal conductivity
ca   = 560.                  # heat capacity in J/kgK
pa   = 2711.0                # density  in kg/m3
kb   = 3.                    # thermal conductivity
cb   = 560.                  # heat capacity in J/kgK
pb   = 2711.0                # density  in kg/m3
kc   = 4.                    # thermal conductivity
cc   = 600.                  # heat capacity in J/kgK
pc   = 3222.0                # density o in kg/m3
kd   = 4.                    # thermal conductivity
cd   = 600.                  # heat capacity in J/kgK
pd   = 3222.0                # density  in kg/m3
F    = 0.01855               # heat flux in W/m^2
dz   = 1                     # spatial step in meters
dt   = 3698.96               # time step in sec (a little more than one hour)
"""

"""
#Model 3
T_surf = Perse
n    = 5.7                   # pressure derivative of the bulk modulus for impact
K0   = 73.3 * (10**9)        # adiabatic bulk modulus at zero pressure (Pa)
ka   = 0.8                   # thermal conductivity
ca   = 600.                  # heat capacity in J/kgK
pa   = 3222.0                # density  in kg/m3
kb   = 0.8                   # thermal conductivity
cb   = 600.                  # heat capacity in J/kgK
pb   = 3222.0                # density  in kg/m3
```

```
kc   = 0.8                    # thermal conductivity
cc   = 600.                   # heat capacity in J/kgK
pc   = 3222.0                 # density o in kg/m3
kd   = 0.8                    # thermal conductivity
cd   = 600.                   # heat capacity in J/kgK
pd   = 3222.0                 # density  in kg/m3
F    = 0.01855                # heat flux in W/m^2
dz   = 1                      # spatial step in meters
dt   = 3698.96                # time step in sec (a little more than one hour)
"""

"""
#Model 4
T_surf = Perse
n    = 5.7                    # pressure derivative of the bulk modulus for impact
K0   = 73.3 * (10**9)         # adiabatic bulk modulus at zero pressure (Pa)
ka   = 0.8                  # thermal conductivity
ca   = 600.                   # heat capacity in J/kgK
pa   = 3222.0                 # density  in kg/m3
kb   = 2.7                   # thermal conductivity
cb   = 1000.                    # heat capacity in J/kgK
pb   = 2600.0                 # density  in kg/m3
kc   = 2.7                   # thermal conductivity
cc   = 1000.                    # heat capacity in J/kgK
pc   = 2600.0                 # density o in kg/m3
kd   = 4.                   # thermal conductivity
cd   = 650.                   # heat capacity in J/kgK
pd   = 2200.0                 # density  in kg/m3
F    = 0.01855                # heat flux in W/m^2
dz   = 1                      # spatial step in meters
dt   = 3698.96                # time step in sec (a little more than one hour)
"""
#-------------------------------------------------------------------
"""
Phoenix site: carbonate (Calcite)
"""
"""
#Model 1 without ice
T_surf = Phoen
n    = 5.7                    # pressure derivative of the bulk modulus for impact
K0   = 73.3 * (10**9)         # adiabatic bulk modulus at zero pressure (Pa)
ka   = 3.                     # thermal conductivity
ca   = 560.                   # heat capacity in J/kgK
```

```
pa   = 2711.0                  # density  in kg/m3
kb   = 3.                      # thermal conductivity
cb   = 560.                    # heat capacity in J/kgK
pb   = 2711.0                  # density  in kg/m3
kc   = 3.                      # thermal conductivity
cc   = 560.                    # heat capacity in J/kgK
pc   = 2711.0                  # density o in kg/m3
kd   = 3.                      # thermal conductivity
cd   = 560.                    # heat capacity in J/kgK
pd   = 2711.0                  # density  in kg/m3
F    = 0.0175                  # heat flux in W/m^2
dz   = 1                       # spatial step in meters
dt   = 3698.96                 # time step in sec (a little more than one hour)
"""
"""
#Model 2 with ice as first layer
T_surf = Phoen
n    = 6.                      # pressure derivative of the bulk modulus for impact
K0   = 13.  * (10**9)          # adiabatic bulk modulus at zero pressure (Pa)
ka   = 2.22                    # thermal conductivity
ca   = 2000.                   # heat capacity in J/kgK
pa   = 915.                    # density  in kg/m3
kb   = 3.                      # thermal conductivity
cb   = 560.                    # heat capacity in J/kgK
pb   = 2711.0                  # density  in kg/m3
kc   = 3.                      # thermal conductivity
cc   = 560.                    # heat capacity in J/kgK
pc   = 2711.0                  # density o in kg/m3
kd   = 3.                      # thermal conductivity
cd   = 560.                    # heat capacity in J/kgK
pd   = 2711.0                  # density  in kg/m3
F    = 0.0175                  # heat flux in W/m^2
dz   = 1                       # spatial step in meters
dt   = 3698.96                 # time step in sec (a little more than one hour)
"""
#prop of ice : Physical Review B, 95(17), p.174111_1-174111_7, Klotz et al,2017

"""
#Model 3 with only ice
T_surf = Phoen
n    = 6.                      # pressure derivative of the bulk modulus for impact
K0   = 13.  * (10**9)          # adiabatic bulk modulus at zero pressure (Pa)
ka   = 2.22                    # thermal conductivity
```

```
ca   = 2000.                    # heat capacity in J/kgK
pa   = 915.                     # density  in kg/m3
kb   = ka                       # thermal conductivity
cb   = ca                       # heat capacity in J/kgK
pb   = pa                       # density  in kg/m3
kc   = ka                       # thermal conductivity
cc   = ca                       # heat capacity in J/kgK
pc   = pa                       # density o in kg/m3
kd   = ka                       # thermal conductivity
cd   = ca                       # heat capacity in J/kgK
pd   = pa                       # density  in kg/m3
F    = 0.0175                   # heat flux in W/m^2
dz   = 1                        # spatial step in meters
dt   = 3698.96                  # time step in sec (a little more than one hour)
"""
#-------------------------------------------------------------------
"""
Syrtis Major: olivine (+ Dacite ?)
"""
"""
T_surf = Syrtis
n    = 4.5                      # pressure derivative of the bulk modulus for impact
K0   = 129  * (10**9)           # adiabatic bulk modulus at zero pressure (Pa)
ka   = 4.                       # thermal conductivity
ca   = 600.                     # heat capacity in J/kgK
pa   = 3222.0                   # density  in kg/m3
kb   = 4.                       # thermal conductivity
cb   = 600.                     # heat capacity in J/kgK
pb   = 3222.0                   # density  in kg/m3
kc   = 4.                       # thermal conductivity
cc   = 600.                     # heat capacity in J/kgK
pc   = 3222.0                   # density o in kg/m3
kd   = 4.                       # thermal conductivity
cd   = 600.                     # heat capacity in J/kgK
pd   = 3222.0                   # density  in kg/m3
F    = 0.01985                  # heat flux in W/m^2
dz   = 1                        # spatial step in meters
dt   = 3698.96                  # time step in sec (a little more than one hour)
"""

#-------------------------------------------------------------------
"""
Nilli Fossae: rich clay : smectic assumption
```

```
"""
"""
T_surf = Nilli
n   = 5.5                    # pressure derivative of the bulk modulus for impact
K0  = 70   * (10**9)         # adiabatic bulk modulus at zero pressure (Pa)
ka  = 0.8                     # thermal conductivity
ca  = 650.                   # heat capacity in J/kgK
pa  = 2200.0                 # density  in kg/m3
kb  = 0.8                    # thermal conductivity
cb  = 650.                   # heat capacity in J/kgK
pb  = 2200.0                 # density  in kg/m3
kc  = 0.8                    # thermal conductivity
cc  = 650.                   # heat capacity in J/kgK
pc  = 2200.0                 # density o in kg/m3
kd  = 0.8                    # thermal conductivity
cd  = 650.                   # heat capacity in J/kgK
pd  = 2200.0                 # density  in kg/m3
F   = 0.0189                 # heat flux in W/m^2
dz  = 1                      # spatial step in meters
dt  = 3698.96                # time step in sec (a little more than one hour)
"""
#-------------------------------------------------------------------
"""
Terra Sabae: Basalt
Test effect of porosity
pa = 2000 vs pa = 2900
"""
"""
T_surf = Terra
n   = 5.5                    # pressure derivative of the bulk modulus for impact
K0  = 19.3 * (10**9)         # adiabatic bulk modulus at zero pressure (Pa)
ka  = 2.                     # thermal conductivity
ca  = 800.                   # heat capacity in J/kgK
pa  = 2000.0                 # density  in kg/m3
kb  = ka                     # thermal conductivity
cb  = ca                     # heat capacity in J/kgK
pb  = pa                     # density  in kg/m3
kc  = ka                     # thermal conductivity
cc  = ca                     # heat capacity in J/kgK
pc  = pa                     # density o in kg/m3
kd  = ka                     # thermal conductivity
cd  = ca                     # heat capacity in J/kgK
pd  = pa                     # density  in kg/m3
```

```
F    = 0.020                    # heat flux in W/m^2
dz   = 1                        # spatial step in meters
dt   = 3698.96                  # time step in sec (a little more than one hour)
"""
# Some helpers constants to build C matrix
alpha1 = dt * ka / (2 * dz * dz * pa * ca)
alpha2 = dt * kb / (2 * dz * dz * pb * cb)
alpha3 = dt * kc / (2 * dz * dz * pc * cc)
alpha4 = dt * kd / (2 * dz * dz * pd * cd)
                              # layer interval is constant and alpha=gamma
H = 5 / np.power(10, 11)  # radiogenic heat production in W/kg
c1 = dt * F / (dz*pa*ca ) #layer a
d1 = H * dt / ca #layer a
c2 = dt * F / (dz*pb*cb) #layer b
d2 = H * dt / (cb) #layer b
c3 = dt * F / (dz*pc*cc ) #layer c
d3 = H * dt / cc #layer c
c4 = dt * F / (dz*pd*cd) #layer d
d4 = H * dt / (cd) #layer d

#-----------------------------------------------------------
#Now for 1 Martian year
#-----------------------------------------------------------

time= np.arange(16056)
#number of second from the start of the year at the start of each month
nh= len(time)
T0= T_surf
zs = np.array(range(0,11+1))  # solar longitude
ts = np.array(range(0,len(T0))) # time steps
#Surface temperature during a martian year (12 martian months )

D = 100. #rim-to-rim diameter of the final crater in m
R = D/2.
v = 10000
# distances from the impact in m: max=crater
rs = np.arange(0.1 ,100, 1)
sin_alpha = np.sin(np.deg2rad(45))
A = pa* (( v * sin_alpha )**2 ) / 4.0
decay = 1.025 #decay exponent
R_p = 1.7
V0 = 1.0/pa
# K0 see layer 1
```

```
P = A * np.power(rs / R_p, -decay)
# n see layer 1
delta_E=(0.5*(P*V0-(2*K0*V0/n))*(1-np.power((P*n/K0)+1,-1./n))) + \
(K0*V0/(n*(1-n)))*(1-np.power((P*n/K0)+1.,1.- 1./n))
T_increase=delta_E/ca

def initTempYears(ini=float(200), nh=len(time), nz=len(zs), T0=T_surf):
    # define a matrix of nh x nz temperatures
    # prepend the column t0
    # nh: number of time steps
    # nz: number of solar longitude
    H = np.zeros((nh,nz))
    H[:,:] = ini
    # prepend the column of initial temperatures
    H[:,0] = T0
    return H

def rowiYears (mt, i) :
  return(mt[i-1,:])

def mkCYears (T0, t, d1, d2, d3, d4, c4):
        return np.array( [T0[t+1] - T0[t]
  , d1 , d1
  , d2 , d2 , d2
  , d3 , d3 , d3
  , d4 , d4 , d4 + c4 ])

def mkCWithImpact(T0, t, d1, d2, d3, d4, c4, T_increase):

    if t == 4000:
        C = np.array( [T0[t+1] - T0[t]
  , d1 + T_increase[1]
  , d1 + T_increase[2]
  , d2 + T_increase[3], d2 + T_increase[4], d2 + T_increase[5]
  , d3 + T_increase[6], d3 + T_increase[7], d3 + T_increase[8]
  , d4 + T_increase[9], d4 + T_increase[10], d4 + c4 + T_increase[11]])
    else:
        C = mkCYears(T0,t,d1,d2,d3,d4,c4)

    return C


#-------------------------------
```

```
#Multilayer
#-------------------------------

def fourlayers(v1,v2,v3,v4):
    allup = tridiagonal(12,v1)
    allmidup = tridiagonal(12, v2)
    allmiddown = tridiagonal(12, v3)
    alldown = tridiagonal(12, v4)
    up = allup[0:3]
    midup = allmidup [3:6]
    middown = allmiddown [6:9]
    down = alldown[9:]
    multi = np.concatenate((up,midup,middown,down))
    return multi

def inner_loopYears(H) :
    (nh, nz) = H.shape
    A = np.linalg.inv (fourlayers(alpha1,alpha2, alpha3,alpha4)) # diag for time +
    B = fourlayers( -alpha1, -alpha2,-alpha3,-alpha4)            # diag for time

    for t in range (0, nh-1): # range doesn't include right bound
        cm = mkCWithImpact(T0, t, d1, d2, d3, d4, c4, T_increase)
        operationYears(A, B, cm, t, H)
    return(H)



def operationYears(am, bm, cm, t, tmY):
        pm = np.dot(bm, rowiYears(tmY, t+1))
        qm = np.add(cm, pm)
        tmY[t+1,:] = np.dot (am, qm) # produit matriciel
        tmY[t,:]   = tmY[t+1,:]
        return tmY

def swapYears(H, T0=T0):
    # first line get the last one
    # first column get initial temperature
    (nh, nz) = H.shape
    H[0,:]   = H[nh-1,:]
    H[:,0]   = T0
    return H

def under_flowYears(tmY, precision):
    (nh,nz) = tmY.shape
```

```
    return (np.abs(rowiYears(tmY, nh) - rowiYears(tmY,1)) / rowiYears(tmY,1) > prec


def not_boundary_conditions(tmY, step, threshold=0.01):
    "Have we reached the boundary conditions (precision and step) ?"
    return (not(under_flowYears(tmY, threshold)) and (step > 0))

def loopTerYears( step = 1000, threshold = 0.01):
    T0 = T_surf #T_surf viens de ls.dat
    H  = initTempYears(ini=float(200), nh=len(time), nz=len(zs), T0=T_surf)
    (nh,nz) = H.shape
    while not_boundary_conditions( H
                                  , threshold= threshold
                                  , step = step):
        H = swapYears(inner_loopYears(H), T0)
        step -= 1

    return(H)


def plt_crank_nicolsonYears(tmY):
    time  = np.arange(16056)
    zs    = np.array(range(0,12)) #layer depths in m
    xs,ys = np.meshgrid(zs, time)
    f     = plt.figure(figsize=(9,4))
    # Configure the contour
    plt.title("Contour of Temperature")
    colorinterpolation = 50
    plt.contourf(ys, xs, tmY, colorinterpolation, cmap = plt.cm.jet)
    # Set Colorbar
    plt.colorbar()
    #isotherms
    #levels=np.array([150,160,165,170,174,176,177,178,179,180,183,186, \
    #190,200,210])
    # Show the result in the plot window
    plt.gca().invert_yaxis()
    CS=plt.contour(ys, xs,tmY,40,colors='black',origin='lower',extend='both', linew
    plt.clabel(CS,inline=True,colors='black' ,fontsize=10,fmt='%1.f')
    # Show the result in the plot window
    plt.gca().invert_yaxis()
    plt.title('Subsurface T for Exomars Model 2',fontsize=15, fontweight="bold")
    plt.xlabel('Time (Martian hours)',fontsize=11)
    plt.ylabel('Depth (meters)',fontsize=11)
```

```
    plt.ylim(10,1)
    plt.show()


#To produce subsurface Temperature of mars for 16 000h
tmY =  loopTerYears(step = 1000, threshold = 0.01)
plt_crank_nicolsonYears(tmY)
```

References

[Abramov, 2006] Abramov, O. (2006). Impact-Induced Hydrothermal Activity on Earth and Mars. Accepted: 2011-12-05T21:51:26Z Publisher: The University of Arizona.

[Ahern et al., 2021] Ahern, A. A., Rogers, A. D., Edwards, C. S., and Piqueux, S. (2021). Thermophysical Properties and Surface Heterogeneity of Landing Sites on Mars From Overlapping Thermal Emission Imaging System (THEMIS) Observations. *Journal of Geophysical Research: Planets*, 126(6):e2020JE006713. _eprint: https://agupubs.onlinelibrary.wiley.com/doi/pdf/10.1029/2020JE006713.

[Amsden et al., 1980] Amsden, A. A., Ruppel, H. M., and Hirt, C. W. (1980). SALE: a simplified ALE computer program for fluid flow at all speeds. Technical Report LA-8095, Los Alamos Scientific Lab., NM (USA).

[Banerdt et al., 2020] Banerdt, W. B., Smrekar, S. E., Banfield, D., Giardini, D., Golombek, M., Johnson, C. L., Lognonné, P., Spiga, A., Spohn, T., Perrin, C., Stähler, S. C., Antonangeli, D., Asmar, S., Beghein, C., Bowles, N., Bozdag, E., Chi, P., Christensen, U., Clinton, J., Collins, G. S., Daubar, I., Dehant, V., Drilleau, M., Fillingim, M., Folkner, W., Garcia, R. F., Garvin, J., Grant, J., Grott, M., Grygorczuk, J., Hudson, T., Irving, J. C. E., Kargl, G., Kawamura, T., Kedar, S., King, S., Knapmeyer-Endrun, B., Knapmeyer, M., Lemmon, M., Lorenz, R., Maki, J. N., Margerin, L., McLennan, S. M., Michaut, C., Mimoun, D., Mittelholz, A., Mocquet, A., Morgan, P., Mueller, N. T., Murdoch, N., Nagihara, S., Newman, C., Nimmo, F., Panning, M., Pike, W. T., Plesa, A.-C., Rodriguez, S., Rodriguez-Manfredi, J. A., Russell, C. T., Schmerr, N., Siegler, M., Stanley, S., Stutzmann, E., Teanby, N., Tromp, J., van Driel, M., Warner, N., Weber, R., and Wieczorek, M. (2020). Initial results from the InSight mission on Mars. *Nature Geoscience*, 13(3):183–189. Bandiera_abtest: a Cg_type: Nature Research Journals Number: 3 Primary_atype: Reviews Publisher: Nature Publishing Group Subject_term: Atmospheric dynamics;Geomagnetism;Geomorphology;Inner planets;Seismology Subject_term_id: atmospheric-dynamics;geomagnetism;geomorphology;inner-planets;seismology.

[Barlow and Boyce, 2016] Barlow, N. G. and Boyce, J. M. (2016). The Role of Target Characteristics in the Formation of Impact Crater Ejecta Morphologies at High Latitudes on Mars. 1926:6019. Conference Name: Sixth International Conference on Mars Polar Science and Exploration.

[Barlow and Perez, 2003] Barlow, N. G. and Perez, C. B. (2003). Martian impact crater ejecta morphologies as indicators of the distribution of subsurface volatiles. *Journal of Geophysical Research: Planets*, 108(E8). _eprint: https://agupubs.onlinelibrary.wiley.com/doi/pdf/10.1029/2002JE002036.

[Boyce et al., 2016] Boyce, J. M., Mouginis-Mark, P. J., and Barlow, N. G. (2016). The Two Types of Double Layer Ejecta (DLE) Craters on Mars. page 1327. Conference Name: Lunar and Planetary Science Conference.

[Boynton et al., 2002] Boynton, W. V., Feldman, W. C., Squyres, S. W., Prettyman, T. H., Brückner, J., Evans, L. G., Reedy, R. C., Starr, R., Arnold, J. R., Drake, D. M., Englert, P. A. J., Metzger, A. E., Mitrofanov, I., Trombka, J. I., d'Uston, C., Wänke, H., Gasnault, O., Hamara, D. K., Janes, D. M., Marcialis, R. L., Maurice, S., Mikheeva, I., Taylor, G. J., Tokar, R., and Shinohara, C. (2002).

Distribution of Hydrogen in the Near Surface of Mars: Evidence for Subsurface Ice Deposits. *Science*, 297:81–85.

[Buffett, 2000] Buffett, B. A. (2000). Clathrate Hydrates. *Annual Review of Earth and Planetary Sciences*, 28(1):477–507. _eprint: https://doi.org/10.1146/annurev.earth.28.1.477.

[Cermak and Rybach, 1982] Cermak, V. and Rybach, L. (1982). Thermal Conductivity and Specific Heat of Minerals and Rocks. pages 305–343.

[Chassefière and Leblanc, 2011] Chassefière, E. and Leblanc, F. (2011). Methane release and the carbon cycle on Mars. *Planetary and Space Science*, 59:207–217.

[Chastain and Chevrier, 2007] Chastain, B. K. and Chevrier, V. (2007). Methane clathrate hydrates as a potential source for martian atmospheric methane. *Planetary and Space Science*, 55:1246–1256.

[Chatti et al., 2005] Chatti, I., Delahaye, A., Fournaison, L., and Petitet, J.-P. (2005). Benefits and drawbacks of clathrate hydrates: a review of their areas of interest. *Energy Conversion and Management*, 46(9-10):1333–1343.

[Chen et al., 2017] Chen, X., Zhang, Y., Hui, D., Chen, M., and Wu, Z. (2017). Study of melting properties of basalt based on their mineral components. *Composites Part B: Engineering*, 116.

[Clifford, 1993] Clifford, S. M. (1993). A model for the hydrologic and climatic behavior of water on Mars. *Journal of Geophysical Research*, 98:10973–11016.

[Collins et al., 2004] Collins, G. S., Melosh, H. J., and Ivanov, B. A. (2004). Modeling damage and deformation in impact simulations. *Meteoritics & Planetary Science*, 39(2):217–231. _eprint: https://onlinelibrary.wiley.com/doi/pdf/10.1111/j.1945-5100.2004.tb00337.x.

[Crumpler, 2021] Crumpler, L. S. (2021). GEOLOGIC MAPPING (1:60K) OF AEOLIS MONS, GALE CRATER, MARS AND SPECTRAL. (2610):2.

[Daubar et al., 2015] Daubar, I., Golombek, M., McEwen, A., Byrne, S., Kreslavsky, M., Schmerr, N., Banks, M., Lognonné, P., Kawamura, T., and Karakostas, F. (2015). Measurement of the Current Martian Cratering Size Frequency Distribution, Predictions for and Expected Improvements from InSight.

[Daubar et al., 2020] Daubar, I. J., Gao, A., Wexler, D., Dundas, C., McEwen, A., Neidhart, T., Miljkovic, K., Eschenfelder, J., Collins, G. S., Piqueux, S., Malin, M., and Posiolova, L. (2020). New Craters on Mars: An Updated Catalog. *LPI Contributions*, 2251:2069.

[Drozdovskiy et al., 2020] Drozdovskiy, I., Ligeza, G., Jahoda, P., Franke, M., Lennert, P., Vodnik, P., Payler, S. J., Kaliwoda, M., Pozzobon, R., Massironi, M., Turchi, L., Bessone, L., and Sauro, F. (2020). The PANGAEA mineralogical database. *Data in Brief*, 31:105985.

[Egea-Gonzalez et al., 2021] Egea-Gonzalez, I., Jiménez-Díaz, A., Parro, L. M., Mansilla, F., Holmes, J. A., Lewis, S. R., Patel, M. R., and Ruiz, J. (2021). Regional heat flow and subsurface temperature patterns at Elysium Planitia and Oxia Planum areas, Mars. *Icarus*, 353:113379.

[Ehlmann and Edwards, 2014] Ehlmann, B. L. and Edwards, C. S. (2014). Mineralogy of the Martian Surface. *Annual Review of Earth and Planetary Sciences*, 42(1):291–315.

[Formisano et al., 2021] Formisano, M., De Sanctis, M. C., Federico, C., De Angelis, S., Ferrari, M., Frigeri, A., Magni, G., Altieri, F., and Ammannito, E. (2021). Thermophysical Modeling of Oxia Planum, Landing Site of ExoMars 2022. page 1894. Conference Name: Lunar and Planetary Science Conference.

[Gary-Bicas and Rogers, 2021] Gary-Bicas, C. E. and Rogers, A. D. (2021). Geologic and Thermal Characterization of Oxia Planum Using Mars Odyssey THEMIS Data. *Journal of Geophysical Research: Planets*, 126(2).

[Gloesener, 2019] Gloesener, E. (2019). *Methane clathrate hydrate stability in the martian subsurface and outgassing scenarios*. PhD thesis, UCL - Université Catholique de Louvain.

[Gloesener et al., 2013] Gloesener, E., Karatekin, O., and Dehant, V. (2013). Martian methane and link with clathrates in the crust of Mars.

[Gloesener et al., 2018] Gloesener, E., Karatekin, O., and Dehant, V. (2018). CH4-rich clathrate hydrate stability zone in the present martian subsurface. page 3.

[Gloesener et al., 2019] Gloesener, E., Karatekin, , and Dehant, V. (2019). Stability of clathrate hydrates and gas transport in the Martian subsurface. page 1.

[Gloesener et al., 2021] Gloesener, E., Karatekin, , and Dehant, V. (2021). Stability and composition of CH4-rich clathrate hydrates in the present martian subsurface. *Icarus*, 353:114099.

[Goossens et al., 2017] Goossens, S., Sabaka, T. J., Genova, A., Mazarico, E., Nicholas, J. B., and Neumann, G. A. (2017). Evidence for a low bulk crustal density for Mars from gravity and topography. *Geophysical Research Letters*, 44(15):7686–7694. _eprint: https://agupubs.onlinelibrary.wiley.com/doi/pdf/10.1002/2017GL074172.

[Haberle et al., 2017] Haberle, R., Clancy, R., Forget, F., Smith, M., and Zurek, R. (2017). The atmosphere and climate of Mars. Cambridge University Press.

[Hahn et al., 2011] Hahn, B. C., McLennan, S. M., and Klein, E. C. (2011). Martian surface heat production and crustal heat flow from Mars Odyssey Gamma-Ray spectrometry. *Geophysical Research Letters*, 38(14). _eprint: https://agupubs.onlinelibrary.wiley.com/doi/pdf/10.1029/2011GL047435.

[Hartmann, 2005] Hartmann, W. K. (2005). Martian cratering 8: Isochron refinement and the chronology of Mars. *Icarus*, 174:294–320.

[Hofmeister, 2019] Hofmeister, A. (2019). *Heat Transport and Energetics of the Earth and Rocky Planets: https://www.elsevier.com/books/heat-transport-and-energetics-of-the-earth-and-rocky-planets/hofmeister/978-0-12-818430-1*.

[Hofmeister, 1991] Hofmeister, A. M. (1991). Pressure derivatives of the bulk modulus. *Journal of Geophysical Research: Solid Earth*, 96(B13):21893–21907. _eprint: https://agupubs.onlinelibrary.wiley.com/doi/pdf/10.1029/91JB02157.

[Ishimaru et al., 2010] Ishimaru, R., Komatsu, G., and Matsui, T. (2010). Solar Insolation-induced Destabilization of Subsurface Clathrates on Mars: Implications for the Martian Atmospheric Methane.

[Ivanov, 2001] Ivanov, B. A. (2001). Mars/Moon Cratering Rate Ratio Estimates. *Space Science Reviews*, 96(1):87–104.

[Jeffrey, 1984] Jeffrey, G. A. (1984). Hydrate inclusion compounds. *Journal of inclusion phenomena*, 1(3):211–222.

[Joiret, 2020] Joiret, S. (2020). Heat Effect of Meteorite Impacts on the Degassing of Methane Trapped in Mars' Icy Soil. Accepted: 2020-07-04T02:04:40Z Publisher: Université de Liège, Liège, Belgique Section: Université de Liège.

[Kadish et al., 2008] Kadish, S. J., Head, J. W., Barlow, N. G., and Marchant, D. R. (2008). Pedestal Craters at High Latitudes on Mars: Marginal Sublimation Pits Implicate Ice and Snow in Pedestal Crater Substrate. page 1751. Conference Name: Lunar and Planetary Science Conference.

[Komatsu et al., 2011] Komatsu, G., Ori, G. G., Cardinale, M., Dohm, J. M., Baker, V. R., Vaz, D. A., Ishimaru, R., Namiki, N., and Matsui, T. (2011). Roles of methane and carbon dioxide in geological processes on Mars. *Planetary and Space Science*, 59(2-3):169–181. Publisher: Elsevier Limited.

[Korablev et al., 2019] Korablev, O., Vandaele, A. C., Montmessin, F., Fedorova, A. A., Trokhimovskiy, A., Forget, F., Lefèvre, F., Daerden, F., Thomas, I. R., Trompet, L., Erwin, J. T., Aoki, S., Robert, S., Neary, L., Viscardy, S., Grigoriev, A. V., Ignatiev, N. I., Shakun, A., Patrakeev, A., Belyaev, D. A., Bertaux, J.-L., Olsen, K. S., Baggio, L., Alday, J., Ivanov, Y. S., Ristic, B., Mason, J., Willame, Y., Depiesse, C., Hetey, L., Berkenbosch, S., Clairquin, R., Queirolo, C., Beeckman, B., Neefs, E., Patel, M. R., Bellucci, G., López-Moreno, J.-J., Wilson, C. F., Etiope, G., Zelenyi, L., Svedhem, H., Vago, J. L., and ACS and NOMAD Science Teams (2019). No detection of methane on Mars from early ExoMars Trace Gas Orbiter observations. *Nature*, 568(7753):517–520.

[Lefèvre and Forget, 2009] Lefèvre, F. and Forget, F. (2009). Observed variations of methane on Mars unexplained by known atmospheric chemistry and physics. *Nature*, 460(7256):720–723. Bandiera_abtest: a Cg_type: Nature Research Journals Number: 7256 Primary_atype: Research Publisher: Nature Publishing Group.

[Madden et al., 2007] Madden, M. E. E., Ulrich, S. M., Onstott, T. C., and Phelps, T. J. (2007). Salinity-induced hydrate dissociation: A mechanism for recent CH4 release on Mars. *Geophysical Research Letters*, 34(11). _eprint: https://agupubs.onlinelibrary.wiley.com/doi/pdf/10.1029/2006GL029156.

[Mangold et al., 2007] Mangold, N., Poulet, F., Mustard, J. F., Bibring, J.-P., Gondet, B., Langevin, Y., Ansan, V., Masson, P., Fassett, C., Head, J. W., Hoffmann, H., and Neukum, G. (2007). Mineralogy of the Nili Fossae region with OMEGA/Mars Express data: 2. Aqueous alteration of the crust. *Journal of Geophysical Research: Planets*, 112(E8). _eprint: https://agupubs.onlinelibrary.wiley.com/doi/pdf/10.1029/2006JE002835.

[Marfil et al., 1996] Marfil, R., Scherer, M., and Turrero, M. J. (1996). Diagenetic processes influencing porosity in sandstones from the Triassic Buntsandstein of the Iberian Range, Spain. *Sedimentary Geology*, 105(3):203–219.

[Mellon et al., 2009] Mellon, M. T., Arvidson, R. E., Sizemore, H. G., Searls, M. L., Blaney, D. L., Cull, S., Hecht, M. H., Heet, T. L., Keller, H. U., Lemmon, M. T., Markiewicz, W. J., Ming,

D. W., Morris, R. V., Pike, W. T., and Zent, A. P. (2009). Ground ice at the Phoenix Landing Site: Stability state and origin. *Journal of Geophysical Research: Planets*, 114(E1). _eprint: https://agupubs.onlinelibrary.wiley.com/doi/pdf/10.1029/2009JE003417.

[Melosh, 1989] Melosh, H. J. (1989). Impact Cratering. A Geologic Process. *Geological Magazine*, 126(6):729–730. Publisher: Cambridge University Press.

[Michot et al., 2008] Michot, A., Smith, D. S., Degot, S., and Gault, C. (2008). Thermal conductivity and specific heat of kaolinite: Evolution with thermal treatment. *Journal of the European Ceramic Society*, 28(14):2639–2644.

[Mo/lgaard and Smeltzer, 1971] Mo/lgaard, J. and Smeltzer, W. W. (1971). Thermal Conductivity of Magnetite and Hematite. *Journal of Applied Physics*, 42(9):3644–3647. Publisher: American Institute of Physics.

[Mousis et al., 2013] Mousis, O., Chassefière, E., Lasue, J., Chevrier, V., Elwood Madden, M. E., Lakhlifi, A., Lunine, J. I., Montmessin, F., Picaud, S., Schmidt, F., and Swindle, T. D. (2013). Volatile Trapping in Martian Clathrates. *Space Science Reviews*, 174(1-4):213–250.

[Mumma et al., 2009] Mumma, M. J., Villanueva, G. L., Novak, R. E., Hewagama, T., Bonev, B. P., Disanti, M. A., Mandell, A. M., and Smith, M. D. (2009). Strong release of methane on Mars in northern summer 2003. *Science (New York, N.Y.)*, 323(5917):1041–1045.

[Munje et al., 2020] Munje, M. J., Daubar, I. J., Doran, G., Wagstaff, K. L., and Mandrake, L. (2020). Large-Scale Automated Detection of Fresh Impacts on Mars Using Machine Learning with CTX Observations. *LPI Contributions*, 2251:2065.

[Osako et al., 2010] Osako, M., Yoneda, A., and Ito, E. (2010). Thermal diffusivity, thermal conductivity and heat capacity of serpentine (antigorite) under high pressure. *Physics of the Earth and Planetary Interiors*, 183(1):229–233.

[Parro et al., 2017] Parro, L. M., Jiménez-Díaz, A., Mansilla, F., and Ruiz, J. (2017). Present-day heat flow model of Mars. *Scientific Reports*, 7:45629.

[Pierazzo and Collins, 2004] Pierazzo, E. and Collins, G. (2004). A Brief Introduction to Hydrocode Modeling of Impact Cratering. In Dypvik, H., Burchell, M. J., and Claeys, P., editors, *Cratering in Marine Environments and on Ice*, Impact Studies, pages 323–340. Springer, Berlin, Heidelberg.

[Pierazzo and Melosh, 2000] Pierazzo, E. and Melosh, H. J. (2000). Understanding Oblique Impacts from Experiments, Observations, and Modeling. *Annual Review of Earth and Planetary Sciences*, 28(1):141–167. _eprint: https://doi.org/10.1146/annurev.earth.28.1.141.

[Piqueux and Christensen, 2009] Piqueux, S. and Christensen, P. R. (2009). A model of thermal conductivity for planetary soils: 1. Theory for unconsolidated soils. *Journal of Geophysical Research: Planets*, 114(E9). _eprint: https://agupubs.onlinelibrary.wiley.com/doi/pdf/10.1029/2008JE003308.

[Putzig et al., 2014] Putzig, N. E., Phillips, R. J., Campbell, B. A., Mellon, M. T., Holt, J. W., and Brothers, T. C. (2014). SHARAD soundings and surface roughness at past, present, and proposed landing sites on Mars: Reflections at Phoenix may be attributable to deep ground ice: SHARAD

RESULTS AT MARS LANDING SITES. *Journal of Geophysical Research: Planets*, 119(8):1936–1949.

[Revil et al., 2002] Revil, A., Grauls, D., and Brévart, O. (2002). Mechanical compaction of sand/clay mixtures. *Journal of Geophysical Research: Solid Earth*, 107(B11):ECV 11–1–ECV 11–15. _eprint: https://agupubs.onlinelibrary.wiley.com/doi/pdf/10.1029/2001JB000318.

[Schwenzer et al., 2012] Schwenzer, S. P., Abramov, O., Allen, C. C., Clifford, S. M., Cockell, C. S., Filiberto, J., Kring, D. A., Lasue, J., McGovern, P. J., Newsom, H. E., Treiman, A. H., Vaniman, D. T., and Wiens, R. C. (2012). Puncturing Mars: How impact craters interact with the Martian cryosphere. *Earth and Planetary Science Letters*, 335:9–17. Publisher: Elsevier.

[Sizemore and Mellon, 2006] Sizemore, H. G. and Mellon, M. T. (2006). Effects of soil heterogeneity on martian ground-ice stability and orbital estimates of ice table depth. *Icarus*, 185(2):358–369.

[Sloan and Koh, 2007] Sloan, E. D. S. and Koh, C. A. (2007). *Clathrate Hydrates of Natural Gases*. CRC Press. Boca raton.

[Temel et al., 2019] Temel, O., Karatekin, , Gloesener, E., Mischna, M. A., and van Beeck, J. (2019). Atmospheric transport of subsurface, sporadic, time-varying methane releases on Mars. *Icarus*, 325:39–54.

[Thomas et al., 2009] Thomas, C., Mousis, O., Picaud, S., and Ballenegger, V. (2009). Variability of the methane trapping in martian subsurface clathrate hydrates. *Planetary and Space Science*, 57(1):42–47.

[Vu et al., 2019] Vu, T. H., Piqueux, S., Choukroun, M., Edwards, C. S., Christensen, P. R., and Glotch, T. D. (2019). Low-temperature specific heat capacity measurements and application to Mars thermal modeling. *Icarus*, 321:824–840.

[Watson, 1964] Watson, K. (1964). *I. The thermal conductivity measurements of selected silicate powders in vacuum from 150°-350° K. II. An interpretation of the Moon's eclipse and lunation cooling as observed through the Earth's atmosphere from 8-14 microns*. phd, California Institute of Technology.

[Webster et al., 2013] Webster, C. R., Mahaffy, P. R., Atreya, S. K., Flesch, G. J., Farley, K. A., and Team, M. S. (2013). Low Upper Limit to Methane Abundance on Mars. *Science*, 342(6156):355–357. Publisher: American Association for the Advancement of Science Section: Report.

[Webster et al., 2015] Webster, C. R., Mahaffy, P. R., Atreya, S. K., Flesch, G. J., Mischna, M. A., Meslin, P.-Y., Farley, K. A., Conrad, P. G., Christensen, L. E., Pavlov, A. A., Martín-Torres, J., Zorzano, M.-P., McConnochie, T. H., Owen, T., Eigenbrode, J. L., Glavin, D. P., Steele, A., Malespin, C. A., Archer, P. D., Sutter, B., Coll, P., Freissinet, C., McKay, C. P., Moores, J. E., Schwenzer, S. P., Bridges, J. C., Navarro-Gonzalez, R., Gellert, R., Lemmon, M. T., and Team, t. M. S. (2015). Mars methane detection and variability at Gale crater. *Science*, 347(6220):415–417. Publisher: American Association for the Advancement of Science Section: Report.

[Webster et al., 2021] Webster, C. R., Mahaffy, P. R., Pla-Garcia, J., Rafkin, S. C. R., Moores, J. E., Atreya, S. K., Flesch, G. J., Malespin, C. A., Teinturier, S. M., Kalucha, H., Smith, C. L., Viúdez-Moreiras, D., and Vasavada, A. R. (2021). Day-night differences in Mars methane suggest nighttime containment at Gale crater. *Astronomy & Astrophysics*, 650:A166. Publisher: EDP Sciences.

[Wünnemann et al., 2006] Wünnemann, K., Collins, G. S., and Melosh, H. J. (2006). A strain-based porosity model for use in hydrocode simulations of impacts and implications for transient crater growth in porous targets. *Icarus*, 180:514–527. ADS Bibcode: 2006Icar..180..514W.

[Yakushev and Istomin, 1992] Yakushev, V. and Istomin, V. (1992). Gas hydrates self-preservation effect. *Physics and Chemistry of Ice*. Hokkaido University Press, Sapporo.

[Zastrow and Glotch, 2021] Zastrow, A. M. and Glotch, T. D. (2021). Distinct Carbonate Lithologies in Jezero Crater, Mars. *Geophysical Research Letters*, 48(9):e2020GL092365. _eprint: https://agupubs.onlinelibrary.wiley.com/doi/pdf/10.1029/2020GL092365.